Fabrication, Modification and Self-assembly of Metallic Nano-Particles for Localized Surface Plasmon Resonance and Surface Enhanced Vibrational Spectroscopy Applications

by

Meikun Fan
M. Sc, Southwest China Normal University, 2002
B. Sc, Southwest China Normal University, 1999

A Thesis Submitted in Partial Fulfillment
of the Requirements for the Degree of

DOCTOR OF PHILOSOPHY

in the Department of Chemistry

University of Victoria

Supervisory Committee

Fabrication, Modification and Self-assembly of Metallic Particles for Localized Surface Plasmon Resonance and Surface Enhanced Vibrational Spectroscopy Applications

by

Meikun Fan
M. Sc, Southwest China Normal University, 2002
B. Sc, Southwest China Normal University, 1999

Supervisory Committee

Dr. Alexandre G. Brolo, (Department of Chemistry)
Supervisor

Dr. David A. Harrington, (Department of Chemistry)
Departmental Member

Dr. Dennis Hore, (Department of Chemistry)
Departmental Member

Dr. Andrew Jirasek, (Department of Physics and Astronomy)
Outside Member

Abstract

Supervisory Committee

Dr. Alexandre G. Brolo, (Department of Chemistry)
Supervisor
Dr. David A. Harrington, (Department of Chemistry)
Departmental Member
Dr. Dennis Hore, (Department of Chemistry)
Departmental Member
Dr. Andrew Jirasek, (Department of Physics and Astronomy)
Outside Member

Metallic nanoparticles (MNPs), especially those made of gold, silver, and copper, are of great importance in many scientific disciplines. The free electrons inside the MNPs can respond collectively to applied electromagnetic fields. This is called the excitation of localized surface plasmon resonance (LSPR).

One of the most important aspects of surface plasmons (SPs) excitation is that it allows the localization of the electromagnetic field at certain regions of the nanostructured surface (or, in other words, the local field is "enhanced"). Based on this, surface enhanced Raman scattering (SERS) and localized surface plasmon resonance (LSPR) sensing can be realized.

The work in this thesis can be divided in two parts: These include the exploration of self-assembled MNPs as new substrates for surface enhanced vibrational spectroscopy; and the sensing applications of these assembled MNPs.

In the first part, the assembly of MNPs on gold electrodes and glass slides were explored.

Firstly, "layer-by-layer" self-assembly of Au NPs on gold electrode was used to construct a highly sensitive and reproducible SERS substrate that can work in an electrochemical environment. The SERS performance, in terms of enhancement and reproducibility, with the the numbers Au NPs "layers", was examined. Meanwhile, the potential window, during which a reproducible *in situ* SERS experiment can be performed, was investigated. The possibility of such kind of substrate to be used in surface enhanced polarization modulation infrared absorption spectroscopy (PM-IRRAS) was also discussed.

The "layer-by-layer" self-assembly idea was extended to Ag NPs supported on glass. The resulted substrate revealed that after multiple time self-assembly, the SERS enhancement performance of the substrate can be 3 to 4 orders of magnitude higher than just one Ag NPs deposition, depending on the wavelength used. Using this substrate, a near-single-molecule sensitivity has been achieved.

In the second part, sensing applications of the assembled MNPs were examined.

The multiple "layers" Au NPs on gold electrode was used to characterize a sample biofuel cell anode, which consists three molecular "layers": the linker 4-hydroxyphenol (HTP), the co-enzyme analog Cibacron blue (CB), and the formaldehyde dehydrogenase (FalDH). (*In situ*) SERS spectra of the sample biofuel cell at different construction stages were recorded and compared.

The work about self-assembly of Ag NPs on glass was extended to fiber optics. The tip of a fiber optic was modified with multiple "layers" of Ag NPs, and the analytical performance for remote sensing of this device was examined by the using of dyes with different structures and charges. It was found that this device was among one of the most sensitive SERS remote sensors when compared to the literature.

Finally, a LSPR biosensor based on self-assembly of Ag NPs on PET, a common type of plastic, has been developed. The advantage of this sensor is that the surface of the Ag NPs was able to be tailored into different functional groups, and therefore met different requirements. Sample analysis for biological relevant species was performed.

Table of Contents

List of Tables

List of Figures

Acronyms

CT mechanism	Charge transfer mechanism
EM mechanism	Electromagnetic mechanism
FWHM	Full-width at half-maximum
LOD	Limit of detection
LSPR	Localized surface plasmons resonance
MNPs	Metallic nanoparticles
NPs-MOFT	Nanoparticles-modified optical fiber tip
OCP	Open circuit potential
OFT	Optical fiber tip
PM-IRRAS	Polarization modulation infrared reflection absorption spectroscopy
RI	Refractive index
RIU	Refractive index unit
RSD	Relative standard deviation
SAM	Self-assembled monolayer
SEIRA	Surface enhanced infrared absorption
SEIRS	Surface-enhanced infra-red spectroscopy
SERS	Surface enhanced Raman scattering
SERRS	Surface enhanced resonance Raman scattering
SNOPS	Silver-nanoparticles-on-plastic sensor
SPR	Surface plasmon resonance

Acknowledgments

I would like to thank:

- My supervisor, Dr. Alexandre G. Brolo, for his supervision, help, support, and patience throughout the course of this thesis.
- Dr. David Harrington, Dr. Andrew Jirasek, and Dr. David Sinton for their help and supervision for related projects.
- Dr. Matthew Moffitt, Dr. Chris Papadopoulos, and Dr. Frank Van Veggel for letting me use their equipments.
- The past Brolo group members for general assistance and useful discussions, especially Dr. Aaron Sanderson, Dr. Gabi Hager, Dr. Jason Anema, Dr. Marcos Santos, Dr. Jacqueline Ferreira, Dr. Gustavo Andrade, Dr. Celly Izumi.
- ALL current Brolo group members, and Amanda Finn, Dr. Manuel Marechal from Harrington group, Cunhai Dong from Van Veggel group for their help and friendship.
- The instrumental shop, chemical store, and machine shop, the chemistry department office for their help.
- NSERC, UVic, CFI and BiopSys network for funding.

Chapter 1: Introduction

This chapter serves to clarify my research goals and to provide the basic background required for the whole thesis. The general objective of this thesis was to explore the application of metallic nanoparticles (MNPs) assemblies in surface-enhanced Raman scattering (SERS) and in localized surface plasmon resonance (LSPR) sensing. A brief discussion on the context of these objectives is presented first. The second part of the chapter presents the organization of the thesis. The third part is to provide some general background for readers from different disciplines. This background includes: the "*abc*" of localized surface plasmon resonance (LSPR); the basics for LSPR sensing; an introduction of surface enhanced vibrational spectroscopy; and, finally, a brief literature review on the application of MNPs as substrate for SERS and LSPR sensing.

1.1 Research Objectives

1.1.1 Motivation

Metallic nanoparticles (MNPs), especially those made of gold, silver, and copper, are of great importance in many scientific disciplines.[1-4] When the size of metallic materials decreases to a certain extent (from a few to ~100 nm), their optical properties substantially changes when compared to the bulk. This is due to the collective oscillation of free electrons in the metal (localized surface plasmon resonance (LSPR)).[3] (Fig. 1-1). For gold, silver, and copper, the frequency for LSPR excitation falls within the visible range. This makes these three metals the top choices for LSPR related applications. For this reason, throughout this work, unless otherwise specified, MNPs only refer to NPs made of one or more of these three metals.

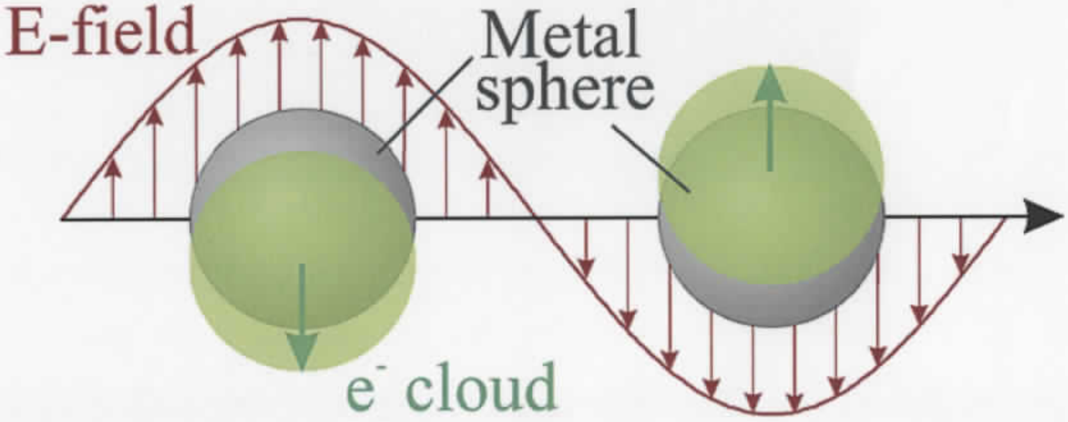

Figure 1- 1 Localized SPR on a MNP excited by free-space light (reproduced with permission, copyright 2003 the American Chemical Society).[38]

One of the most important aspects of LSPR excitation is that it allows the localization of the electromagnetic field at certain regions of the nanostructured surface (or, in other words, the local field is "enhanced"). The efficiency of low probability optical phenomena, such as Raman scattering, can be greatly enhanced due to this localization of electromagnetic field (surface enhanced Raman scattering (SERS)). This is particularly true at the junctions of MNPs (Fig. 1-2).[5-6] In fact, SERS has become one of the most powerful analytical tools, since it can provide single-molecule detection limit together with the molecular vibrational signature .[7]

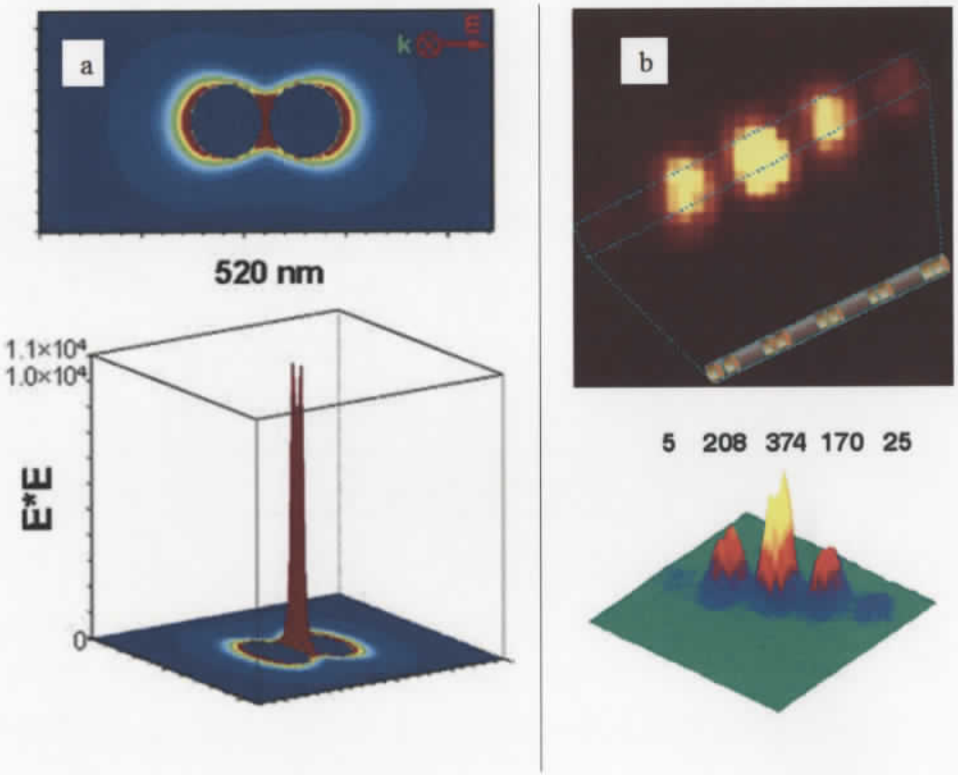

Figure 1- 2 a, theoretical calculation shows the electric field around (up panel) and between (lower panel) silver NPs dimmer separated by 2 nm (reproduced with permission, copyright 2004 the American Institute of Physics);[5] b, confocal Raman mapping of MNPs with different separation distances (reproduced with permission, copyright 2006 the National Academy of Sciences, U.S.A.).[8]

Though MNPs have been widely used in SERS experiment soon after its discovery,[9-10] SERS substrates fabricated from direct aggregation of MNPs suffers from an inherent reproducibility problem. To solve this issue, self-assembly of MNPs on solid support as

SERS substrate has attracted the attention of different groups from all around the world.[11-13] However, despite the large body of work done in this area, several issues still need to be addressed. For instance, the question of how the number of deposited MNPs "layers" will affect the sensitivity and the spatial variation of the final substrate has not been fully explored. The performance of such "multi-layers" structures in electrochemical environment is another issue that has not been tackled before. Systematic examination of such structures as substrate for surface enhanced polarization modulation infrared reflection absorption spectroscopy (PM-IRRAS) has not been reported.

Furthermore, the characterization of multi-layers adsorbates on surfaces by SERS technique is not common,[14-16] even though the multi-layers adsorbate structure is very important in many fields, such as in biofuel cell and biosensor development.[17-18]

Finally, fiber optics based SERS remote sensors have been widely reported but several issues related to reproducibility and detection limit were not fully explored.[19-21]

In a different application, LSPR can be used for detecting molecular adsorption, since the adsorption of analytes on the surface of the MNPs will perturb the SPR field and cause a shift of the absorption maximum.[22-24] The same principle is widely explored in planar SPR devices that use very thin (50 nm) gold films. The application of LSPR for sensing offers a few advantages. For example, the LSPR sensor has normally high spatial resolution. They have fast response times and can be easily miniaturized and integrated into a lab-on-chip.[25-26]

For MNPs based LSPR sensor, the ultimate goal is to develop simple, rapid, inexpensive yet durable sensors for point-of-care diagnostic. To fulfill this, different supporting substrates for MNPs, such as glass,[22, 27-28] paper,[29-30] have been reported. Surprisingly, a more interesting substrate, polyethylene terephthalate (PET), or plastics in general, have not been used yet as the supporting substrate for LSPR sensors.

1.1.2 The general objective

The general objective in this thesis is then to fabricate MNPs assemblies on different solid supports, and explore their applications in surface enhanced vibrational spectroscopy and LSPR sensing. The effect of assembly numbers (number of MNPs "layers") on the sensitivity (enhancement) and reproducibility (spatial variation, sample-to-sample variation) is the focus. The electrochemical stability and the sensing application for multi-layer adsorbates will also be examined.

1.2 Organization of the Thesis

This thesis is divided into 4 parts: I) the introduction; II) surface enhanced vibrational spectroscopy using MNPs assembly on solid support; III) sensing applications of MNPs; followed by IV) a summary chapter.

Other than the introduction and summary, each chapter is a paper that has been published or is under consideration. Supporting information for each respective paper (chapter) were also included.

Part I (chapter 1) is intended to provide some general theoretical background of the topics involved in this work, such as the physics of LSPR, SERS and surface-enhanced infrared absorption (SEIRA) spectroscopy. It also contains a literature overview of the current research status involving MNPs.

Part II comprises of two chapters (chapters 2 and 3).

Chapter 2 deals with the self-assembly of Au NPs on gold slides and its application as substrate for (*in situ*) vibrational spectroscopy. This chapter follows-up on previous work from our research group on the investigation of the self-assembly of Au NPs on glass.[31] Our results showed that ~2 orders of magnitude increase in the SERS signal was achieved after 9 depositions when compared to one deposition, with a electrochemical stable window from -800 mV to +200 mV (versus Ag|AgCl). For SEIRA, only one deposition of Au NPs was sufficient to yield good IR signal.

Chapter 3 focuses on self-assembly of Ag NPs on glass surface as ultrasensitive SERS substrate. Our results showed that by increasing the deposition numbers, not only the enhancement efficiency, but also the sample-to-sample reproducibility between substrates were also improved. The substrates were capable of providing near single molecule sensitivity, with a spatial variation of less than 20%, after 7 Ag NPs depositions.

Part III is concerned with the sensing applications of MNPs-based materials, and it is divided into 3 chapters (chapters 4-6).

In chapter 4, the fabrication of a sample biofuel cell anode was successfully characterized using the substrate described in chapter 2. The sample biofuel cell consisted of three "layers": the linker 4-hydroxythiophenol (HTP), which worked as anchor for immobilizing the coenzyme analog Cibacron Blue (CB), and the latter was used to immobilize enzyme FalDH though affinity interaction. *In situ* and *ex situ* SERS and PM-IRRAS techniques were used to monitor each step.

In chapter 5, Ag NPs were self-assembled on optical fibers and were used as a prototype of remote sensor. The sensitivity and the adaptability of the remote sensor was shown by detecting of analytes with different charges and structures. It was found that the sensitivity of the device for remote sensing Rhodamine 6G (R6G) in water is one of the best ever reported.

Chapter 6 is about a LSPR sensor based on self-assembly of Ag NPs on plastics. The plastic PET was first modified with amine functionality to facilitate the adsorption of Ag NPs. The sensor showed moderate sensitivity to bulk refractive indices changes. The analytical performance of the sensor for biosensing was examined. A linear response for detecting streptavidin was found in the range between 9.5 nM to 189.4 nM, with a limit of detection (LOD) estimated to be 3.5 nM. The capability of using this sensor to monitor protein-protein interaction was also shown.

Part IV (chapter 7) is the summary of the findings in this thesis. The main results from part II and III are revised, discussed, and placed in a proper context. Meanwhile, future directions for this work are suggested.

1.3 General Background

Each result chapter (parts II and III) has its own short introduction. However, some general information, useful for readers from different backgrounds, is presented here. This information will include some basic physics of LSPR, SERS and SEIRA. Meanwhile, the application of the MNPs in surface enhanced spectroscopy and LSPR is also briefly reviewed.

1.3.1 The physics of surface plasmons

The collective fluctuation of surface free electrons at the interface between conductors and dielectrics is called surface plasmons (SPs) or surface plasmon resonance (SPR).[32-33] The word 'plasmon' was coined by David Pines in 1950s,[33] who theoretically described the energy loss caused by the collective oscillation of free electrons in the metal, and borrowed the concept from the plasma physics. The free electrons in metal can be treated as an electron liquid of high density, and the collective electron fluctuation can be considered as plasma oscillation.[32] A generic term for this is "surface plasmon polaritons",[34] since it involves the interaction between surface charge and electromagnetic field (light).

There are two different forms of SPs: propagating SPR and localized SPR. The former refers to the freely propagating electron density waves along the metal surfaces, and the latter describes the localized free charge oscillations on MNPs.

There are two important facts about propagating SPR. Firstly, by solving Maxwell's equation, the relationship between the free space wave vector, k_0, and the SP wave vector, k_{SP}, can be described as following:[34]

$$k_{SP} = k_0\sqrt{\frac{\varepsilon_d\varepsilon_m}{\varepsilon_d+\varepsilon_m}} \qquad (1.1)$$

Where ε_m and ε_d are the frequency dependent permittivity of the metal and dielectric material, respectively.

Equation 1.1 clearly shows that there is momentum mismatch between the free space light and the SPs at the same frequency. This mismatch can be corrected by, for example, introducing a prism.

Another important fact about SPs is that, although the SPs propagate along the surface of the metal, the electromagnetic field perpendicular to this surface decays exponentially with the distance from the surface. Typically, the decay length is half the wavelength of the excitation light.[34]

Since early 1990s, the application of SPs in bio-sensing has attracted tremendous attention. The binding of molecules to the metal (gold) surface changes the surface dielectric constant, and it can be monitored in real time with very high sensitivity (eqn. 1.1). Most importantly, this is a "label-free" technique; i.e., the detection scheme does not require any chemical modification of the analyte.

a b

Figure 1- 3 The Lycurgus Cup in reflected (a) and transmitted (b) mode (courtesy of Celly M. S. Izumi, Brazil).

In contrast to propagating SPR, the phenomenon of LSPR from MNPs has been observed since a very long time; much before it was fully understood.

Fig. 1-3 shows an example of the application of the LSPR effect of MNPs in early civilizations. It is the famous Lycurgus Cup made in ancient Roman time, somewhere in the fourth century A.D. The most remarkable property of this cup is that it presents the color of jade under direct light (Figure 1-3 a). However, the color of the cup changes dramatically into a ruby color once light is shining through the cup (Figure 1-3 b).

This behavior puzzled people for centuries. In 1959, researchers at General Electric Company Ltd found trace amounts of gold, silver and other elements in the glass. Although they believed that these trace elements were responsible for the so called "dichroic effect", they still didn't fully understand the mechanism.[35] The idea that the presence of Au:Ag alloy NPs, of 50~100 nm diameter, is responsible for the dichroic effect become well accepted in the late 1980s. These alloy NPs present LSPR frequencies around 400~520 nm. Hence, when the Lycurgus cup is under direct illumination, it will scatter more in that frequency range, leading to the jade color appearance. Once the illumination is through the cup, light at the same frequency range will be scattered/absorbed, and the ruby color will appear due to the complementary color effect.

The mechanism for excitation of LSPR, or particles plasmons/Mie plasmons,[10] is quite different from that of propagating SPR.

For an isolated MNP under resonance conditions, when the size of the NPs is in the range of the penetration depth of light (e.g., ~20 nm for silver in the visible range), the free electrons in the whole MNP will oscillate together with the applied electromagnetic field. In other words, the MNP can be basically treated as a "molecule". In response to applied field, for the simplest case, the free electrons will be shifted to one side, while the opposite side will be positively charged (Fig. 1-1). Thus, the MNP response looks like a dipole oscillating in response to applied field. In reality, this oscillator will rely on both the electron density and the geometry of the MNP.[33] As a result, the amplitude of the induced electromagnetic field (LSP field) around the surface of the MNPs can be 1 or 2 orders [33] of magnitude higher than the field in the absence of the MNP. Note that this is the simplest approximation for the excitation of LSPR. The MNPs can have more than one single oscillation mode (i.e. higher order oscillation modes), which means that the charge and field distribution can be quite different from Fig. 1-1.

The Mie solution is a widely accepted classical description of the excitation of LSPR on MNPs. When only the dipole oscillation contributes significantly to the extinction cross-section, the Mie solution can be reduced to the following equation: [1, 3, 36-39]

$$\sigma_{ext}(\omega) = \frac{9V\varepsilon_d^{3/2}}{c} \cdot \frac{\omega\varepsilon_2(\omega)}{[\varepsilon_1(\omega)+2\varepsilon_d]^2+\varepsilon_2(\omega)^2}, \qquad (1.2)$$

where $\sigma_{ext}(\omega)$ is the extinction cross-section, V is the volume of the MNP, ω is the angular frequency of the exciting light, c is the speed of light in vacuum, ε_d and $\varepsilon_m(\omega) = \varepsilon_1(\omega) + i\varepsilon_2(\omega)$ are the dielectric function of surrounding medium and the metal, respectively. It is clear that when $\varepsilon_1(\omega) = -2\varepsilon_d$, and ε_2 is small or weakly dependent on ω, the surface plasmon resonance absorption band appears.

Equation 1.2 indicates no size dependent effects for the LSPR frequency and bandwidth in MNPs. This is, indeed, in contradiction with the experimental results. As shown in Fig. 1-4, both parameters, resonance position and bandwidth, change with size. Even for MNPs smaller than 20 nm, there are still size-dependent effects. For MNPs in the size range between 2 and 20 nm, a $1/r$ dependency is observed for the LSPR bandwidth. Equation 1.2 fails to describe the size dependent effect due to the assumption that the optical properties of the MNPs are the same as they are in bulk forms.[36-37] Hence, a more complicated form of the dielectric function of the MNPs, which is both frequency and particle size dependant ($\varepsilon(\omega, r)$), is introduced to better match the experimental results.[36]

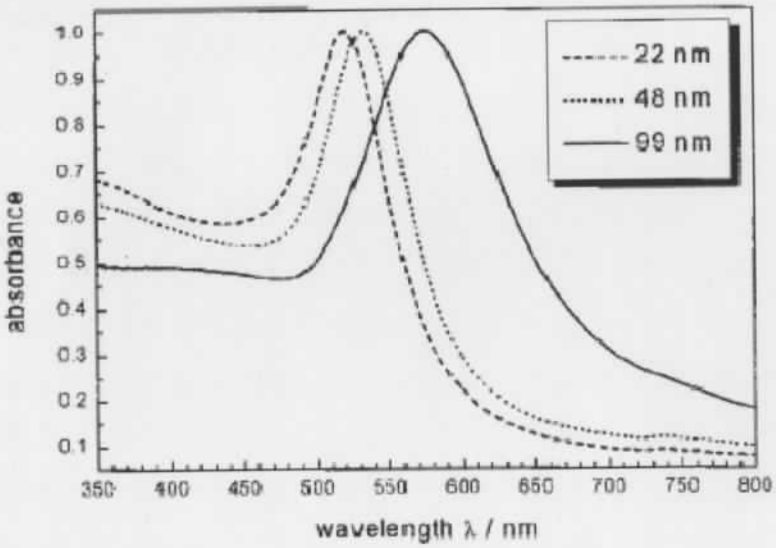

Figure 1- 4 Size effect in surface plasmon absorption in gold spherical NPs (reproduced with permission, copyright 2000 the Taylor & Francis).[36]

For larger MNPs, where the size is comparable to the wavelength of light, the MNPs can no longer be homogenously polarized. Higher order oscillation modes become more important in this regime. These higher order modes locate at lower energy position.[36]

Therefore, the surface plasmon absorption red shifts compared to the small particle situation.

The Mie solution can also been extended for cylindrical or oblate MNPs[1] by introducing depolarization factors.

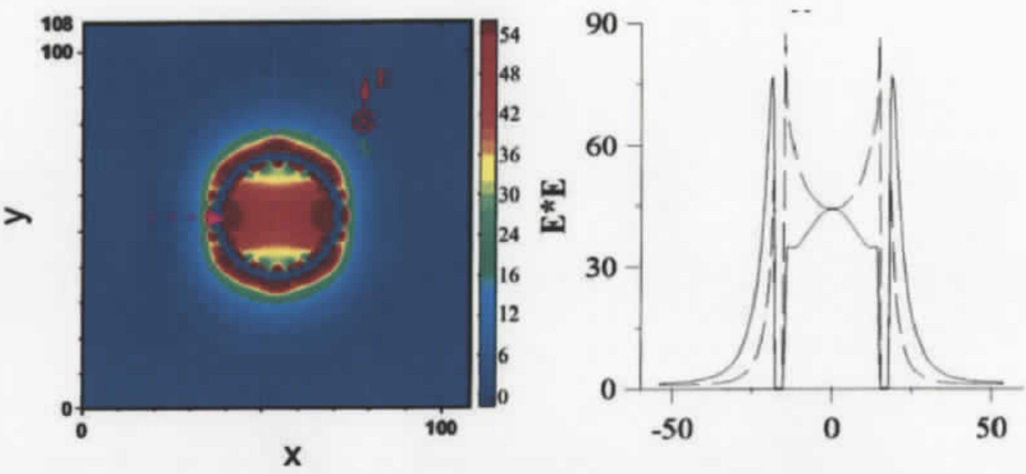

Figure 1- 5 E-field enhancement contours (left) and line analysis (right) external to a gold nanoshell (18 nm in radii and 3 nm in thickness) (reproduced with permission, copyright 2004 the American Chemical Society).[40]

1.3.2 LSPR sensing basics

Equation 1.2 indicates that, for a given size, shape, and material of the MNPs, the extinction coefficient is dependent on the dielectric constant of the surrounding medium. This is the basis for sensing of adsorbates using MNPs. It should also be noted that LSPR is a near field effect.[5, 33, 40] As shown in Fig. 1-5, the field decays exponentially away from the interface. Depending on the materials and the size, the decay length in the case of LSPR is normally in the order of one or a few 10s nm.[40] This is much smaller compared with the planar SPR, which makes the apparent sensitivity of LSPR analysis lower than that of planar SPR, but also provides better special resolution.

However, equation 1.2 uses dielectric function of the surrounding material to predict the changes of the resonance frequency, which is not convenient in sensing. Hence, the refractive index (RI), a property closely related with the dielectric constant ε,[10] is most used in the calculations for (L)SPR sensing.

For bulk RI changes and in a narrow range of wavelength, the equation $\Delta\lambda = m(\eta_{final} - \eta_{initial})$ holds,[41] where m is a sensitivity factor and η is the RI (Fig. 1-6). Generally, the sensitivities of LSPR sensing based on MNPs range from ~100 to ~1000 nm per RI unit.[42-43] Recently, a report indicates that the bulk sensitivity for LSPR sensors based on Au nanorod arrays can be even as high as 32000 nm per RI unit change.[44]

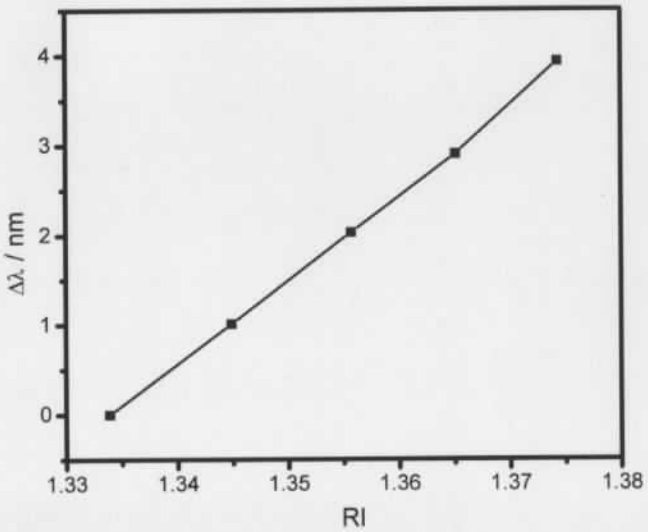

Figure 1- 6 Response of self-assembled Ag NPs to bulk RI changes (glucose solution).

For LSPR sensing, the shift in absorption maximum position depends on the interaction of the analyte of interest and the bulk with the decaying SP field. Therefore, the refractive index must be properly weighted, according to:[25, 41]

$$\Delta\lambda = m\Delta n[1 - \exp(-2d/l_d)] \qquad (1.3),$$

where Δn is the RI difference between a thin uniform film of adsorbates on the sensor surface and the solution above the adsorbates, d is the effective thickness of the adsorbates layer, and l_d is the characteristic decay length of the local field.

1.3.3 Surface-enhanced vibrational spectroscopy

Vibrational spectroscopy, specifically infrared absorption spectroscopy and Raman spectroscopy, is among the most important analytical methods. This is because they can provide a "fingerprint" of the target molecule.[45] However, normal Raman scattering suffers from a problem of low sensitivity.

Surface enhanced vibrational spectroscopy (SEVS), which "deals with the enhanced spectra of molecules on specially fabricated nanostructures with the ability to support surface plasmons and to enhance optical signals",[10] has triggered tremendous interests in scientific community since the discovery of SERS (1970s[46-48]) and SEIRA (1980s[49]).

SERS as an analytical method, is well known for its high sensitivity and specificity.[45] Today, SERS not only serves as one of the most powerful tools for exploring material properties at single molecule level, but also plays very important role in several basic research applications. SERS-based methods can, for instance, monitor the chemical reactions inside a single cell,[50] or probe different cancer markers.[51]

The signal enhancement in SEIRA is believed to be in the range from 1 to 3 orders of magnitude,[49, 52-54] although only 10 to 100 fold - enhancement is commonly observed.[52] The advantage of SEIRA is that it does not have as strict requirement as SERS in terms of substrate material (i.e., mainly Au, Ag, and copper for SERS). Recently, SEIRA on metal Ni mesh substrate has also been reported and used to monitor the catalytic reduction of methanol.[54] This opens the possibility of standardized SEIRA analysis in industrial settings, since the enhancement is large (>100) and Ni meshes are commercially available.

In the next section, some of the basic theories for both SERS and SEIRA will be discussed.

1.3.3.1 Surface enhanced Raman scattering

Raman spectroscopy

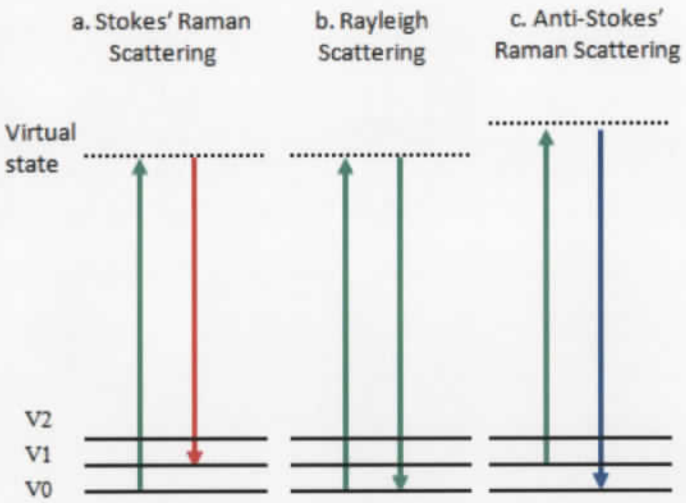

Figure 1- 7 Schematic energy diagram describing the light scattering process.

When photon hits a molecule and is not absorbed (i.e., does not promote an electronic transition), it will be immediate re-emitted (scattered). Generally, only 1 in 1000 incident photons will be scattered by molecules in the visible range.[55] Eventually (1 in 1000 scattered photons), there is an energy exchange between the molecule and the photon in a process called Raman scattering. Raman scattering was first experimentally observed in 1928 by C. V. Raman.[45] The initial experiments were realized using sun light as the excitation source and some color filters. Raman observed what he called "a new type of secondary radiation" that later led to a publication in Nature and a Nobel Prize in physics in 1930.

As shown in Fig. 1-7a, when a photon from a laser beam with energy $h\nu_L$ hits a molecule in its ground vibrational state, the molecule can be excited to a virtual state (this state depends on the energy of the laser). When the photon is re-emitted, some energy is transferred to the molecule leaving it in an excited vibrational state. The Raman scattering frequency is the *difference* between the incident and scattered frequencies. That is:

$$\nu_{Raman} = \nu_L - \nu_S \qquad (1.4),$$

where ν_L is the frequency of the incident laser and ν_S is the frequency of the scattered light. In the special case shown in 1-7a, the emitted radiation is called "Stokes Raman scattering" and the energy of the scattered photon is smaller than that of the incident photon. Usually Raman scattering frequency (Raman Shift) is presented in wave numbers (cm^{-1}) If the incident laser wavelength is λ_L nm and the scattered light is λ_S nm, then equation 1.4 can be written as:

$$\bar{\nu}_{Raman} = 10^7/\lambda_L - 10^7/\lambda_S \qquad (1.5).$$

Another situation, illustrated in Fig. 1-7 c occurs when the molecule is excited initially from its first excited vibrational state. The re-emitted photon will leave with more than the incident energy as the molecule returns to its ground state. This process is called "anti-Stokes Raman scattering". In this case, the emitted photon gained energy from the molecule, Equation 1.5 still holds, but the Raman shift will be mathematically negative. However, the anti-Stokes Raman scattering is much weaker than its counterpart. This is due to the Boltzmann distribution of the molecular population on different energy levels.[55] The population of molecules on their excited vibrational states is smaller than that on ground state at room temperature. Hence, the probability of Raman scattering from these *excited* molecules should be much smaller.

Classically, Raman scattering can be explained in terms of the induced dipole moment, p:[10, 56-57]

$$p = \alpha E \qquad (1.6),$$

where α is the polarizability tensor describes the response function of the molecular electronic cloud to an external field, and E is the incident field vector of the excitation radiation (note: for simplicity, the proper representations for vectors and tensors are omitted).

The polarizability tensor can be written as a series expansion about the equilibrium geometry (for diatomic molecule):

$$\alpha = \alpha_0 + \left(\frac{\partial \alpha}{\partial q}\right)_0 q + \frac{1}{2}\left(\frac{\partial^2 \alpha}{\partial q^2}\right)_0 q^2 + \cdots \qquad (1.7).$$

In equation 1.7, α_0 is the equilibrium value, and subscript 0 simply means the equilibrium value. q is the displacement of position from equilibrium, and can be described using the following equation:

$$q = q_0 \cos(\omega_0 t) \qquad (1.8)$$

where q_0 is the equilibrium position, and ω_0 is the (vibrational) frequency of the oscillation.

Combining equation 1.6 and 1.7 (with q limited at its first order), and replacing E for given laser frequency ω_1 by:

$$E = E_0 cos\,(\omega_1 t) \qquad (1.9),$$

we have:

$$p = \alpha_0 E_0 \cos(\omega_1 t) + \left(\frac{\partial \alpha}{\partial q}\right)_0 q_0 E_0 \cos(\omega_1 t)\cos(\omega_0 t) \qquad (1.10).$$

Since $\cos(x)\cos(y) = \frac{1}{2}[\cos(x+y) + \cos(x-y)]$, equation 1.10 can be written as:

$$p = \alpha_0 E_0 \cos(\omega_1 t) + \frac{1}{2}\left(\frac{\partial \alpha}{\partial q}\right)_0 q_0 E_0 \cos[(\omega_1 + \omega_0)t] + \frac{1}{2}\left(\frac{\partial \alpha}{\partial q}\right)_0 q_0 E_0 \cos[(\omega_1 - \omega_0)t]$$

(1.11)

The first term in the right side of equation 1.11, accounts for the Rayleigh scattering, where there is no energy exchange between the molecule and the incident photon (Fig. 1-7 b); the second term is the anti-Stokes Raman scattering (Fig. 1-7 c); and the third term is the Stokes Raman scattering (Fig. 1-7 a). One more piece of very important information that can be extracted from equation 1.11 is the selection rule in Raman scattering: there has to be a change in the polarizability with the vibration for a specific normal mode to be Raman active. That is, $\left(\frac{\partial\alpha}{\partial q}\right)_0 \neq 0$.

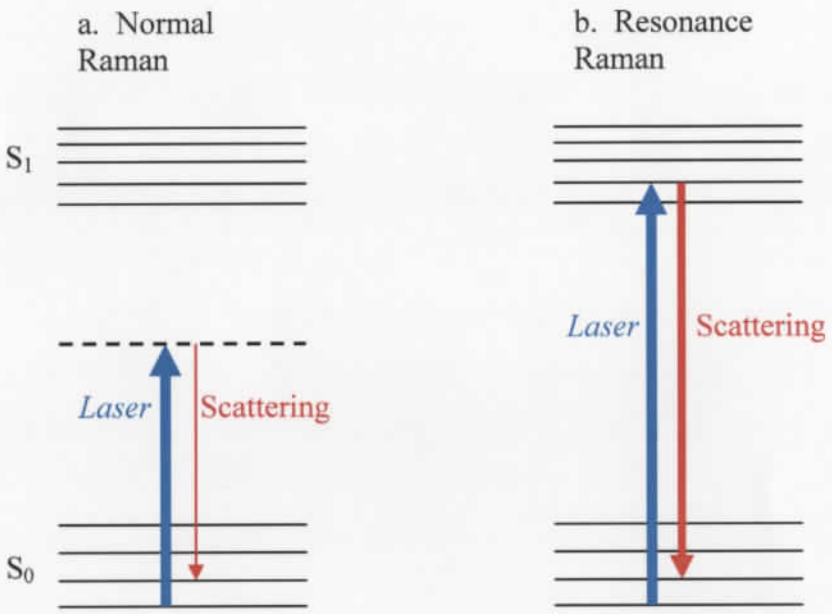

Figure 1- 8 Schematic diagram of normal Raman scattering and resonance Raman scattering (RRS).

Resonant Raman Scattering

Normal Raman scattering is not very efficient (only 1 in 10^6 incident photons scatter as Raman). One way to improve the performance of the Normal Raman is to carefully choose laser frequencies that match real electronic states of the molecule of interest (Fig. 1-8 b). This is called resonance Raman scattering (RRS) and it is a process that greatly increases the probability of Raman scattering. It is estimated that up to 10^6 times enhancement can be achieved compared with normal Raman scattering.[10, 58]

Surface enhanced Raman scattering (SERS)

The SERS phenomenon was discovered in 1970s, when an abnormal intense Raman scattering was observed for pyridine adsorbed on electrochemically roughened silver electrode.[46-48] Up to 10^{10} times of enhancement relative to the normal Raman response has been reported for species at "hot spots" of the SERS substrate,[59] though normally an average of 10^6 is observed. Single molecule SERS detection has been widely reported,[60-62] even for molecules adsorbed on electrochemically roughened electrode.[63]

There are two classes of mechanisms that describe the origin of SERS.[64-67] The first accounts for most of the observed features in SERS and is called the electromagnetic (EM) mechanism.[66] The second one is the charge transfer (CT) mechanism.[67]

The main aspects of the EM mechanism involve the excitation of LSPR. The general features of the theory can be obtained by considering a single spherical MNP,[66] experiencing an electromagnetic field E_0 from the incident laser. Due to the excitation of LSPR, the magnitude of the average field radiated by the MNP, E_s, will be: $E_s = gE_0$, where g is the field enhancement factor. Therefore, the Raman field strength (E_R) for a molecule adsorbed on the surface of the MNP will be: $E_R \propto \alpha_R E_s \propto \alpha_R g E_0$, where α_R is the Raman tensor. However, this is not the ultimate scattered field yet. The MNP can also scatter light at the Raman-shifted frequency enhanced by a factor, g'. Hence, for SERS, the amplitude of the scattered field can be expressed as: $E_{SERS} \propto \alpha_R g g' E_0$. Since the intensity is just the square of the amplitude of the field, the SERS intensity now can be described as:

$$I_{SERS} \propto |\alpha_R|^2 |gg'|^2 I_0 \qquad (1.12),$$

where I_0 is the intensity of the incident light.

For low vibrational frequencies (small Raman shift), the energy of the scattered photon is very close to the wavelength of the incident light, such that $g \cong g'$. Therefore, equation 1.12 can be re-written as:

$$I_{SERS} \propto |\alpha_R|^2 |g|^4 I_0 \qquad (1.13).$$

The SERS intensity would be proportional to the fourth power of the enhanced local field in this case.

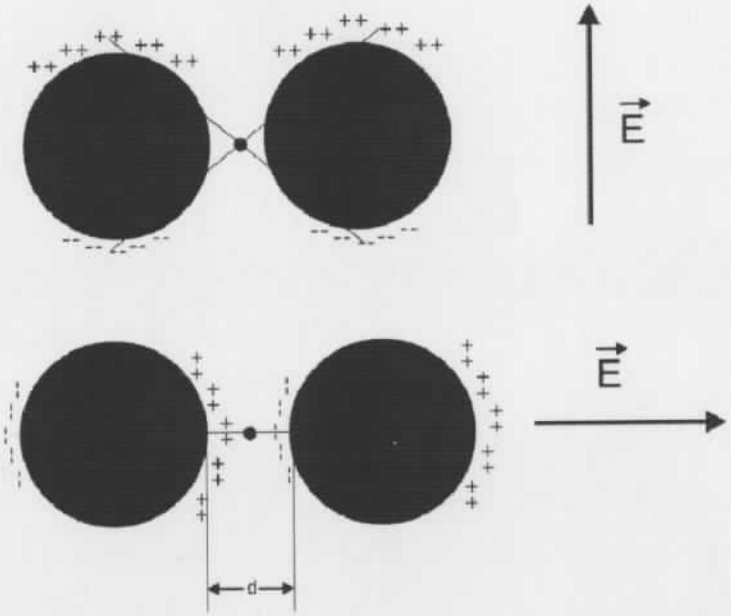

Figure 1- 9 "Interacting" MNPs pair under different light polarization. The sign near the MNPs are the charges (reproduced with permission, copyright 2005 John Wiley and Sons).[9]

For interacting MNPs (i.e., MNPs that are close enough to each other to couple through their dipoles), extremely large local field strength may be found in the gap between them (Fig. 1-2, 1-9).[9-10, 45, 66] As shown in Fig. 1-9, lower panel, if the light is polarized along the axis formed by connecting the centers of the two MNPs, electromagnetic coupling between the two induced dipoles occurs within a certain distance range. As a result, molecules located within these junctions will experience a much higher field, and hence contributes most to the observed SERS signal. This effect has been both theoretically (Fig. 1-2 a) and experimentally (Fig. 1-2 b) justified in the literature. These junctions are examples of SERS hot spots and are the basis for single molecule SERS measurements.[10, 45, 66] It is also interesting to note that, due to this type of coupling, the peak position of the LSPR shifts to longer wavelength. This shift can be rationalized by using a molecular orbital analogy. In molecular orbital theory, the coupling of two molecular orbitals will produce a bonding and an anti-bonding molecular orbitals, with the former locates at lower energy level. The same principle can be applied in LSPR coupling. The red-shifted extinction spectrum of MNPs aggregates is the result of forming "bonding" LSPR states.[120]

On the other hand, if the polarization direction of the field is perpendicular to the axis, as the case shown in Fig. 1-9 upper panel, the coupling effect will be absent. Hence, fractal structures that do not have polarization preference will be superior for SERS. This, indeed, justifies the tremendous effort of building different aggregated MNPs as highly sensitive SERS substrates, including the work in this thesis.

It is also very important to point out that the EM enhancement is strongly dependent on the distance between the target molecule and the metal surface. This is due to the nature of the LSPR as pointed out in section 1.3.1. One should also keep in mind that the decay for LSPR field is not linear.[45, 68]

LSPR plays main role in most of the observed SERS phenomena, but some experiments indicate that other mechanisms may also apply.[64-65, 67] One important contribution comes from "CT mechanism". When molecules adsorbed onto metal surfaces with atomic level roughness, they interact with adatoms to form complexes. Due to the complex formation, the energy gap between the metal's Fermi level and the molecular frontier orbitals may match the energy of the incident laser photon producing a resonance-Raman-scattering-like process. The enhancement from CT processes may not be as strong as that from LSPR field. However, since the Fermi level of metal can be adjusted by applying an external potential, it provides an extra controllable parameter in electrochemical SERS experiments (Fig. 1-10). It is worth mentioning that CT effects are strictly limited to the "first layer", i.e., only the molecules that are in direct contact to the surface (MNPs, electrodes) will benefit from this effect.[10, 65, 67]

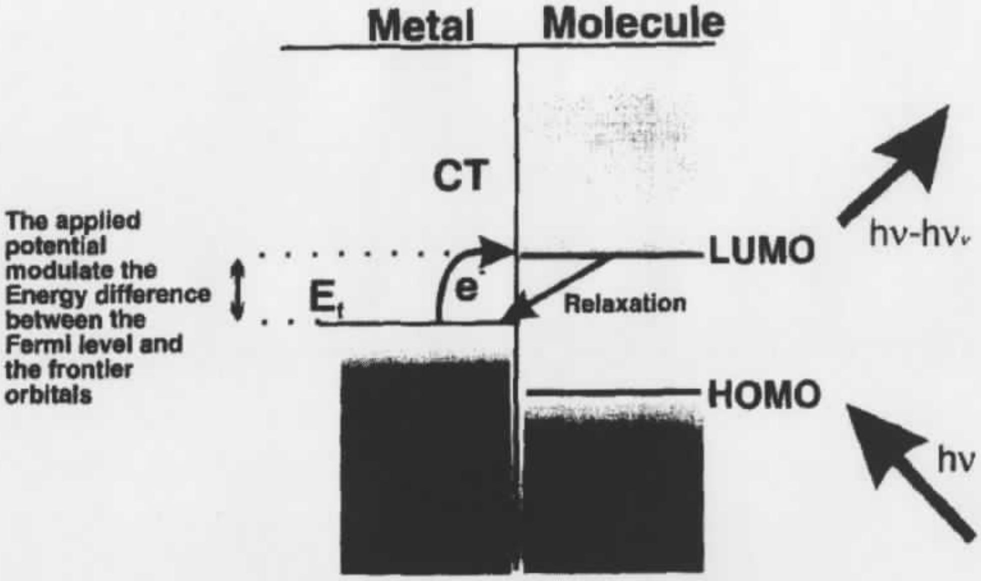

Figure 1- 10 CT mechanism on an electrode (reproduced with permission, copyright 1997 the Elsevier).[65]

1.3.3.2 Surface enhanced infrared absorption

Infrared absorption spectroscopy

A molecule in a vibrational energy level E_n can be excited to a higher vibrational energy level (with energy E_m) when illuminated by a photon with energy $h\nu$ that matches the difference in energy between E_m and E_n: [69]

$$h\nu = E_m - E_n \tag{1.14}$$

$$|m - n| = 1 \tag{1.15}$$

Equation (1.15) defines a selection rule for a harmonic oscillator. Not all vibrational modes are IR active, but only the ones with vibrations that are accompanied by a change in the electric dipole moment of the molecule.

In classical mechanics, the vibrations of polyatomic molecules can be decomposed into normal vibrations, where all atoms are moving at the same frequency and passing through their equilibrium positions simultaneously. The frequency of the vibration of a diatomic molecule can be expressed as:

$$\nu = \frac{1}{2\pi} \cdot \sqrt{\frac{k}{M}} \qquad (1.16),$$

where k is the force constant, and M is the reduced mass of the two atoms, A and B, and can be expressed as:

$$M = \frac{m_A \cdot m_B}{m_A + m_B} \qquad (1.17).$$

Where m_A and m_B are the atomic masses in Kg.

Polarization modulation infrared reflection absorption spectroscopy (PM-IRRAS) [70]

When the infrared beam is linear polarized and strikes a metallic surface at grazing incidence, as shown in Fig. 1-11, the electric field vanishes for *s*-polarized light. This is due to the destructive interference of the incident and reflected radiation at the surface. In the case of *p*-polarized light, constructive interference will occur at the surface and the electric field will be actually enhanced. Considering a molecule adsorbed on a Au surface with a transition dipole moment perpendicular to the surface, it will only interact with *p*-polarized infrared light which will be selectively absorbed. However, molecules that are not adsorbed on the Au surface will have no discrimination against the two orthogonal polarized beams (*s*- and *p*-polarized). As a result, the difference between the two beams will only contain the information of the species adsorbed on the Au surface. This is the working principle of the PM-IRRAS on metal surfaces.

The signal in PM-IRRAS can be expressed by the following equation:[70]

$$\frac{\Delta R}{R} = \frac{|R_s - R_p|}{(R_s + R_p)/2} \qquad (1.18)$$

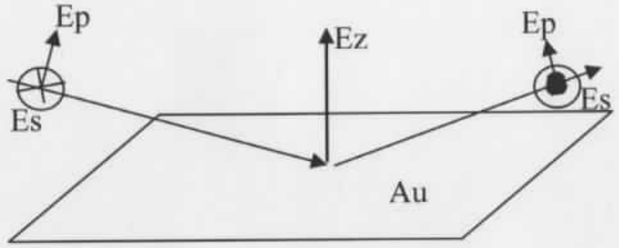

Figure 1- 11 Schematic representation of linear polarized light reflected on Au surface. *p*- and *s*- are for light polarized parallel and perpendicular to the plane of incidence.

Surface enhanced infrared absorption (SEIRA) spectroscopy

SEIRA was first observed in 1980 by Hartstein et al.[71] The origin of SEIRA is generally considered to be similar to SERS, where electromagnetic fields (SPs and phonons) play major roles.[10, 49] However, one should keep in mind that the resonance-Raman- like enhancement due to CT mechanism in SERS does not exist in SEIRA.[10] According to the electric dipole approximation, the SEIR absorption can be written as:[49]

$$A \propto |\frac{\partial\mu}{\partial q} \cdot E_{loc}|^2 \qquad (1.19),$$

where μ is the dipole moment of the molecule, q is the normal coordinates, and E_{loc} is the enhanced local field.

SEIRA enhancements of 3 orders of magnitude is possible for phonon-based processes. The average absorption cross section is 9 orders of magnitude higher than that of Raman scattering, and the materials that can support enhanced IR signal are not only limited to precious metals. These advantages makes SEIRA quite attractive in comparison with SERS.[52] Metallic islands, as well as metallic NPs, dielectric NPs such as SiC and Al_2O_3, and even Nickel meshes,[54] have been used to support SEIRA.[10, 49, 52]

1.3.4 MNPs for SERS and chemical sensing: a brief review

1.3.4.1 SERS substrate development: an overview

Electrochemically roughened Ag electrode was the very first SERS substrate discovered in 1974.[47] Today, SERS substrates made through electrochemical oxidation and reduction cycle (ORC) are still widely used when electrochemistry is involved.[72] The "activation" procedures for the popular electrodes were suggested by Brolo[65] and Tian.[72] However, this technique does not allow much control over the size and shape of the nanofeatures, leading to low reproducibility and high spatial variation.

The most popular SERS substrates are MNPs in suspension in a liquid and MNPs supported on a planar substrate (including vacuum evaporated metal island materials).[45, 73] MNPs have been widely used in SERS experiment since 1977.[9-10, 73] The advantages of using MNPs are that they are easy to make through regular wet chemistry and their size and shape are controllable. The LSPR can be tuned to match different laser excitations. Meanwhile, aggregation of MNPs by simply adding salts into the suspension leads to the formation of SERS hot spots. However, the problem with MNPs suspended in liquid phase is lack of reproducibility in terms of SERS enhancement.[45] Self-assembly of MNPs on glass for SERS was first reported by Freeman et al,[13] in an attempt to solve the reproducibility issue. The immobilization on a solid support seems to improve sample-to-sample reproducibility, and the SERS hot spot density is more easily controlled through the MNPs' size and inter-particle distance.[74]

It is interesting to note that, besides the size and shape effect, alloy and core-shell MNPs[75-81] can also be used to tune the SERS performance. Some reports showed that NPs made of both gold and silver metals can provide higher SERS activity[78-80, 82-84] than pure gold or silver NPs.

More recently, modern nanofabrication methods allow tailoring of the nanostructures for maximum enhancement, and the fabrication of reproducible nanofeatures even in a large area.[85-87] For example, periodic arrays of sub-wavelength apertures (nanoholes) [88-91] and inverted pyramids structures[45] have been shown to be successful SERS substrates.

In the following sections, some examples of the applications of MNPs in SERS will be discussed.

1.3.4.2 MNPs as SERS substrate

The use of MNPs in SERS only started from late 1970s,[73] but they remains as one of the most popular type of SERS substrates due to the great freedom they offer for tuning the LSPR.[45] Currently, the active research interest in this area aims at improving both their sensitivity and the reproducibility. The former involves the synthesis of MNPs with different structures, shapes, and materials; the latter is realized by controlling the size and shape distributions, and by their self-assembly on solid support.[45]

The most common MNPs used as SERS substrates are spherical gold and silver.[45] A comparison of NPs made by these two different metals are discussed in the literature.[45] In general, Au NPs are more stable at different conditions and their chemical modifications are well-understood. On the other hand, due to their dielectric property, Ag NPs are believed to be able to provide better electromagnetic enhancement in the visible range.

There are several preparation methods for Au NPs presented by different authors.[3-4, 92-93] Among all the methods developed, the most widely used is the citrate reduction of gold salts. A modified citrate-based method proposed by Grabar et al[94] provides very reproducible 13 nm spherical NPs. Ag NPs can also be synthesized by reducing silver salts with citrate. The most commonly used is ~ 60 nm in size, and they were first reported by Lee et al.[4, 45, 93, 95] It is worth noting that Ag NPs fabricated by citrate reduction are not very stable.[45]

Preparation methods of MNPs with different sizes and shapes for better SERS performance have been reviewed in the literature.[95-96] Other optimization atempts[97] involve controlling the surface charge of the MNPs to allow specific analytes to reach closer to the surface, yielding better SERS signal.

The tuning of the SPs resonance can also be accomplished by varying the composition in core-shell structures.[45, 68] The core can be either a metal or a dielectric material. It is possible to prepare MNPs with SPR that matches a specific laser frequency using this approach. This is especially important when working with biological samples, where longer wavelength excitation is preferred to avoid background fluorescence.[68] The first examples of MNPs core-shell structures were reported back in 1989.[98] Core-shell structures with defects on the shell can provide an one-order-of-magnitude increase in SERS efficiency when compared to those without deffects.[40, 77, 80] However, the exact reason for this phenomenon is still being debated.[77, 79]

It is a consensus in the SERS community that SERS hot spots are present in aggregated MNPs.[10, 45, 68] Although it is possible to simply add salts into the MNPs solution to introduce aggregation,[51] this approach leads to poor reproducibility.[68, 99] There are considerable efforts in the literature towards finding controlled ways of producing MNPs aggregates.[45, 68, 99] In order to limit the coverage in this introduction, only those approaches that involve the immobilization of MNPs from a suspension will be discussed. Interested readers are encouraged to check the reviews by Vo-Dinh[99] and Baker[68] for other approaches.

Inspired by the self-assembly of organized organic film on metal surfaces, Freeman[13] used silane chemistry to functionalize a glass surface with amino groups, which were used as linkers for the immobilization of MNPs. The concept behind these "2-D SERS substrates", as referred by Freeman, was followed by several groups.[13, 100] The general approach for substrate fabrication involves an initial surface modification of the solid support, either though thiol (for metal) or silane/polymer (for glass),[101] followed by the adsorption of MNPs. It is found that the SERS enhancement factors of the substrates fabricated through this procedure are indeed a function of both the size and population (i.e., particle-to-particle distance) of the deposited MNPs.[74, 102]

Another approach to build 2-D SERS structure is based on capillary forces and van der Waals attraction.[84, 102-108] The self-assembly occurs at the liquid/air or liquid/solid interface [103] and the distance between MNPs can be tuned from 0.4 nm[108] to 10 nm.[106] It was found that the inter-particle distance tuned the SERS signal enhancement,[102] which is in agreement with other theoretical[5] and experimental[8] works. Modification of the MNPs with surfactants was found to be useful to tune the inter-particle distance, and hence yield a better SERS and SEIRA performance.[102, 107]

The third approach, to build a particular interesting SERS substrate, is to embed MNPs in a temperature-controllable polymer.[109] Temperature changes affect the packing of the polymeric chain, tuning the inter-particle distance and the SERS intensity. This is an interesting example of a "smart" SERS substrate.

There are also efforts to build "3-D structures" for SERS applications.[11, 31, 100, 102] These "3-D structures" provide larger surface area for analyte adsorption as well as higher density of hot spots.[102] They also offer the capability of tuning structures according to the laser frequency.[31] The 3-D SERS substrate can be further divided into two groups: template assisted/supported 3-D SERS substrate,[102] and 3-D MNPs substrate fabricated through layer-by-layer assembly.[11, 31, 100] In the first group, the template can be self-assembled polystyrene beads, synthetic nanoporous semiconductors, and photonic crystal fibers.[102] While in the latter case, the MNPs-"linker"-MNPs multilayer structures can be achieved though polymers[11] or dithiols.[31] It is worth noting that, as pointed out by Addison and Brolo,[31] there is an optimum number of "layers" of MNPs that matches a specific laser frequency.

1.3.4.3 MNPs as LSPR sensing material

80 nm Ag NPs can have scattering cross-section one million times larger than the fluorescence cross-section of fluorescein, because of the excitation of LSPR.[27] Meanwhile, MNPs do not suffer from the photo-quenching problem. These are important advantages that encourage the application of LSPR with MNPs in immunoassay and biochemical sensing.[27, 42] The MNPs structures used in those applications include metal-evaporated structures (nanosphere lithography method,[110] colloidal lithography, and soft lithography),[24, 42, 111] electrochemical grown nanorods,[44] and MNPs suspended in liquids.[30, 112] There are also examples of top-down lithography nano-structures used as LSPR sensors,[42, 113] but they are beyond the scope of this introduction.

In this section, only those LSPR sensors fabricated from suspensions of MNPs will be discussed. Examples of other approaches to prepare LSPR sensors are discussed in reviews[27, 42, 93, 114-115] published recently.

MNPs suspensions were firstly employed for detecting DNA hybridization[114, 116-118] and in immunoassays.[23, 114] The detection schemes in those cases were based on LSPR coupling (through small range inter-particle interaction), and on RI induced LSPR frequency shift, respectively. The latter is the same principle used in planar SPR analysis. However, LSPR analysis from MNPs suspensions also suffers from stability issues. Furthermore, the approach is not suitable for high throughput analysis,[22] as is the case for MNPs immobilized on a solid support.[25, 28, 30, 44, 119]

There are two different approaches to solve the issues encountered in the direct application of the colloidal suspension for LSPR sensing. The first approach is to use a controlled aggregation.[42] In this case, the MNPs are firstly modified with enzymes, aptamers, or even some crown ligands. As a result, the MNPs (most cases, gold) will form a grey to purple aggregates (in case of gold). In the presence of the analyte of interest, the Au NPs will dissociate and turn back to the original bright red color.

In the other approach shown in Fig. 1-12, the MNPs are immobilized on a solid support, usually glass. Later, the surface of the MNPs is modified with specific recognizing element to detect the desired analyte(s). The binding events can be monitored by regular UV-Vis spectrometer through changes either in the wavelength on in the absorbance.[42] The sensitivity of immobilized MNPs based LSPR sensor to bulk RI changes ranges from ~100 to 1000 nm/RIU, depending on the material, size and shape of the MNPs.[42, 114]

A significant advantage of MNPs- based LSPR sensors is that the sensing can be done at the single MNP level. This is particular important for biosensing, where the samples are expensive and in limited amounts.[42] This also allows the incorporation of MNPs-based LSPR sensor into a microfluidic system, and is also suitable for multiplexing detection.[27]

However, there are still limitations for this type of sensor.[42, 114] MNPs-based LSPR sensors are lack of sensitivity to bulk RI changes when compared with traditional propagating SPR. Kabashin et al reported a nanorod array with LSPR sensitivity of 32,000 nm/RIU,[44] but this is an atypical example. Secondly, the MNPs fabrication methods have to be improved to achieve better size and shape reproducibility. Thirdly, similar to its counterpart planar SPR, LSPR sensors are not specific and the surface must be properly modified to target a particular molecule. Finally, more supporting solid substrates should be explored, other than glass, to offer different material alternatives in the implementation of LSPR sensors for point-of-care diagnostics.[42]

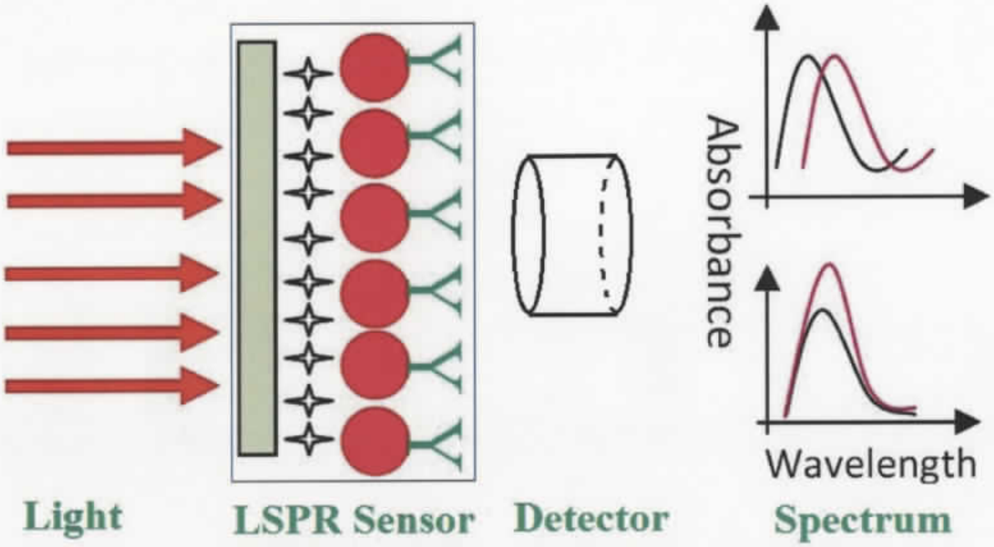

Figure 1- 12 Schematic illustration of the working principle of LSPR sensor. There are two detecting schemes, one as spectrum shift and another one as absorbance change, as shown in the left.

1.4 References:

1. Burda, C.; Chen, X. B.; Narayanan, R.; El-Sayed, M. A., *Chemical Reviews* **2005,** *105* (4), 1025-1102.

2. Daniel, M. C.; Astruc, D., *Chemical Reviews* **2004,** *104* (1), 293-346.

3. Hutter, E.; Fendler, J. H., *Advanced Materials* **2004,** *16* (19), 1685-1706.

4. Bauer, G.; Hassmann, J.; Walter, H.; Haglmuller, J.; Mayer, C.; Schalkhammer, T., *Nanotechnology* **2003,** *14* (12), 1289-1311.

5. Hao, E.; Schatz, G. C., *Journal of Chemical Physics* **2004,** *120* (1), 357-366.

6. Qin, L. D.; Zou, S. L.; Xue, C.; Atkinson, A.; Schatz, G. C.; Mirkin, C. A., *Proceedings of the National Academy of Sciences of the United States of America* **2006,** *103* (36), 13300-13303.

7. Aroca, R. F.; Alvarez-Puebla, R. A.; Pieczonka, N.; Sanchez-Cortez, S.; Garcia-Ramos, J. V., *Advances in Colloid and Interface Science* **2005,** *116* (1-3), 45-61.

8. Qin, L.; Zou, S.; Xue, C.; Atkinson, A.; Schatz, G. C.; Mirkin, C. A., *Proceedings of the National Academy of Sciences* **2006,** *103* (36), 13300-13303.

9. Moskovits, M., *Journal of Raman Spectroscopy* **2005,** *36* (6-7), 485-496.

10. Aroca, R., *Surface enhanced vibrational spectroscopy*. Wiley: Hoboken, NJ, 2006; p xxv, 233 p.

11. Goulet, P. J. G.; dos Santos, D. S.; Alvarez-Puebla, R. A.; Oliveira, O. N.; Aroca, R. F., *Langmuir* **2005,** *21* (12), 5576-5581.

12. Han, Y.; Sukhishvili, S.; Du, H.; Cefaloni, J.; Smolinsko, B., *Journal of Nanoscience and Nanotechnology* **2008,** *8* (11), 5791-5800.

13. Freeman, R. G.; Grabar, K. C.; Allison, K. J.; Bright, R. M.; Davis, J. A.; Guthrie, A. P.; Hommer, M. B.; Jackson, M. A.; Smith, P. C.; Walter, D. G.; Natan, M. J., *Science* **1995,** *267* (5204), 1629-1632.

14. Jiao, L. S.; Wang, Z. J.; Niu, L.; Shen, J.; You, T. Y.; Dong, S. J.; Ivaska, A., *Journal of Solid State Electrochemistry* **2006,** *10* (11), 886-893.

15. Joo, S. W.; Han, S. W.; Kim, K., *Langmuir* **2000,** *16* (12), 5391-5396.

16. Kudelski, A., *Vibrational Spectroscopy* **2003,** *33* (1-2), 197-204.

17. Barton, S. C.; Gallaway, J.; Atanassov, P., *Chemical Reviews* **2004,** *104* (10), 4867-4886.

18. Kim, J.; Jia, H. F.; Wang, P., *Biotechnology Advances* **2006,** *24* (3), 296-308.

19. Stoddart, P. R.; White, D. J., *Analytical and Bioanalytical Chemistry* **2009,** *394* (7), 1761-1774.

20. Beam, B. M.; Armstrong, N. R.; Mendes, S. B., *Analyst* **2009,** *134* (3), 454-459.

21. Polwart, E.; Keir, R. L.; Davidson, C. M.; Smith, W. E.; Sadler, D. A., *Applied Spectroscopy* **2000,** *54* (4), 522-527.

22. Nath, N.; Chilkoti, A., *Analytical Chemistry* **2002,** *74* (3), 504-509.

23. Englebienne, P., *Analyst* **1998,** *123* (7), 1599-1603.

24. Haes, A. J.; Chang, L.; Klein, W. L.; Van Duyne, R. P., *Journal of the American Chemical Society* **2005,** *127* (7), 2264-2271.

25. Willets, K. A.; Van Duyne, R. P., *Annual Review of Physical Chemistry* **2007,** *58*, 267-297.

26. Chen, H. J.; Kou, X. S.; Yang, Z.; Ni, W. H.; Wang, J. F., *Langmuir* **2008,** *24* (10), 5233-5237.

27. Anker, J. N.; Hall, W. P.; Lyandres, O.; Shah, N. C.; Zhao, J.; Van Duyne, R. P., *Nature Materials* **2008,** *7* (6), 442-453.

28. Endo, T.; Kerman, K.; Nagatani, N.; Hiepa, H. M.; Kim, D. K.; Yonezawa, Y.; Nakano, K.; Tamiya, E., *Analytical Chemistry* **2006,** *78* (18), 6465-6475.

29. Zhao, W.; Brook, M. A.; Li, Y. F., *ChemBioChem* **2008,** *9* (15), 2363-2371.

30. Zhao, W. A.; Ali, M. M.; Aguirre, S. D.; Brook, M. A.; Li, Y. F., *Analytical Chemistry* **2008,** *80* (22), 8431-8437.

31. Addison, C. J.; Brolo, A. G., *Langmuir* **2006,** *22* (21), 8696 -8702.

32. Raether, H., *Surface Plasmons on Smooth and Rough Surfaces and on Gratings*. Springer-Verlag: Berlin, 1986.

33. Brongersma, M. L.; Kik, P. G.; SpringerLink (Online service), Surface Plasmon Nanophotonics. In *Springer series in optical sciences,* [Online] Springer: Dordrecht, 2007. http://dx.doi.org/10.1007/978-1-4020-4333-8.

34. Barnes, W. L.; Dereux, A.; Ebbesen, T. W., *Nature* **2003,** *424* (6950), 824-830.

35. Freestone, I.; Meeks, N.; Sax, M.; Higgitt, C., *Gold Bulletin* **2007,** *40* (4), 270-277.

36. Link, S.; El-Sayed, M. A., *International Reviews in Physical Chemistry* **2000,** *19* (3), 409-453.

37. Link, S.; El-Sayed, M. A., *Journal of Physical Chemistry B* **1999,** *103* (40), 8410-8426.

38. Kelly, K. L.; Coronado, E.; Zhao, L. L.; Schatz, G. C., *Journal of Physical Chemistry B* **2003,** *107* (3), 668-677.

39. Noguez, C., *Journal of Physical Chemistry C* **2007,** *111* (10), 3806-3819.

40. Hao, E.; Li, S. Y.; Bailey, R. C.; Zou, S. L.; Schatz, G. C.; Hupp, J. T., *Journal of Physical Chemistry B* **2004,** *108* (4), 1224-1229.

41. Jung, L. S.; Campbell, C. T.; Chinowsky, T. M.; Mar, M. N.; Yee, S. S., *Langmuir* **1998,** *14* (19), 5636-5648.

42. Stewart, M. E.; Anderton, C. R.; Thompson, L. B.; Maria, J.; Gray, S. K.; Rogers, J. A.; Nuzzo, R. G., *Chemical Reviews* **2008,** *108* (2), 494-521.

43. Miller, M. M.; Lazarides, A. A., *Journal of Physical Chemistry B* **2005,** *109* (46), 21556-21565.

44. Kabashin, A. V.; Evans, P.; Pastkovsky, S.; Hendren, W.; Wurtz, G. A.; Atkinson, R.; Pollard, R.; Podolskiy, V. A.; Zayats, A. V., *Nature Materials* **2009,** *8* (11), 867-871.

45. Le Ru, E. C.; Etchegoin, P. G., *Principles of surface-enhanced Raman spectroscopy : and related plasmonic effects*. 1st ed.; Elsevier: Amsterdam ; Boston, 2009; p xxiii, 663.

46. Albrecht, M. G.; Creighton, J. A., *Journal of the American Chemical Society* **1977,** *99* (15), 5215-5217.

47. Fleischm.M; Hendra, P. J.; McQuilla.Aj, *Chemical Physics Letters* **1974,** *26* (2), 163-166.

48. Jeanmaire, D. L.; Vanduyne, R. P., *Journal of Electroanalytical Chemistry* **1977,** *84* (1), 1-20.

49. Osawa, M., Surface-enhanced infrared absorption. In *Near-Field Optics and Surface Plasmon Polaritons*, SPRINGER-VERLAG BERLIN: Berlin, 2001; Vol. 81, pp 163-187.

50. Ruan, C. M.; Wang, W.; Gu, B. H., *Analytical Chemistry* **2006,** *78* (10), 3379-3384.

51. Qian, X. M.; Nie, S. M., *Chemical Society Reviews* **2008,** *37* (5), 912-920.

52. Aroca, R. F.; Ross, D. J.; Domingo, C., *Applied Spectroscopy* **2004,** *58* (11), 324A-338A.

53. Enders, D.; Puccia, A., *Applied Physics Letters* **2006,** *88* (18).

54. Coe, J. V.; Williams, S. M.; Rodriguez, K. R.; Teeters-Kennedy, S.; Sudnitsyn, A.; Hrovat, F., *Analytical Chemistry* **2006,** *78* (5), 1384-1390.

55. Harris, D. C.; Bertonlucci, M. D., *Symmetry and spectroscopy: an introduction to vibrational and electronic spectroscopy*. Oxford Uninversity Press: New York, 1989; p 93.

56. Sanderson, A. C.; Brolo, A. G.; University of Victoria (B.C.). Dept. of Physics and Astronomy.; University of Victoria (B.C.). Surface-enhanced raman scattering from a modified silver electrode. 2007.

57. Long, D. A., *The Raman Effect: A Unified Treatment of the Theory of Raman Scattering by Molecules*. John Wiley & Sons Ltd: Baffins Lane, Chichester, 2002; p 584.

58. Petry, R.; Schmitt, M.; Popp, J., *Chemphyschem* **2003,** *4* (1), 14-30.

59. Le Ru, E. C.; Blackie, E.; Meyer, M.; Etchegoin, P. G., *Journal of Physical Chemistry C* **2007,** *111* (37), 13794-13803.

60. Kneipp, K.; Wang, Y.; Kneipp, H.; Perelman, L. T.; Itzkan, I.; Dasari, R.; Feld, M. S., *Physical Review Letters* **1997,** *78* (9), 1667-1670.

61. Delfino, I.; Bizzarri, A. R.; Cannistraro, S., *Chemical Physics* **2006,** *326* (2-3), 356-362.

62. Pieczonka, N. P. W.; Aroca, R. F., *Chemical Society Reviews* **2008,** *37* (5), 946-954.

63. dos Santos, D. P.; Andrade, G. F. S.; Temperini, M. L. A.; Brolo, A. G., *Journal of Physical Chemistry C* **2009,** *113* (41), 17737-17744.

64. Campion, A.; Kambhampati, P., *Chemical Society Reviews* **1998,** *27* (4), 241-250.

65. Brolo, A. G.; Irish, D. E.; Smith, B. D., *Journal of Molecular Structure* **1997,** *405* (1), 29-44.

66. Moskovits, M., Surface-enhanced Raman spectroscopy: a brief perspective. In *Surface-Enhanced Raman Scattering: Physics and Applications*, 2006; Vol. 103, pp 1-17.

67. Otto, A.; Futamata, M., Electronic mechanisms of SERS. In *Surface-Enhanced Raman Scattering: Physics and Applications*, 2006; Vol. 103, pp 147-182.

68. Baker, G. A.; Moore, D. S., *Analytical and Bioanalytical Chemistry* **2005,** *382* (8), 1751-1770.

69. Christy, A. A.; Ozaki, Y.; Gregoriou, V. G., *Modern Fourier Transform Infrared Spectroscopy*. 1 ed.; ELSEVIER: 2001; Vol. XXXV.

70. Zamlynny, V. Electrochemical and Spectroscopic Studies of Pyridine Surfactants at the Gold-Electrolyte Interface. University of Guelph, Ottawa, 2002.

71. Hartstein, A.; Kirtley, J. R.; Tsang, J. C., *Physical Review Letters* **1980,** *45* (3), 201-204.

72. Wu, D. Y.; Li, J. F.; Ren, B.; Tian, Z. Q., *Chemical Society Reviews* **2008,** *37* (5), 1025-1041.

73. Kerker, M., *Selected papers on surface-enhanced raman scattering*. SPIE Optical Engineering Press: Bellingham, Wash., USA, 1990; p xix, 696 p.

74. Zhu, Z. H.; Zhu, T.; Liu, Z. F., *Nanotechnology* **2004,** *15* (3), 357-364.

75. Ferrando, R.; Jellinek, J.; Johnston, R. L., *Chemical Reviews* **2008,** *108* (3), 845-910.

76. Alvarez-Puebla, R. A.; Ross, D. J.; Nazri, G. A.; Aroca, R. F., *Langmuir* **2005,** *21* (23), 10504-10508.

77. Cao, L. Y.; Diao, P.; Tong, L. M.; Zhu, T.; Liu, Z. F., *Chemphyschem* **2005,** *6* (5), 913-918.

78. Cui, Y.; Ren, B.; Yao, J. L.; Gu, R. A.; Tian, Z. Q., *Journal of Physical Chemistry B* **2006,** *110* (9), 4002-4006.

79. Freeman, R. G.; Hommer, M. B.; Grabar, K. C.; Jackson, M. A.; Natan, M. J., *Journal of Physical Chemistry* **1996,** *100* (2), 718-724.

80. Kumar, G. V. P.; Shruthi, S.; Vibha, B.; Reddy, B. A. A.; Kundu, T. K.; Narayana, C., *Journal of Physical Chemistry C* **2007,** *111* (11), 4388-4392.

81. Zhan, P.; Wang, Z. L.; Dong, H.; Sun, J.; Wu, J.; Wang, H. T.; Zhu, S. N.; Ming, N. B.; Zi, J., *Advanced Materials* **2006,** *18* (12), 1612-+.

82. Cui, Y.; Gu, R. A., *Chemical Journal of Chinese Universities-Chinese* **2005,** *26* (11), 2090-2092.

83. Ling, L.; Xu, M. M.; Gu, R. A.; Yao, J. L., *Acta Chimica Sinica* **2007,** *65* (9), 779-784.

84. Wang, H. H.; Liu, C. Y.; Wu, S. B.; Liu, N. W.; Peng, C. Y.; Chan, T. H.; Hsu, C. F.; Wang, J. K.; Wang, Y. L., *Advanced Materials* **2006,** *18* (4), 491-+.

85. Natan, M. J., *Faraday Discussions* **2006,** *132*, 321-328.

86. Henzie, J.; Lee, M. H.; Odom, T. W., *Nature Nanotechnology* **2007,** *2* (9), 549-554.

87. Kwak, E. S.; Henzie, J.; Chang, S. H.; Gray, S. K.; Schatz, G. C.; Odom, T. W., *Nano Letters* **2005,** *5* (10), 1963-1967.

88. Gordon, R.; Brolo, A. G.; McKinnon, A.; Rajora, A.; Leathem, B.; Kavanagh, K. L., *Physical Review Letters* **2004,** *92* (3).

89. Lesuffleur, A.; Kumar, L. K. S.; Brolo, A. G.; Kavanagh, K. L.; Gordon, R., *Journal of Physical Chemistry C* **2007,** *111* (6), 2347-2350.

90. Gordon, R.; Sinton, D.; Kavanagh, K. L.; Brolo, A. G., *Accounts of Chemical Research* **2008,** *41* (8), 1049-1057.

91. Anema, J. R.; Brolo, A. G.; Marthandam, P.; Gordon, R., *Journal of Physical Chemistry C* **2008,** *112* (44), 17051-17055.

92. Daniel, M.-C.; Astruc, D., *Chemical Reviews* **2004,** *104* (1), 293-346.

93. Schwartzberg, A. M.; Zhang, J. Z., *Journal of Physical Chemistry C* **2008,** *112* (28), 10323-10337.

94. Grabar, K. C.; Freeman, R. G.; Hommer, M. B.; Natan, M. J., *Analytical Chemistry* **1995,** *67* (4), 735-743.

95. Lu, X. M.; Rycenga, M.; Skrabalak, S. E.; Wiley, B.; Xia, Y. N., *Annual Review of Physical Chemistry* **2009,** *60*, 167-192.

96. Skrabalak, S. E.; Chen, J. Y.; Sun, Y. G.; Lu, X. M.; Au, L.; Cobley, C. M.; Xia, Y. N., *Accounts of Chemical Research* **2008,** *41* (12), 1587-1595.

97. Alvarez-Puebla, R. A.; Aroca, R. F., *Analytical Chemistry* **2009,** *81* (6), 2280-2285.

98. Barnickel, P.; Wokaun, A., *Molecular Physics* **1989,** *67* (6), 1355-1372.

99. Vo-Dinh, T., *Trac-Trends in Analytical Chemistry* **1998,** *17* (8-9), 557-582.

100. Shipway, A. N.; Katz, E.; Willner, I., *ChemPhysChem* **2000,** *1* (1), 18-52.

101. Aroca, R. F.; Goulet, P. J. G.; dos Santos, D. S.; Alvarez-Puebla, R. A.; Oliveira, O. N., *Analytical Chemistry* **2005,** *77* (2), 378-382.

102. Ko, H.; Singamaneni, S.; Tsukruk, V. V., *Small* **2008,** *4* (10), 1576-1599.

103. Binder, W. H., *Angewandte Chemie-International Edition* **2005,** *44* (33), 5172-5175.

104. Genov, D. A.; Sarychev, A. K.; Shalaev, V. M.; Wei, A., *Nano Letters* **2004,** *4* (1), 153-158.

105. Ko, H.; Tsukruk, V. V., *Small* **2008,** *4* (11), 1980-1984.

106. Qiu, T.; Wu, X. L.; Shen, J. C.; Chu, P. K., *Applied Physics Letters* **2006,** *89* (13).

107. Wang, H.; Kundu, J.; Halas, N. J., *Angewandte Chemie-International Edition* **2007,** *46* (47), 9040-9044.

108. Wei, A.; Kim, B.; Sadtler, B.; Tripp, S. L., *ChemPhysChem* **2001,** *2* (12), 743-+.

109. Lu, Y.; Liu, G. L.; Lee, L. P., *Nano Letters* **2005,** *5* (1), 5-9.

110. Zhao, J.; Jensen, L.; Sung, J. H.; Zou, S. L.; Schatz, G. C.; Van Duyne, R. P., *Journal of the American Chemical Society* **2007,** *129* (24), 7647-7656.

111. Malinsky, M. D.; Kelly, K. L.; Schatz, G. C.; Van Duyne, R. P., *Journal of the American Chemical Society* **2001,** *123* (7), 1471-1482.

112. Nusz, G. J.; Curry, A. C.; Marinakos, S. M.; Wax, A.; Chilkoti, A., *ACS Nano* **2009,** *3* (4), 795-806.

113. Eftekhari, F.; Escobedo, C.; Ferreira, J.; Duan, X. B.; Girotto, E. M.; Brolo, A. G.; Gordon, R.; Sinton, D., *Analytical Chemistry* **2009,** *81* (11), 4308-4311.

114. Sepulveda, B.; Angelome, P. C.; Lechuga, L. M.; Liz-Marzan, L. M., *Nano Today* **2009,** *4* (3), 244-251.

115. LaFratta, C. N.; Walt, D. R., *Chemical Reviews* **2008,** *108* (2), 614-637.

116. Elghanian, R.; Storhoff, J. J.; Mucic, R. C.; Letsinger, R. L.; Mirkin, C. A., *Science* **1997,** *277* (5329), 1078-1081.

117. Storhoff, J. J.; Lucas, A. D.; Garimella, V.; Bao, Y. P.; Muller, U. R., *Nature Biotechnology* **2004,** *22* (7), 883-887.

118. Li, H. X.; Rothberg, L., *Proceedings of the National Academy of Sciences of the United States of America* **2004,** *101* (39), 14036-14039.

119. Ling, J.; Li, Y. F.; Huang, C. Z., *Analytical Chemistry* **2009,** *81* (4), 1707-1714.

120. Wang, H., Brandl, D. W., Nordlander, P., Halas, N. J., *Accounts of Chemical Research* **2007**, 40. 53-62.

Chapter 2: Self-assembled Au Nanoparticles as Substrates for Surface-enhanced Vibrational Spectroscopy: Optimization and Electrochemical Stability

This chapter is published in the journal ***ChemPhysChem*** *(2008, 9 (13), 1899-1907).*

3-D nanostructured metallic substrates for enhanced vibrational spectroscopy were fabricated by self-assembly. Nanostructures consisting of 1 to 21 depositions of 13 nm-diameter Au nanoparticles (NPs) on Au films were prepared and characterized by AFM and UV-Vis reflection-absorption spectroscopy. Surface-enhanced polarization modulation infrared reflection-absorption spectroscopy (PM-IRRAS) was observed from Au NPs modified by the probe molecule 4-hydroxythiophenol (4-HTP). The limitation of this kind of substrate for surface-enhanced PM-IRRAS is discussed. Surface-enhanced Raman scattering (SERS) from the same probe molecule, 4-HTP, was also observed and the effect of the number of Au NPs depositions on the SERS efficiency was studied. The SERS signal from the probe molecule maximized after eleven Au NPs deposition and the absolute SERS intensities from different batches were reproducible within 20%. In situ electrochemical SERS measurements showed that these substrates were stable within the potential window between –800mV to +200mV (vs. Ag/AgCl/sat. Cl-).

2.1 Introduction

The analytical spectroscopic signal from species adsorbed on metallic nanostructures can be significantly enhanced relative to the signal from the same species in solution.[1-2] For instance, surface-enhanced Raman scattering (SERS) as high as 10^{14}-10^{15} times the normal Raman response have been reported for species located at the "hot spots" of nanostructured silver.[3] SERS and surface-enhanced infra-red absorption (SEIRA) spectroscopy are vibrational spectroscopy tools and the uniqueness of the vibrational signature makes it possible to identify target molecules.[2] The SERS technique is particularly attractive for label-free trace analysis, such as for the detection of high explosives, nerve stimulants agents, and environmental pollutants.[4]

It is currently widely accepted that there are mainly two kinds of contributions to the observed SERS[1, 4-5] and SEIRS:[6-7] the chemical contribution and the electromagnetic (EM) contribution. The charge transfer (CT) mechanism originates from resonant transitions involving the metal's Fermi level and the adsorbed molecule's frontier orbitals (in case of SERS).[5, 8] In electrochemical environment, this contribution can be tuned by adjusting the applied potential. The CT is thought to be a short range effect, which affects mainly the species in direct contact to the metal surface (in case of SERS). Localized surface Plasmon resonance (LSPR) can be directly excited on nanostructured noble metal surfaces using visible radiation, and these resonances are considered to provide the main contributions to the EM mechanism.[5-8] LSPR result in strong EM fields localized in certain regions of the nanostructured surface (for example, sharp tips and troughs between nanoprotrusions[9]) which accounts for most of the observed enhancement. The frequency of the LSPR resonance is tunable by the surface morphology.[10-18]

A variety of substrates that support SERS are being explored by various groups.[1, 4, 19] Typically, an ideal SERS substrate for analytical applications should be robust, easy to prepare and use, provide a large enhancement of the interference-free Raman signal of the analyte, and present a high degree of reproducibility.[4] Substrate development is also a high-active area in SEIRS research. Among the substrates developed specifically for SEIRS include vacuum deposited metal islands,[6] nano-rod arrays,[20] sub-wavelength holes,[21] and nanoparticles.[6-7, 22-27] Recently, a SEIRA enhancement factor of 2000 was achieved by "*in-situ*" tailoring of the size of the metallic nanofeatures.[24]

Metallic nanoparticles (NPs) are probably the most common type of substrate for SERS and SEIRA. They are easy to prepare (with numerous choices of sizes and shapes, which means tunable LSPR), and can be simply characterized by UV-Vis spectroscopy. Metallic NPs aggregate in the presence of salts leading to large enhancement factor.[4] However, the morphology of the aggregates and the reproducibility of the enhanced signal[19] are strongly affected by the experimental conditions, such as temperature, ionic strength, pH and even the presence of adsorbates.[4]

Au and Ag NPs can be self-assembled into monolayer or multilayer 3D-structures on a flat surface.[15, 28] This kind of approach for SERS substrate preparation has recently attracted much attention.[11, 28-34] The self-assembled structures are fabricated by alternate dipping the initially flat surface into solutions containing a bifunctional cross-linker and the NPs. The resultant morphology can be tuned by the desired number of NPs depositions, tailoring the substrate performance for SERS. The sizes of the linker molecules and of the NPs are adjustable, providing more dimensions to tune the resonances. It also has been shown that it is possible to use this approach to fabricate a specific substrate that matches the excitation condition (laser wavelength) of the SERS experiment, leading to optimized enhancement conditions.[29] However, the self-assembled nanostructures multilayer approach, describe above, have not yet been explored to develop substrate for SEIRS.

Metallic NPs-modified electrodes also provide advantages over the traditional "bulk" electrodes used in electrochemistry. [35-37] For example, NPs usually demonstrate extra catalytic activities, even for those metals normally recognized as inert, such as Au.[37] Furthermore, NPs-modified electrode can provide higher signal-to-noise ratio for electrochemical currents measurements as a result of their large effective surface area.[36] In fact, theoretical calculations reveal that an electrode composed of 10 nm NPs in an array format can enhance the peak current in two orders of magnitude compared to a bulk electrode.[35]

All these advantages have attracted several groups to the development of metallic NPs- modified electrodes for both electrocatalysis and *in situ* SERS.[14, 38-40] These activities have even expanded towards non-traditional SERS-active metals. For instance, Gomez et al.[14] reported that Pt NPs deposited on a flat conducting electrode surface provided a significantly larger SERS enhancement factor than an electrochemically roughened Pt electrode. Guo et al.[40] found that 3 nm Fe NPs made by microemulsion also demonstrated remarkable SERS activity when coated onto a flat silver electrode. Potential dependent-SERS spectra of pyridine were recorded from the Fe NPs with an enhancement factor of two to three orders of magnitude.[40] Despite all this activity in the field, there is no report yet on the application of 3D self-assembly using more common NPs for surface-enhancement, such as gold, on smooth electrode surfaces for SEIRA and for *in situ* electrochemical SERS applications. These structures should provide high SERS signal enhancement,[29-30] as well as the good electrical conductivity required for electrocatalysis.[28, 33-34]

Previously, we demonstrated that a step-wise deposition of Au NPs on glass produced a highly sensitive SERS substrate.[29] It was found that, at optimum conditions, the SERS intensity could be at least ten times stronger than that of a monolayer of Au NPs. More importantly, by changing the number of depositions we were able to tune the surface morphology to match the laser wavelength, producing an optimized SERS substrate for a given condition for surface plasmon (SP) excitation. In this work, we fabricated similar structures on a gold thin film instead. The conditions for optimum surface-vibrational spectroscopy were evaluated and the performance of the substrate for *in situ* electrochemical SERS measurements was probed.

2.2 Results and Discussion

2.2.1 Characterization of the substrates by atomic force microscope (AFM) and UV-Vis reflection-absorption spectroscopy

Figure 2-1 presents selected AFM images of the substrates prepared with different numbers of Au NPs deposition. The AFM pictures indicate that both the surface roughness and the average size of the features increased with the number of depositions. The size of the features after one Au NPs deposition was around 10 nm (Fig. 2-1a) which is consistent with the diameter of the NPs used. Fig. 2-1b shows that a large number of aggregates were formed after nine NPs depositions. In this case, the average height was about 50nm, but features as large as 100 nm could be found when a large area of the substrate (100 μm x 100 μm) was imaged (data not shown).

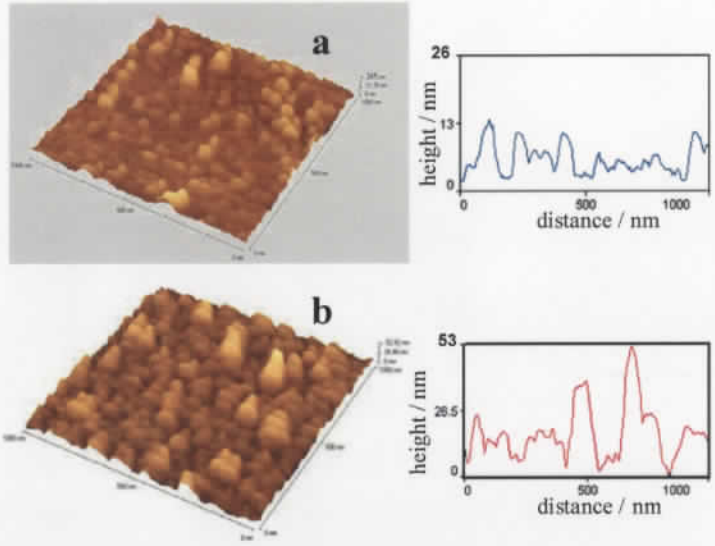

Figure 2- 1 Topographic and representative line-scan AFM images of the Au NPs modified substrates (a) one Au NP deposition; (b) nine Au NPs depositions.

Figure 2-2 shows the UV-Vis reflection-absorption spectra from substrates with different numbers of Au NPs deposition. The UV-Vis spectrum after one Au NPs deposition presents an absorption maximum at around 524 nm, which is very close to the observed from the NPs in water (520 nm). The small red-shift relative to the absorption of Au NPs in water and the peak width suggest a small degree of aggregation for the monolayer of immobilized NPs, in agreement with the AFM data from Fig. 2-1. The 524 nm-peak broadened and shifted to longer wavelength as the number of Au NPs deposition increased. A similar trend was observed for Au NPs deposited on glass. [29] These changes were accompanied by an increase in absorption in the region between 600 and 800 nm. All these are evidence of increasing aggregation with the number of Au NPs deposition. The total absorbance, given by the integrated area of the absorption spectrum, also increased. However, the changes are not as pronounced after 9 Au NPs depositions, which is similar to our observations in a previous publication. [29]

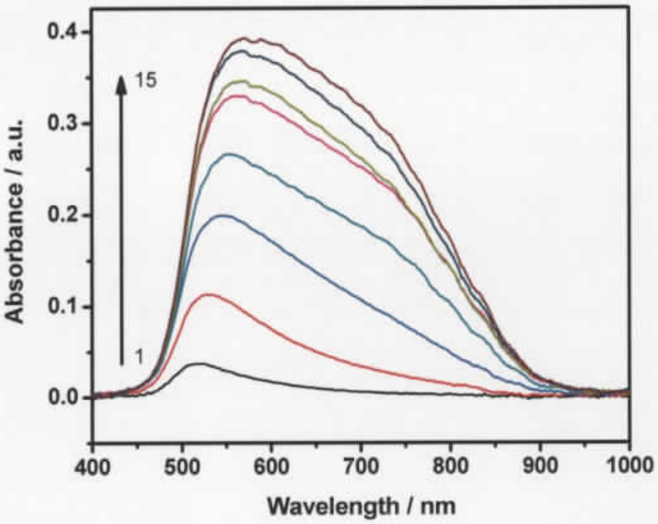

Figure 2- 2 UV-Vis reflection-absorption spectra for the substrates with different numbers of Au NPs deposition on Au slides. The spectra were calculated using: Absorbance = -log(R_{NP}/R_{bareAu}), where R_{NP} is the reflectivity from the Au slide modified with Au NPs (the average from different positions on the same slide is presented); and R_{bareAu} is the reflectivity from the Au slide without Au NPs. The detection system was equipped with a filter that cuts off at 450 nm.

A comparison between the results presented in Fig. 2-2 (for Au NPs deposited on Au films) with our previous results (for Au NPs deposited on glass[29]) shows a few differences in the shape of the absorption profiles and their evolution with the number of Au NPs deposition. These differences can be attributed to the differences in the experimental procedures, surface chemistry and optical properties of the underlying substrate (glass vs. gold film).

2.2.2 Application of the substrates to enhanced vibrational spectroscopy

Substrate optimization and application in surface-enhanced PM-IRRAS spectroscopy

Representative PM-IRRAS spectra of the Au-NPs assembly are shown in Figure 2-3, and they contain several vibrational features that can be readily assigned to the linker molecule (PDT) used to immobilize the Au NPs to the gold electrode (see scheme 1). The main vibrational bands in Figure 2-3 at 1419, 1323, 1288, and 1234 cm^{-1} have been previously assigned to the CH_2 bending/scissoring, the CH_2 wagging, the CH_2 twisting and the CH_2 twisting/wagging modes of PDT, respectively.[41] The complete assignment has been confirmed by our own ab initio calculation (DFT rb3lyp/6-311^{++}g(3df,3pd)). It should be pointed out that PDT presents three conformers, and the dominant conformation of the adsorbed molecule may be different than PDT in solution.[41-42]

In Fig. 2-3c, the spectrum with zero Au NPs deposition corresponds to the flat gold surface modified with a monolayer of PDT (in the absence of NPs). In this case, the IR features are weak and the band due to the CH_2 bending-mode (~1419 cm^{-1}) is missing. The lack of band due to the CH_2 bending is an indication that only one thiol end of the PDT is directly adsorbed to the gold surface as pointed out by Joo et al. [42] When only one of the thiols of the PDT binds to the surface, leaving the main chain almost perpendicular to the gold surface, the changes in dipole momentum due to the CH_2 bending would be parallel to the surface. According to the surface selection rules, only vibrational modes with transition dipole components perpendicular to the metallic surface contribute to the IR intensity.[43] Hence, this result indicates that an organized self assembled monolayer (SAM) of PDT was formed.

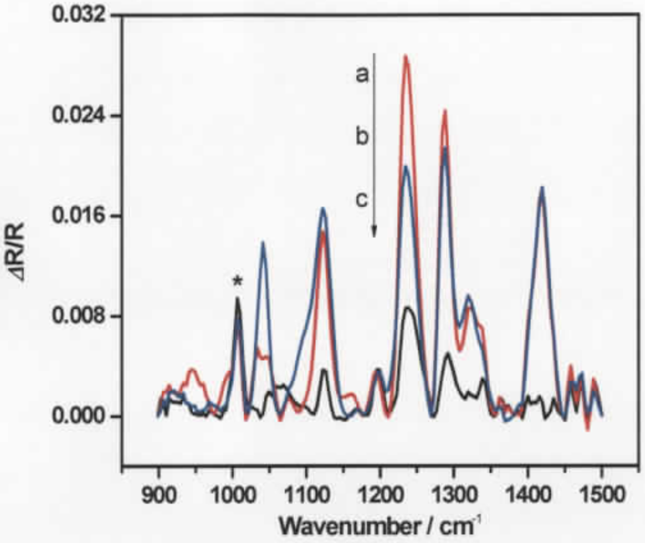

Figure 2- 3 PM-IRRAS spectra: a) one deposition of Au NPs; b) two depositions of Au NPs; c) zero deposition of Au NPs - monolayer of PDT on a flat gold substrate. All spectra were background corrected. The peak at 1008 cm^{-1} (marked with an asterisk) is an artefact from the instrument. Also note that the amount of adsorbed PDT in *a)* and *c)* are the same, and it is smaller than the amount of PDT adsorbed in *b)* (see text and scheme 1).

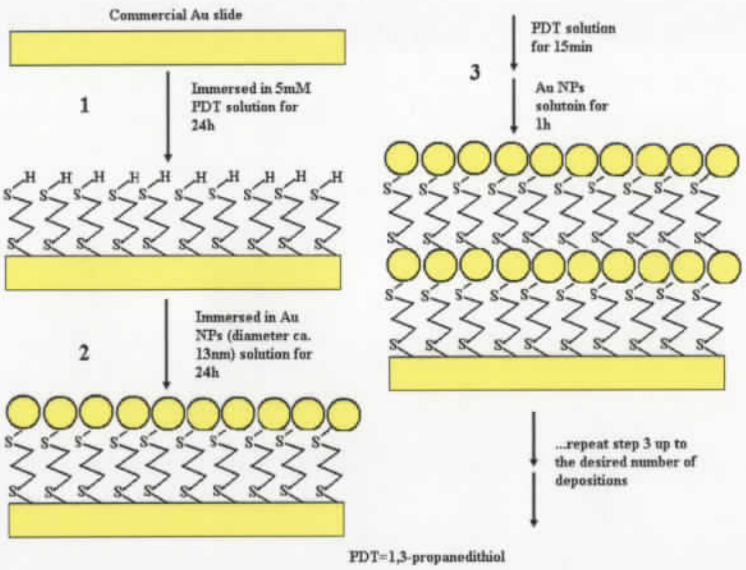

Scheme 2- 1 Schematic representation of the procedure for Au NPs deposition on a gold thin film. This diagram is not to scale. Notice that the amount of PDT before and after step 2 is the same.

Figure 2-3 also shows a significant increase in the IR absorption after the PDT monolayer was covered with a layer of Au NPs. Notice that the amount of PDT on a flat Au surface (a monolayer) was the same before and after the Au NPs deposition (because the Au NPs are deposited on top of the PDT monolayer – see scheme 2-1). However, the IR intensity of the latter was about 4 times larger at ~1234 cm^{-1}, as shown in Fig. 2-3. It is well known that Au NPs can be used as substrate for SEIRS measurements.[24-26, 44] Therefore, the increase in the IR absorption relative to the smooth surface is attributed to the SEIRS effect. However, as it can be seen in Fig. 2-3, the IR absorption at ~1234 cm^{-1} actually decreased with additional NPs deposition (although after the first layer of Au NPs, the amount PDT increases with the number of Au NPs deposition – see scheme 2-1). This effect is better illustrated in Figure 2-4 which shows the dependence of the IR absorption of all PDT bands from 1000 to 1500 cm^{-1} region vs. the number of Au NPs depositions. It is clear from Fig. 2-4 that after five Au NPs deposition, the intensities of the different bands were comparable to the observed from a smooth gold surface modified with a PDT monolayer. These observations can be rationalized considering the operation principle of the PM-IRRAS technique. In PM-IRRAS, the incident light is modulated between *p*- and *s*- linear polarizations and the surface is probed by reflection. According to the surface selection rules for IR spectroscopy in external reflection configuration, the *s*-polarization is not absorbed by the surface species on a highly reflective metal, while *p*-polarization incident light is absorbed. Therefore, the difference between the IR reflection-absorption from both polarizations eliminates the background, providing an IR absorption related only to the surface species. However, as the number of Au-NPs deposition increased, the substrate surface become rougher. Rough structures are depolarizing (i.e. have a tendency to scramble polarized fields),[45-46] and in turn decrease the response towards the difference between *s*- and *p*- polarized incident light.

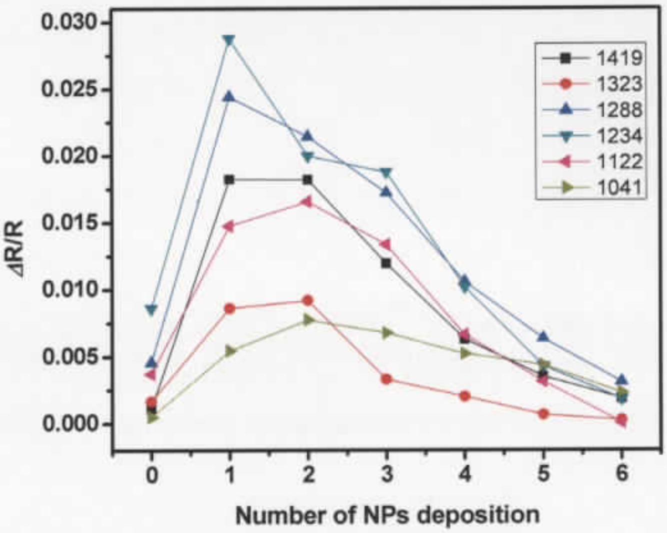

Figure 2- 4 Dependence of the surface IR intensities of PDT bands on the number of Au NPs deposition.

Figures 2-3 and 2-4 showed that the maximum surface-enhanced PM-IRRAS for this class of substrates (Au NPs immobilized on a flat gold film using a dithiol linker) is obtained within the first few layers of Au NPs deposition. The relative intensities of the IR absorption bands also changed with the number of Au-NPs deposition. For instance, the 1234 cm^{-1}-band was almost twice as large as the 1122 cm^{-1}-band after the deposition of a monolayer of Au NPs; however, the ratio between these two bands was closer to one after two Au NPs depositions (Figure 2-3). These changes in relative intensities are explained by considering the average orientation of PDT. After adsorption, the PDT species covering the NPs are oriented randomly relative to the underlying gold surface. Therefore, the changes in relative intensities can be attributed to an increased distribution of orientations of PDT with the addition of Au NPs. Notice that the amount of adsorbed PDT increased linearly after the deposition of the second layer of Au NPs (see scheme 2-1).

Considering the results from Figs. 2-3 and 2-4, we concluded that the substrate prepared with just one Au NPs deposition yielded a reasonable enhancement and decided to use it for the surface-enhanced IR absorption investigation of a probe molecule (4-HTP). Moreover, since the PDT links the Au NPs to the Au surface, the remaining area of the NPs not in contact with the surface is free of PDT and may readily interact with the probe molecule (see scheme 2-1), when the substrate with just one NP deposition is used.

Figure 2-5 shows the surface-enhanced IR spectra of 4-HTP adsorbed on the optimized substrate (Fig. 2-5a). The spectra of a monolayer of 4-HTP adsorbed on a smooth Au surface (Fig. 2-5b) and from the substrate in the absence of 4-HTP (Fig. 2-5c) are also shown. A comparison between Figs. 2-5a and 2-5b shows that the vibrational bands of the probe molecule were enhanced in presence of Au NPs. It is believed that surface area increase can also contribute to the observed SEIRS signal.[6] Using AFM, it was found that the surface area after 1 Au NPs deposition was typically less than 1.2 times of the value for the smooth gold surface. Electrochemical measurements, using a reversible redox pair ($[Fe(CN)_6]^{3-}$½$[Fe(CN)_6]^{4-}$), didn't show an increase in the electrochemical surface area after the first Au NPs deposition (data not shown). These findings were consistent with the results reported by Sivanesan et al,[47] where similar electrochemical experiment was performed for Au NPs self-assembly onto 1,6-hexanedithiol SAM. Meanwhile, the enhancement factor for 4-HTP (about 4 times relative to the smooth surface) is about the same as of PDT, where the role of the surface area was absent, since the amount of PDT did not change after the NP deposition. Thus, the increase in IR absorption for HTP adsorbed on Au NPs (Fig. 2-5a) relative to HTP adsorbed on the smooth surface (Fig. 2-5b) is assigned mainly to a surface-enhancement effect. On the other hand, we should point out that the surface enhancement factor observed here (about 4) is smaller than the values reported by other authors.[6, 24]

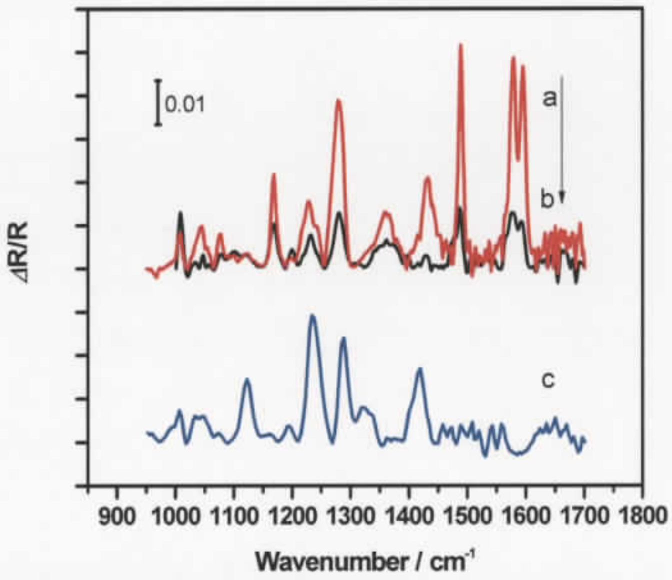

Figure 2- 5 PM-IRRAS spectra of a) 4-HTP on one deposition of Au NPs modified slide; b) 4-HTP on bare Au slide; c) one deposition of Au NPs modified slide in the absence of HTP (SEIRS signal from the PDT). All spectra were background corrected.

It can also be seen in Fig. 2-5 that absorptions from the linker PDT (shown in Fig. 2-5c) interfere with the final spectrum of 4-HTP on Au NPs modified substrate, since PDT and 4-HTP both have absorption bands around 1230, 1280, and 1420 cm^{-1}. In conclusion, although some vibrational bands from 4-HTP can be uniquely assigned, the interference from the linker is significant in this particular case. This problem severely limits the applicability of self-assembled Au NPs using linkers in surface-enhanced IR. Moreover the enhancement factor obtained by this substrate was only at the lower end of that reported by other groups.[6] Therefore, other approaches for Au NPs immobilization, which do not include organic linkers, seem to be more suitable for SEIRS.[24-26]

Substrate optimization for SERS

4-HTP was also used as a probe to evaluate the SERS efficiency of the substrates. Figure 2-6 shows the SERS spectra of substrates prepared with different numbers of Au NPs deposition with and without the SERS probe (4-HTP). The spectra in Fig. 2-6 were baseline corrected for a fluorescence-like background[48] that was observed in all experiments. The background increased with the deposition of NPs. The main features in the SERS of 4-HTP agrees well with the report by Lee et al.[49] There are two important points that can be observed from Fig. 2-6: Firstly, the SERS bands due to the linker (PDT) are present even in the absence of the 4-HTP. This SERS background, however, is much weaker than the signal from the probe molecule. The SERS bands of PDT can be readily identified as weak features in the SERS spectra containing 4-HTP, as illustrated in Fig. 2-6d. Secondly, the magnitude of the SERS signal (from both the background linker and the probe) increased with the number of Au NP depositions. This trend is further illustrated in Fig. 2-7, where a plot of the SERS signal from the ring breathing mode of 4-HTP against the number of Au NPs deposition is shown. The SERS intensity increased with the number of NPs deposition, reaching a maximum value around eleven Au NPs depositions. The results from Fig. 2-7 were not corrected for surface area variations. This procedure is justified by our surface area determinations using two independent techniques, AFM and electrochemistry. AFM showed an average increase in surface area of 20~30% relative to the smooth surface only after 9 Au NPs depositions. The relatively small increase in surface area with the number of Au NPs deposition is consistent with our previous work[50]. The 20% variation in the electrochemical surface area is actually within the uncertainty of SERS measurement.[51] Hu et al[13] and Yun et al[52] also reported SERS intensity dependence with the morphology of the metallic nanostructure without taking into consideration the surface area, which was also assumed to have a minor effect compared to the SP contribution to the enhancement of the Raman signal.[53]

Previously, we investigated the relationship between the SERS signal and the number of Au NPs depositions on a glass substrate.[29] It was found that the maximum SERS signal was dependent on the excitation wavelength, since different conditions for optimized surface plasmon resonance were encountered for distinct morphologies. An optimized SERS substrate for 632.8 nm excitation (He-Ne) was found after nine Au NPs depositions on glass.[29] On the other hand, the maximum in Fig. 2-7 occurred after 11 Au NPs depositions; the SERS signal decreased by roughly 30% and remained stable (within the uncertainty of the SERS measurements) after the maximum. We attribute the discrepancy with our previous report to the differences in electromagnetic field distribution around the nanofeatures for Au NPs deposited in either glass or a flat gold film. These may include further contributions from additional plasmon hybridization, which is expected from the interaction between the metallic NPs with the metallic film.[54] Another factor is the structure of the linker used to build the first layer of Au NPs. When a gold film is used, the Au NPs are deposited on a monolayer of PDT. On the other hand, the glass surface was modified by 3-(mercaptopropyl) trimethoxysilane to allow the binding with Au NPs. Comparing the AFM results from Fig. 2-1 with our former report[29], it is found that, although the heights of the features were similar for the same number of Au NPs deposition, the line scan shows that the features for Au NPs deposited on glass slide were somehow sharper, and the bumps were more isolated. These factors should significantly alter the conditions for SP excitation in these substrates, leading to differences in the trends with the number of Au NPs depositions.

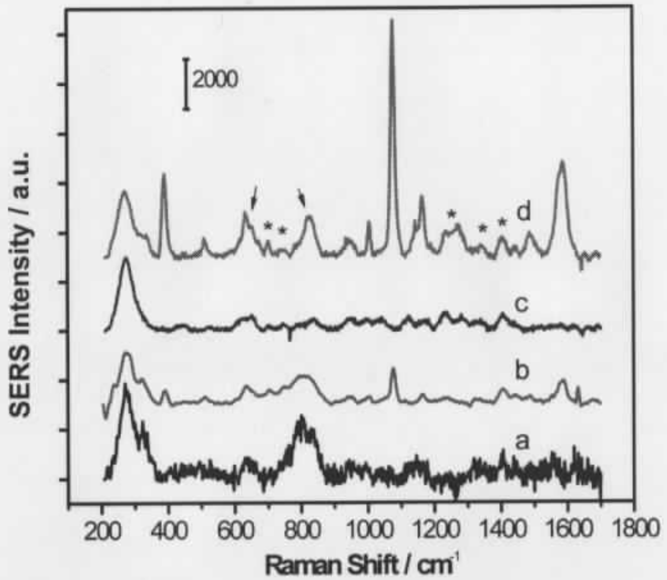

Figure 2- 6 SERS spectra from Au NPs-modified substrates in the absence and presence of 4-HTP. a). SERS spectra from one deposition of Au NPs (without 4-HTP); b). 4-HTP adsorbed on one deposition of Au NPs; c). SERS spectra from nine depositions of Au NPs (without 4-HTP); d). 4-HTP adsorbed on nine depositions of Au NPs. Spectra a and b were multiplied by a factor of 10. All spectra were baseline corrected and they are an average of 4 measurements on different regions on the same slide. Asterisks indicate the PDT bands. Arrows indicate bands with contribution from both PDT and 4-HTP.

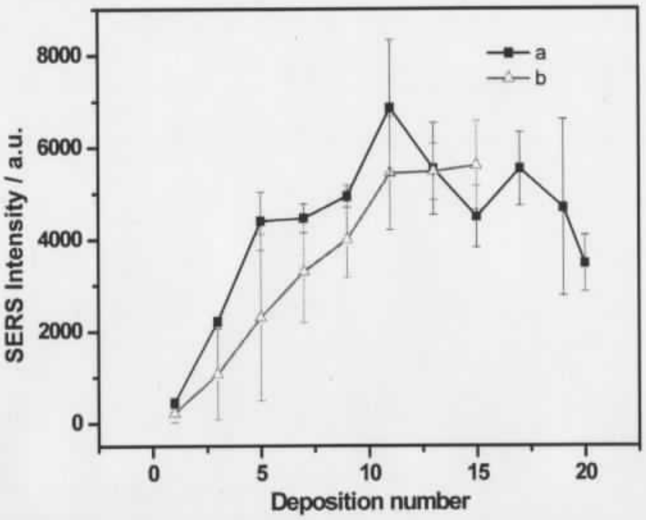

Figure 2- 7 SERS intensity of 4-HTP band at 1078 cm^{-1} versus the number of Au NPs deposition. a) Averages from a single batch preparation, and the error bars are the results of 4 measurements on the same slide (different spots). b) Averages from 3 different batches preparations.

The two curves in Fig. 2-7 are for averages calculated from SERS measurements realized in different spots of the same slides (Fig. 2-7a) and averages obtained from three different batches (Fig. 2-7b). The calculated percent relative standard deviation (RSD%) of the SERS intensities measured at different positions on a single slide ranged between 20% to 40%, which is within the normal spatial variability encountered in conventional random SERS substrates.[51] The spatial variability, measured as RSD%, decreased with the increasing number of Au NPs depositions. Furthermore, the variability of the SERS signal among batches (RSD%) was less than 20% after nine Au NPs depositions. These results imply that the variability in the SERS signal (both the spatial variability within a slide and the sample to sample variability) is within 20% after nine Au NPs depositions;

in other words, the variability of the SERS signal decreased with the number of NPs deposition. This is an important finding, since the reproducibility of the SERS signal is generally a concern that precludes the widespread application of the SERS technique in analytical problems. Another important aspect investigated was the long term stability of the substrates. No deterioration was found in the SERS performance even for three-month old substrates that were stored in the dark.

2.2.3 Application of the substrates for in situ electrochemical SERS

Another objective of this work was to use this class of substrates for *in situ* electrochemical SERS measurement. The Au NPs were immobilized using a thiol linker. The Au-S bonds can be electrochemically dissociated; therefore, the electrochemical stability of the substrate needs to be evaluated prior to the introduction of a SERS probe. Moreover, Fig. 2-6 shows that the SERS signal of the linker is always present as weak features in the SERS spectrum. These features, however, may interfere with the ones from the species of interest. It is well known that both position and intensities of the SERS bands can be potential-dependent, hence, a detailed study of the SERS response of the substrate in the absence of a SERS probe was carried out.

In situ SERS of the substrates without a probe molecule

Figures 2-8 and 2-9 show the results of the electrochemical stability tests in experiments without any SERS probe. The insets in Figures 2-8 and 2-9 present the raw SERS spectra of the substrate at different potentials. The background fluorescence and the vibrational bands of the PDT can be readily seen in the insets. Fig. 2-8 corresponds to SERS spectra obtained after each potential was stepped towards negative values from a starting potential of 0 V.

In order to better illustrate the changes in the SERS bands, all spectra were divided by the initial spectrum (0V). This spectrum ratio was calculated for each potential using the raw SERS data (without baseline correction to eliminate the fluorescence) and the results are plotted in Fig. 2-8. The ratios were close to 1 at all frequencies in the potential window between 0 and –800mV, indicating that no significant change in either peak position or intensity was observed in that range. Even the fluorescence background didn't significantly change. When the applied potential reached –900 mV, a few changes, represented by arrows in Fig. 2-8, were found in the electrochemical SERS spectra. New SERS bands growing at around 270, 600-700, and 1409 cm^{-1} were evident from the spectrum ratio at -900 mV and they were accompanied by an increase in the florescence background. These features (new vibrational bands and increased fluorescence background) became more evident as the potential was moved towards more negative potential values than -900 mV (Fig. 2-8). The changes observed at –900mV are attributed to the electroactivity of PDT at potentials more negative than -800 mV, since the desorption of alkanethiol from gold usually happens in the potential region between -800mV[55] and -1100mV[56] versus Ag/AgCl. Therefore, we conclude that -800 mV is the limit in the negative range where the substrate is electrochemically inert and can be used for *in situ* SERS.

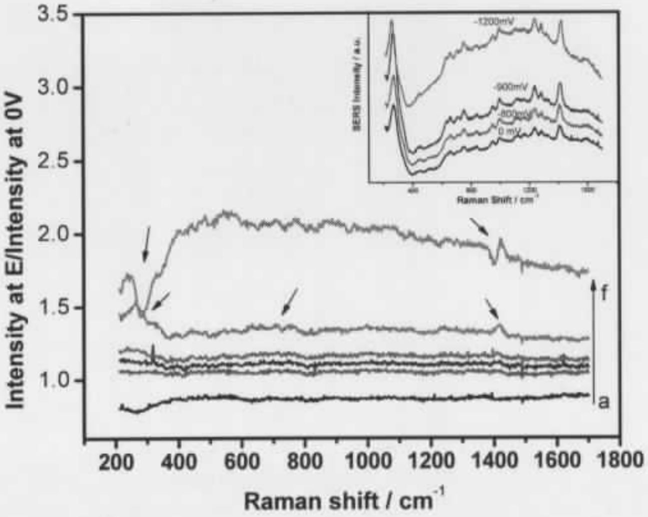

Figure 2- 8 *In situ* SERS of the substrate. Applied potential from 0 mV to -1200 mV (vs. Ag/AgCl). Acquisition time, 180s. Electrolyte, 0.1M KCl. Ratio of the SERS spectrum at E = (a) -200mV, (b) -400mV, (c) -600mV, (d) -800mV, (e) -900mV, (f) -1200mV over that of E=0 mV. Arrows emphasize the spectral changes. Inset shows the original spectra (raw data).

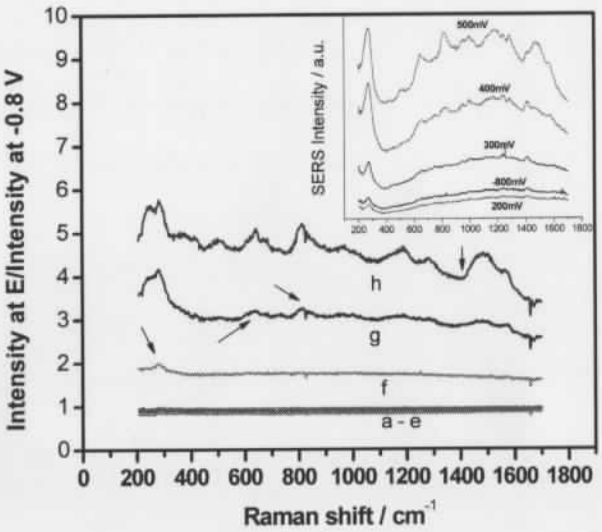

Figure 2- 9 *In situ* SERS of the substrate. Applied potential from -800 mV to +500 mV (vs. Ag/AgCl). Acquisition time, 180s. Electrolyte, 0.1M KCl. Ratio of the SERS spectrum at E = (a) -600mV, (b) -400mV, (c) -200mV, (d) 0 mV, (e) +200 mV, (f) +300 mV, (g) +400 mV and (h) +500 mV over that of E=-800 mV. The ratios (a) through (e) basically overlap. Arrows emphasize some spectral changes. Inset shows the original spectra (raw data).

Similarly, *in situ* SERS tests were performed in the positive potential range. In this case, the starting potential was -800 mV and the normalized SERS spectra were calculated using the spectrum at this potential as reference. The raw spectra (inset) and the ratios can be found in Fig. 2-9. The ratios were again constant in the potential range between –800 mV to +200 mV, but significant changes were observed after that positive potential limit. It is also worth noting that after a full run beyond +200 mV, the original

SERS signal decreased and could not be recovered by stepping the potential back to values more negative than +200 mV. This indicates that irreversible structure changes take place after the limit of +200 mV.

The results from Figs. 2-8 and 2-9 indicate that the substrate is not stable at potentials more negative than -800 mV and more positive than +200 mV. The SERS features of the background do not change significantly in the potential range between –800 mV to +200 mV. This implies that the substrates can be used for *in situ* SERS within that range, and that the potential-independent SERS signal from the interference (linker) could be subtracted.

In situ SERS of the substrates in the presence of 4-HTP

Figure 2-10 presents the *in situ* SERS spectra of the probe molecule,4-HTP, on a Au NPs-modified surface at different applied potentials (within the potential range of the substrate stability determined in the previous section). The main features of 4-HTP can be readily identified at around 392, 636, 818, 1008, 1080, 1164 and 1584 cm^{-1}, corresponding to the 7a, 12, 6a, 18a, 1, 9a and 8 (8a and 8b are mixed) modes, respectively, in terms of the Wilson's notation.[49] Bands attributed to PDT are indicated by asterisks. The SERS signal from PDT is weak and provides a small interference. More importantly, the signal from PDT does not change with potential. The inset in Fig. 2-10 shows a plot of the SERS intensity of the breathing mode of 4-HTP (1080 cm^{-1}) versus the applied potential. A maximum SERS signal was observed at around -600 mV. A decrease of SERS signal at more negative potential is expected, since the desorption of 4-HTP will happen as seen in cyclic voltammetric experiments involving thiols. The measurement of the electrochemical SERS trend of 4-HTP from the self-assembled substrate was possible. Hence, this substrate can be used in electrochemical SERS measurements provide that the experiments are realized within the potential range of substrate stability and that the interferences from the PDT bands are recognized. The self-assembled substrates suggested here present better spatial and sample-to-sample reproducibility of the SERS spectra than the more conventional electrochemically-roughened Au electrode. This is an important advantage of this substrate that could be further explored for the *in situ* investigation of electrocatalytic process from nanostructured gold surfaces.

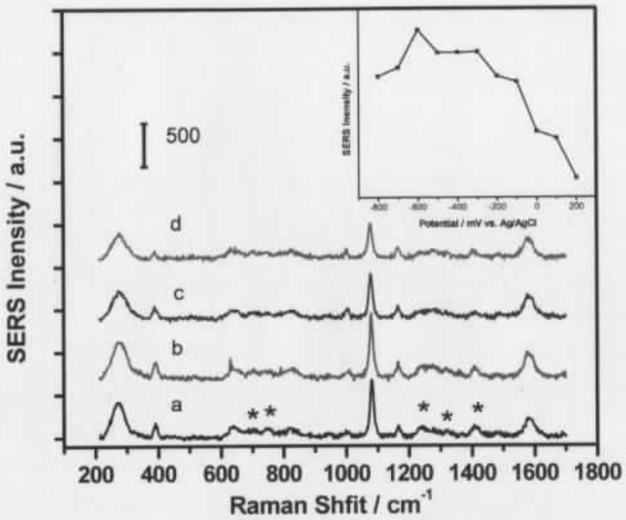

Figure 2- 10 *In-situ* SERS response of 4-HTP. a. -800 mV; b, -400 mV; c, 0 mV; d, 200mV vs. Ag/AgCl. Electrolyte, 0.1 M KCl. Asterisks indicate the PDT bands (interference). Inset shows the change of SERS intensity of 4-HTP at 1080 cm^{-1} upon applying potential. Asterisks on spectrum "a" indicates the position of some of the PDT bands.

2.3 Conclusion

3-D nanostructured substrates were fabricated by the deposition of Au NPs on Au slides, and these substrates were used for surface-enhanced vibrational spectroscopy. The substrates were prepared by immersing the slide into a PDT solution followed by incubation on Au NPs solution, and this procedure was repeated until the desired number of Au NPs deposition was achieved. A substrate with only one Au NPs deposition provided the best enhancement for the probe molecule 4-HTP in surface-enhanced PM-

IRRAS measurements. However, the linker PDT introduced some significant spectral interferences reducing the applicability of this substrate in IR measurements. It was found that substrates made by eleven Au NPs deposition yielded the best SERS of the probe molecule HTP for the 632.8 nm excitation. More importantly, the substrates with more than 9 Au NPs depositions presented a good spatial and batch-to-batch reproducibility (% RSD is lower than 20%). In situ SERS measurements showed that these substrates are stable in the potential window from –800mV to +200mV versus Ag/AgCl. In this region, SERS spectral interferences from the linker (PDT) didn't change with the applied potential and was easily identified as weak features in the spectra. In situ SERS measurement of the probe molecule, 4-HTP, was obtained within the potential window of electrochemical stability of the substrate. The results discussed here also provide a baseline for further application of this immobilization strategy for the fabrication of electrodes and substrates for high-sensitive, SERS-based sensors.

2.4 Experimental Section

Chemicals: Unless otherwise mentioned, ACS grade chemicals were used. $HAuCl_4$, sodium citrate dihydrate, 1,3-propanedithiol (PDT), and 4-hydroxythiophenol (4-HTP) were obtained from Sigma-Aldrich. HPLC grade methanol was obtained from Caledon Laboratories Ltd. Gold slides (100 nm thick Au deposited on glass – a 5 nm Cr layer is used to help the adhesion of the gold to the glass) were obtained from Evaporated Metal Films Inc. Ultrapure water with a resistivity of 18.2 MΩ cm (from Barnstead NANOpure Diamond water purification system) was used throughout the experiments.

NPs synthesis: The glassware was cleaned by soaking into a hot sulphuric acid bath overnight. After that, it was rinsed thoroughly with ultrapure water. The synthesis of Au NPs is described in the literature.[57] Briefly, $HAuCl_4$ solution (1 mM, 500 mL) was brought to a rolling boil with stirring. Then, sodium citrate solution (38.8 mM, 50 mL) was added and the heating and stirring were kept for 10 min. After that, the heating was stopped and the stirring was kept for additional 15 min to finish the reaction. The product was a wine-red color solution. The as-prepared Au NPs solution was stored in an amber bottle in a fridge at 4 C.

Procedure for Au NP deposition: The commercial Au slides were cleaned in oxygen plasma for 15min and then rinsed with methanol. The procedure for NPs deposition, represented in scheme 1, was as following: Firstly, a gold slide was soaked into PDT methanolic solution (5mM) for 24h. A self-assembled monolayer (SAM) of PDT was spontaneously formed on the gold surface. The slide modified with the PDT SAM was removed, rinsed with excess amount of methanol and water, and then incubated in a Au NPs solution for another 24h. After that, the slide was removed from the solution, dried with N_2, and rinsed with water. The resulting slide contained a monolayer of Au NPs. Subsequent Au NPs depositions were accomplished by repeating the following steps: rinsing the slide containing immobilized NPs with methanol and immersing it into PDT solution (5mM) for 15min to get the PDT self assembled onto the Au NPs surface. The substrate was then rinsed with methanol and water and immersed into Au NPs solution for 1h to deposit Au NPs. After the NPs deposition, the slide was dried with N_2 and rinsed with copious amount of water. All samples were stored in water if not used immediately.

Application of the probe molecule 4-HTP: 4-HTP coated slides were prepared by immersing the SERS substrates into 4-HTP ethanolic solution (1mM) for 24 h. The samples were then rinsed with copious amount of ethanol and dried with N_2.

Characterization: The characterization by AFM was accomplished by using a ThermoMicroscopes Digital AFM instrument. It was operated under ambient conditions and noncontact mode. Noncontact AFM tips were obtained from ThermoMicroscopes (model 1650 - 00). An area of 1000 nm by 1000 nm was always scanned (200 lines in the scan area), and scan rate was 950nm/s. Other parameters were optimized for each scan. UV-Vis reflection-absorption spectra of the as prepared Au NPs modified slide was measured using an USB miniature fiber optic spectrometer (Ocean Optics), attached to the ocular of an Olympus BHSM microscope. The halogen lamp of the microscope was used as light source. The experiments were realized in back reflection using a 20X microscope objective.

PM-IRRAS measurement: PM-IRRAS measurement was performed on a Equinox 55 (Bruker) equipped with a photoelastic modulator (PEM-90 with II/ZS50 ZnSe 50 kHz optical head, HINDS instruments) and a liquid N_2 cooled MCT IR detector (Kolmar

Technologies). An external reflection configuration was used. The IR beam was directed to the sample surface at a grazing angle. The acquisition time was 10 min for the difference spectra and 2 min for the sum spectra. The resolution was set at $4cm^{-1}$. The final spectra were obtained by dividing the difference spectra by the sum spectra. The data presented were background subtracted.

Ex situ and *in situ* SERS measurement: All the Raman measurements were accomplished using a Raman microscope system equipped with He-Ne laser source (632.8 nm, Melles Griot). *Ex situ* measurements were taken in air with the samples directly mounted on the stage of the Olympus BHSM microscope. The *in situ* measurements were taken with the substrate immersed in an electrolyte and under electrochemical control. The spectroelectrochemical cell used for *in situ* measurements was also mounted on the stage of the microscope. The Raman experiments were realized in a backscattering configuration, where the exciting laser and the scattered radiation passed through the same 50x Olympus microscope objective. An ultra long working distance objective (NA=0.55) was used for *in situ* measurements; and a regular (NA=0.80) objective was used for the ex situ measurements. A Kaiser super notch filter was used to remove the unwanted radiation at the laser frequency. A Kaiser Holospec f/1.4 spectrograph equipped with an Andor CCD detector (model DV-401-BV) was coupled to the microscope. For *in situ* measurement, a three-compartment spectroelectrochemical cell with 1 mm glass window was used. The Au NPs modified slides were used as working electrodes. A Ag/AgCl was used as reference electrode and a Pt wire was used as a counter electrode. Typically, 30s of acquisition time was applied for ex situ measurements while 120s was used for *in situ* SERS. An Autolab PGSTAT 30 potentiostat/galvanostat was used to control the applied potential.

2.5 References:

1. Vo-Dinh, T., *Trac-Trends in Analytical Chemistry* **1998,** *17* (8-9), 557-582.

2. Aroca, R., *Surface enhanced vibrational spectroscopy*. Wiley: Hoboken, NJ, 2006; p xxv, 233 p.

3. Nie, S. M.; Emery, S. R., *Science* **1997,** *275* (5303), 1102-1106.

4. Baker, G. A.; Moore, D. S., *Analytical and Bioanalytical Chemistry* **2005,** *382* (8), 1751-1770.

5. Brolo, A. G.; Irish, D. E.; Smith, B. D., *Journal of Molecular Structure* **1997,** *405* (1), 29-44.

6. Osawa, M., Surface-enhanced infrared absorption. In *Near-Field Optics and Surface Plasmon Polaritons*, SPRINGER-VERLAG BERLIN: Berlin, 2001; Vol. 81, pp 163-187.

7. Osawa, M., *Bulletin of the Chemical Society of Japan* **1997,** *70* (12), 2861-2880.

8. Campion, A.; Kambhampati, P., *Chemical Society Reviews* **1998,** *27* (4), 241-250.

9. Kho, K. W.; Shen, Z. X.; Zeng, H. C.; Soo, K. C.; Olivo, M., *Analytical Chemistry* **2005,** *77* (22), 7462-7471.

10. Mosier-Boss, P. A.; Lieberman, S. H., *Analytical Chemistry* **2005,** *77* (4), 1031-1037.

11. Olson, L. G.; Uibel, R. H.; Harris, J. M., *Applied Spectroscopy* **2004,** *58* (12), 1394-1400.

12. Li, H. G.; Cullum, B. M., *Applied Spectroscopy* **2005,** *59* (4), 410-417.

13. Hu, X. G.; Cheng, W. L.; Wang, T.; Wang, Y. L.; Wang, E. K.; Dong, S. J., *Journal of Physical Chemistry B* **2005,** *109* (41), 19385-19389.

14. Gomez, R.; Perez, J. M.; Solla-Gullon, J.; Montiel, V.; Aldaz, A., *Journal of Physical Chemistry B* **2004,** *108* (28), 9943-9949.

15. Freeman, R. G.; Grabar, K. C.; Allison, K. J.; Bright, R. M.; Davis, J. A.; Guthrie, A. P.; Hommer, M. B.; Jackson, M. A.; Smith, P. C.; Walter, D. G.; Natan, M. J., *Science* **1995,** *267* (5204), 1629-1632.

16. Bao, L. L.; Mahurin, S. M.; Dai, S., *Analytical Chemistry* **2004,** *76* (15), 4531-4536.

17. Aroca, R. F.; Goulet, P. J. G.; dos Santos, D. S.; Alvarez-Puebla, R. A.; Oliveira, O. N., *Analytical Chemistry* **2005,** *77* (2), 378-382.

18. Aroca, R. F.; Alvarez-Puebla, R. A.; Pieczonka, N.; Sanchez-Cortez, S.; Garcia-Ramos, J. V., *Advances in Colloid and Interface Science* **2005,** *116* (1-3), 45-61.

19. Mulvaney, S. P.; Keating, C. D., *Analytical Chemistry* **2000,** *72* (12), 145R-157R.

20. Leverette, C. L. J., S. A.; Shanmukh, S.; Chaney, S. B.; Dluhy, R. A.; Zhao, Y.-P, *Applied Spectroscopy* **2006,** *60* (8), 906-913.

21. Coe, J. V.; Williams, S. M.; Rodriguez, K. R.; Teeters-Kennedy, S.; Sudnitsyn, A.; Hrovat, F., *Analytical Chemistry* **2006,** *78* (5), 1384-1390.

22. Huo, S.-J.; Xue, X.-K.; Li, Q.-X.; Xu, S.-F.; Cai, W.-B., *Journal of Physical Chemistry B* **2006,** *110* (51), 25721 -25728.

23. Huo, S. J.; Li, Q. X.; Yan, Y. G.; Chen, Y.; Cai, W. B.; Xu, Q. J.; Osawa, M., *Journal of Physical Chemistry B* **2005,** *109* (33), 15985-15991.

24. Enders, D.; Puccia, A., *Applied Physics Letters* **2006,** *88* (18).

25. Brown, C. W.; Li, Y.; Seelenbinder, J. A.; Pivarnik, P.; Rand, A. G.; Letcher, S. V.; Gregory, O. J.; Platek, M. J., *Analytical Chemistry* **1998,** *70* (14), 2991-2996.

26. Enders, D.; Rupp, S.; Kuller, A.; Pucci, A., *Surface Science* **2006,** *600* (23), L305-L308.

27. Miki, A.; Ye, S.; Osawa, M., *Chemical Communications* **2002,** (14), 1500-1501.

28. Musick, M. D.; Keating, C. D.; Keefe, M. H.; Natan, M. J., *Chemistry of Materials* **1997,** *9* (7), 1499-1501.

29. Addison, C. J.; Brolo, A. G., *Langmuir* **2006,** *22* (21), 8696 -8702.

30. Sztainbuch, I. W., *Journal of Chemical Physics* **2006,** *125* (12).

31. Olson, L. G.; Lo, Y. S.; Beebe, T. P.; Harris, J. M., *Analytical Chemistry* **2001,** *73* (17), 4268-4276.

32. Abdelrahman, A. I.; Mohammad, A. M.; Okajima, T.; Ohsaka, T., *Journal of Physical Chemistry B* **2006,** *110* (6), 2798-2803.

33. Musick, M. D.; Pena, D. J.; Botsko, S. L.; McEvoy, T. M.; Richardson, J. N.; Natan, M. J., *Langmuir* **1999,** *15* (3), 844-850.

34. Musick, M. D.; Keating, C. D.; Lyon, L. A.; Botsko, S. L.; Pena, D. J.; Holliway, W. D.; McEvoy, T. M.; Richardson, J. N.; Natan, M. J., *Chemistry of Materials* **2000,** *12* (10), 2869-2881.

35. Welch, C. W.; Compton, R. G., *Analytical and Bioanalytical Chemistry* **2006,** *384* (3), 601-619.

36. Hernandez-Santos, D.; Gonzalez-Garcia, M. B.; Garcia, A. C., *Electroanalysis* **2002,** *14* (18), 1225-1235.

37. Daniel, M. C.; Astruc, D., *Chemical Reviews* **2004,** *104* (1), 293-346.

38. Gómez, R.; Solla-Gullón, J.; Pérez, J. M.; Aldaz, A., *Journal of Raman Spectroscopy* **2005,** *36* (6-7), 613 - 622.

39. Li, X.-Y.; Huang, Q.-J.; Petrov, V. I.; Xie, Y.-T.; Luo, Q.; Yu, X.; Yan, Y.-J., *Journal of Raman Spectroscopy* **2005,** *36* (6-7), 555 - 573.

40. Guo, L.; Huang, Q. J.; Li, X. Y.; Yang, S. H., *Physical Chemistry Chemical Physics* **2001,** *3* (9), 1661-1665.

41. Som, J. N.; Mukherjee, D. K., *Journal of Molecular Structure* **1975,** *26* (1), 120-123.

42. Joo, S. W.; Han, S. W.; Kim, K., *Journal of Physical Chemistry B* **2000,** *104* (26), 6218-6224.

43. Bernad, S.; Mantele, W., *Analytical Biochemistry* **2006,** *351* (2), 214-218.

44. Seelenbinder, J. A.; Brown, C. W.; Pivarnik, P.; Rand, A. G., *Analytical Chemistry* **1999,** *71* (10), 1963-1966.

45. Bahar, E.; Huang, G. R.; Lee, B. S., *Radio Science* **1995,** *30* (3), 525-544.

46. Bicout, D.; Brosseau, C.; Martinez, A. S.; Schmitt, J. M., *Physical Review E* **1994,** *49* (2), 1767-1770.

47. Sivanesan, A.; Kannan, P.; John, S. A., *Electrochimica Acta* **2007,** *52* (28), 8118-8124.

48. Itoh, T.; Biju, V.; Ishikawa, M.; Kikkawa, Y.; Hashimoto, K.; Ikehata, A.; Ozaki, Y., *Journal of Chemical Physics* **2006,** *124* (13).

49. Lee, H. M.; Kim, M. S.; Kim, K., *Vibrational Spectroscopy* **1994,** *6* (2), 205-214.

50. Addison, C. J.; Brolo, A. G. Fabrication, characterization and optical properties of three-dimensional colloidal gold nanostructures. Thesis (M Sc), University of Victoria, (Canada). 2005.

51. Tourwe, E.; Hubin, A., *Vibrational Spectroscopy* **2006,** *41* (1), 59-67.

52. Yun, S.; Park, Y. K.; Kim, S. K.; Park, S., *Analytical Chemistry* **2007,** *79*, 8584-8589.

53. Qin, L. D.; Zou, S. L.; Xue, C.; Atkinson, A.; Schatz, G. C.; Mirkin, C. A., *Proceedings of the National Academy of Sciences of the United States of America* **2006,** *103* (36), 13300-13303.

54. Le, F.; Lwin, N. Z.; Steele, J. M.; Kall, M.; Halas, N. J.; Nordlander, P., *Nano Letters* **2005,** *5* (10), 2009-2013.

55. Wano, H.; Uosaki, K., *Langmuir* **2005,** *21* (9), 4024-4033.

56. Walczak, M. M.; Popenoe, D. D.; Deinhammer, R. S.; Lamp, B. D.; Chung, C. K.; Porter, M. D., *Langmuir* **1991,** *7* (11), 2687-2693.

57. Grabar, K. C.; Freeman, R. G.; Hommer, M. B.; Natan, M. J., *Analytical Chemistry* **1995,** *67* (4), 735-743.

Chapter 3: Silver Nanoparticles Self Assembly as SERS Substrates with Near Single Molecule Detection Limit

This chapter is a paper published on ***Phys. Chem. Chem. Phys.*** *(2009, 11 (34), 7381-7389).*

Reproduced by permission of the PCCP Owner Societies.

Link: http://www.rsc.org/publishing/journals/CP/article.asp?doi=b904744a

Highly sensitive SERS substrates with limit of detection in the zeptomole (for nile blue A and oxazine 720) range were fabricated through a bottom-up strategy. Ag nanoparticles (Ag NPs) were self-assembled onto glass slides by using 3-mercaptopropyl-trimethoxysilane (MPTMS) sol-gel as linker. The substrates were characterized by UV-Vis and AFM after each deposition of Ag NPs. It was found that the glass slide presented just a few Ag NPs aggregates scattered throughout the surface after just one deposition. The glass surface was gradually covered by a homogeneous distribution of Ag NPs aggregates as the deposition number increased. Surface-enhanced Raman scattering (SERS) of the substrates was examined at different numbers of Ag NPs deposition using nile blue A and oxazine 720 as probe molecules and two laser excitations (632.8 nm and 785 nm). Optimum SERS was observed after six depositions of Ag NPs. SERS mapping indicated that at lower deposition numbers (less than 3 Ag NPs depositions) the substrates presented a few SERS "hot–spots" randomly distributed at the surface. After 7 Ag NPs depositions, spatial distribution of the SERS signal followed Gaussian statistics, with a percent relative standard deviation (RSD%) of ~19%. In addition, the sample-to-sample reproducibility of the SERS intensities under both laser excitations was lower than 20%. It was also found that these substrates can provide giant Raman signal enhancement. At optimum condition and with 632.8 nm laser, the signal from an estimated of only ~44 probe molecules (100× objective) can still be detected.

3.1 Introduction

After more than 30 years of development, surface-enhanced Raman scattering (SERS)[1-4] has been proven as a versatile analytical technique.[5] This is not only due to its high sensitivity but also because SERS provides vibrational (fingerprint) information of target molecules. The analytical capabilities of SERS have been explored in several fields, including environmental sciences and biomedicine.[6-10] For example, SERS has been used to detect DNA,[11] enzymes,[7] and even to follow enzymatic activity in a single cell.[6] In addition, SERS-based immunoassays are widely reported and provide several advantages relative to other labeling techniques, in terms of sensitivity, selectivity and multiplexing.[9-10] SERS detection has also been used in environmental analysis for the detection of polycyclic aromatic hydrocarbons in aqueous solution.[12-13]

The enhancement of local electromagnetic fields via localized surface plasmon modes in metallic nanostructures is mostly responsible for the SERS phenomena.[5, 14-16] This field localization is controlled by the nanostructure morphology. Hence, there are tremendous efforts to explore different nanostructures that support SERS, aiming at optimized substrates with high sensitivity and reproducibility.

SERS substrates can be prepared using either the bottom-up or the top-down strategy. The electrochemical roughening of electrodes through oxidation-reduction cycles (ORCs) is among the simplest example of a SERS substrate.[1, 17] However, this technique does not allow much control over the size and shape of the nanofeatures, leading to low reproducibility. Recently, more elaborated top-down strategies become accessible due to the latest developments in nanolithography. Modern nanofabrication methods allow tailoring of the nanostructures for maximum enhancement, and the fabrication of reproducible nanofeatures even in a large area.[18-20] For example, periodic arrays of sub-wavelength apertures (nanoholes) have been proved to be a successful SERS substrate.[21-24] SERS from single nanoholes has also been observed.[25] Other top-down fabricated nanostructures for SERS reported recently include: Au nanoparticle arrays;[26-27] "multi-bowtie"[28] structures; Au nano-disks with different thickness and separation distances;[29]and gold moon crescent structures.[30] Some of these structures were proved to have close to single-molecule detection limit.[25, 28, 30] However, the common disadvantage among some of these top-down methodologies is their high cost per fabricated sample and their serial character (such as in focused-ion beam milling and in electron beam lithography). A cheaper alternative is the preparation of SERS substrates by the self-assembly of metallic nanoparticles (bottom-up approach). The building blocks in this case are nanoparticles (NPs) of different shapes (nanospheres, nanorods, nanocubes) and compositions, including core-shell structures.[31] The NPs are immobilized in a planar platform through either covalent[32-36] or non-covalent[37-43] interactions with linkers. The "linkers" generally used for non-covalent self-assembly are organic polymers[44] and polymer dendrimers,[38, 45] DNAs,[37] and proteins;[42-43] as for covalent self-assembly, organic silane[32] and dithiols[33-35] are common choices. The preparation of positively charged Ag NPs[46] and their application in the multi-layer self-assembly of oppositely charged NPs as SERS substrates[47-48] has also been reported. The bottom-up approach, however, commonly provides less spatial and sample-to-sample reproducibility than the nanolithographic methods.

Previously, we have reported a bottom-up strategy to fabricate SERS substrate using Au NPs.[33-34] 1,3-propanedithiol was used as linker for the multiple depositions of Au NPs onto both glass and gold slides. It was found that the SERS signal maximizes after a certain number of Au NPs depositions at a given excitation energy. Meanwhile, the spatial variation of the SERS signal and the optimized sample to sample reproducibility obtained by this procedure were lower than 20%.[34]

In this report, we will present a self-assembled substrate for SERS based on Ag NPs as building blocks and 3-mercaptopropyltrimethoxysilane (MPTMS) sol-gel as linker. Although dithiols was proved to be good linkers for the stepwise deposition of Au NPs,[33-35] they are not as efficient for Ag NPs deposition. Alternative approaches for Ag immobilization include thiol-exchange reactions[49] and layer-by-layer deposition through electrostatic interactions.[37-38, 40, 47-48] The limited success of the application of dithiol as linker to the fabrication of self-assembled Ag structures is probably due to the strong affinity of the thiol functionality towards the Ag surface which favors the simultaneous interaction of both thiol groups of the dithiol with the Ag, leaving no free thiol group to interact with the adjacent layer.[50] Hydrolyzation of MPTMS leads to the formation of a sol-gel rich in free thiol functionalities,[51] which guarantees the availability of thiol groups after binding to the bottom layer of Ag NPs. It was found in this report that the SERS efficiency increases with the number of Ag NPs deposition, stabilizing after 6 depositions for both 632.8 nm and 785 nm laser excitations. These results agree with our previous work involving Au NPs deposition on Au films.[34] The spatial variation of the SERS signal also decreased with increasing Ag NPs depositions, as revealed by SERS mapping. In addition, slide-to-slide variations in SERS intensities proved to be less than 20% for both lasers used. Finally, this class of substrates is very sensitive, allowing the detection of about 44 Nile blue A (NBA) molecules at 632.8 nm excitation using a 100× objective.

3.2 Experimental section

3.2.1 Chemicals

Unless otherwise mentioned, ACS grade chemicals were used. $AgNO_3$, sodium citrate dihydrate, 3-mercaptopropyltrimethoxysilane (MPTMS), Oxazine 720 and Nile blue A (NBA) perchlorate were obtained from Sigma-Aldrich. Ultrapure water with a resistivity of 18.2 MΩ.cm (from Barnstead NANOpure Diamond water purification system) was used throughout the experiments. Glass slides are 1×1 inch regular microscope slides.

3.2.2 Synthesis of Ag NPs and MPTMS sol-gel

The preparation of Ag NPs followed the procedure reported in the literature.[52] Briefly, a 500 mL $AgNO_3$ solution (1 mM) was heated to ~90 *°C* (initial boiling) under vigorous stirring. Then, 20 mL of 1% sodium citrate solution was quickly added. The solution was kept on a hotplate with stirring until it turned into an apparent luminescent yellow. After that, the hotplate was removed but stirring was kept until the solution cooled down to the room temperature (about 25^0C). The as prepared Ag NPs showed an absorption peak at 407 nm.

The MPTMS sol-gel preparation also follows the literature[51] but with some modifications. Briefly, 600 μL of MPTMS and 500 μL of 0.1M HCl were added into 50 mL of water. The solution was vigorously stirred for at least 1 hour. The sol-gel solution should be used the same day.

3.2.3 Preparation of the SERS substrate

The glass slides were cleaned using piranha solution and rinsed thoroughly with water. Then, they were dried using a nitrogen flow, rinsed with methanol and soaked into 10 mM MPTMS methanolic solution for 24 hours. The modified slides were then rinsed with copious amount of methanol, dried with nitrogen, rinsed again with water, and finally immersed into the Ag NPs solution for another 24 hours. For the deposition of additional Ag NPs, the slides were removed from the Ag NPs solution, thoroughly rinsed with water and dipped into the MPTMS sol-gel for 20min and then immersed again in the Ag NPs solution for 1 hour. This procedure was repeated until the desired number of Ag NPs depositions was achieved. Rigorous rinsing was performed after each step.

3.2.4 Characterization of the SERS substrate

The UV-Vis spectra of the slides were obtained using a UV-Visible spectrometer (Agilent, model 8453). The spectrum of a clean glass in air was used as background. AFM scans were accomplished using a Nanonics Imaging AFM model MV-1000. Intermittent contact mode was used with a pulled glass fiber tip. The image was analyzed with WSXM software.

3.2.5 SERS measurement

All the Raman measurements were accomplished using RENISHAW inVia Raman microscope system equipped with a He-Ne and a diode near IR as laser sources. The He-Ne excitation, at 632.8 nm (6.7 μW), presented a circular laser spot at the sample with a diameter (FWHM) equal to 0.9 μm for the 50× objective and equal to 0.5 μm for the 100× objective. The laser spot of the diode near IR laser, at 785 nm (0.317 mW), was a rectangle of 2.6μm×5.8μm for the 50× objective.

The SERS probes (nile blue A and oxazine 720) were added to the substrates as following: An appropriate amount of the dyes were dissolved in methanol. Then, 50 μL of the solution was dropped onto the 1×1 inch substrate. This amount of solution covered the whole surface. The slides then were left in air to dry.

To calculate the amount of probe molecules in the laser spot region, the number of moles of the probe molecule was calculated from the solution concentration and then divided by the surface area of the glass slide, yielding moles per unit area, which was then multiplied by the size of the laser spot. Note that this calculation is based on the assumption that the binding constant of the probe molecules to the substrate is infinitely high. Thus, the estimated number N of adsorbed molecules is an upper limit.

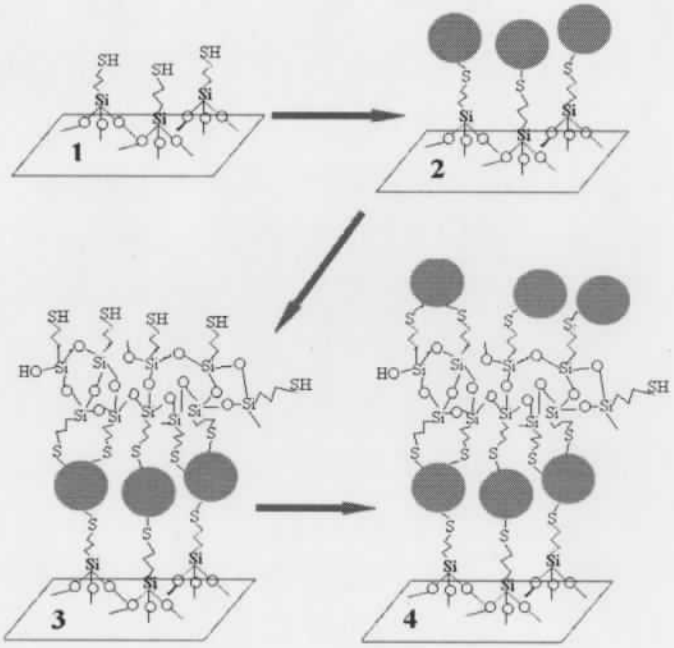

Scheme 3- 1 Preparation of the SERS substrates. This diagram is not to scale. Step 1: The surface of a clean glass slide is modified by MPTMS to yield pedant thiol groups; Step 2: The modified glass slide is immersed in a solution of Ag NPs (grey circles), which will adhere to the surface by interacting with the thiol groups; Step 3: The slide is dipped in sol-gel of MPTMS to add more thiol functionalities to the surface; Step 4: The substrate is immersed again in a solution of Ag NPs to receive an additional layer of Ag NPs. Steps 3 and 4 are repeated until the desired number of depositions is achieved.

3.3 Results and discussion

3.3.1 Substrate characterization

Scheme 3-1 represents the procedure used in the preparation of the SERS substrates used in this work. A clean glass slide was initially modified with MPTMS. The modified slide was dipped into an Ag NPs solution for 24h. The Ag NPs interact with the pendent thiol groups of the MPTMS, forming the first layer of NPs. Further addition of NPs was accomplished by dipping the slide with the first layer of Ag NPs in MPTMS sol-gel for 20 min. The MPTMS sol-gel "polymer" attach to the Ag NPs but leaves free thiols for the deposition of the next Ag NPs layer. The last two steps were repeated until the desired number of Ag NPs depositions was achieved.

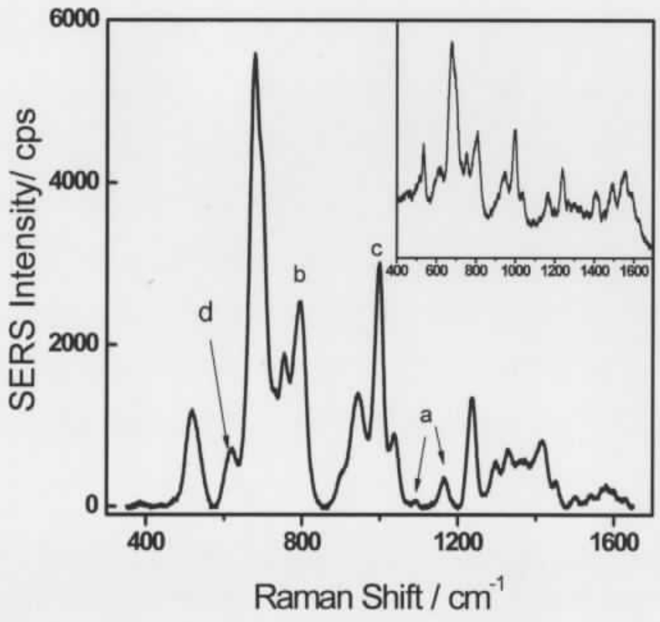

Figure 3- 1 SERS spectrum from Ag NPs substrate after 7 Ag NPs depositions. There are no probe molecules adsorbed at the silver surface and the spectrum corresponds to the background due to the sol-gel polymer. Laser excitation at 785 nm. The inset shows the spectrum of the same sample obtained using 632.8nm excitation.

A common disadvantage of linker-based SERS substrates is the Raman signature of the linker molecules (the sol-gel "polymer", in our case), which will be a constant background in the SERS experiments. Fig. 3-1 shows spectra of the SERS substrate after the deposition of 7 Ag NPs "layers" for both lasers excitations used in this work. The Raman signature in Fig. 3-1 is typical for hydrolized MPTMS. For instance, the bands labeled as *a* have been assigned to the longitudinal and transverse optical (LO and TO) stretching modes of Si-O-Si, and the *b* band is the symmetrical stretch of the Si-O-Si network.[53-54] The peaks labeled *c* and *d* are from SiOH modes, implying some defects in the polymeric network.[53, 55] The background spectrum presented in Fig. 3-1 will not be a significant spectral interference for SERS of strong scatters. However, the background become important during the detection of a small number of adsorbates, as it will be discussed later.

The morphologies of the SERS substrates prepared in this work were monitored by AFM, and a few representative images are presented in Fig. 3-2. It is clear from the AFM that the packing density and the homogeneity of the surface features increased with the number of Ag NPs deposition. The height of the features in Fig. 3-2a was between 40-90 nm, which is in agreement with the particle size distribution of the synthesized Ag colloid.[52] All AFM images presented features with average lateral dimensions between 200-400 nm, except for Fig. 3-2a (1 Ag NP deposition) that shows a few clusters with lateral dimension of less than 100 nm.

Fig. 3-3 shows the UV-Vis absorption of the substrates prepared with different numbers of Ag NPs depositions. A typical surface plasmon absorption band was observed at 409 nm for the substrate with just one deposition of Ag NPs. This absorption maximum red-shifted with the increasing number of Ag NPs deposition, quickly reaching 446 nm after 7 depositions of Ag NPs, and shifting only slightly after that. An absorption shoulder at around 680 nm appears after 3 depositions of Ag NPs, and the absorption band tails towards the near IR (ca 1000 nm) region as the number of Ag NPs deposition increases. These results are common indications of Ag NPs aggregation, which become more significant with the increase in the amount of Ag NPs.[44] The optical data agrees with the increase in nanoparticle density with the number of Ag NPs depositions shown in the AFM images in Fig. 3-2.

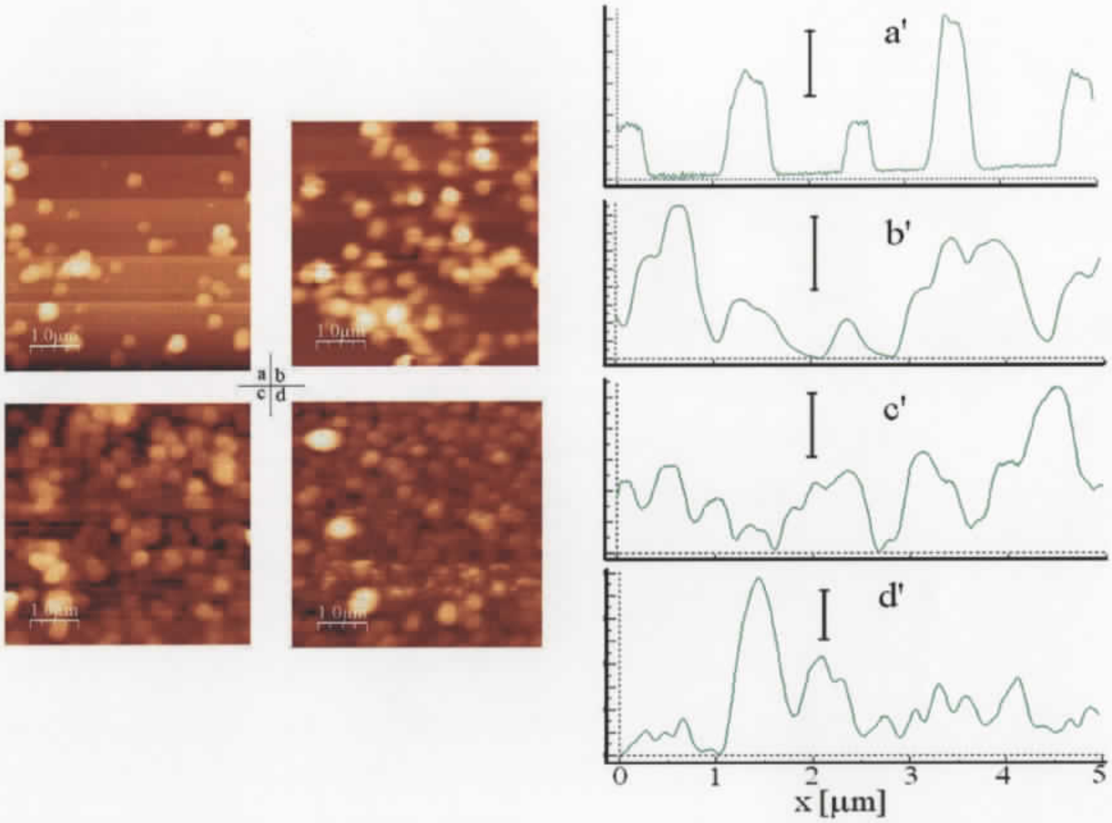

Figure 3- 2 AFM images of the Ag NPs substrates after a) 1; b) 3; (c) 5; and d) 7 depositions of Ag NPs. The representative line profiles of the images are shown in a', b', c' and d', respectively. Scale bar shows 40 nm.

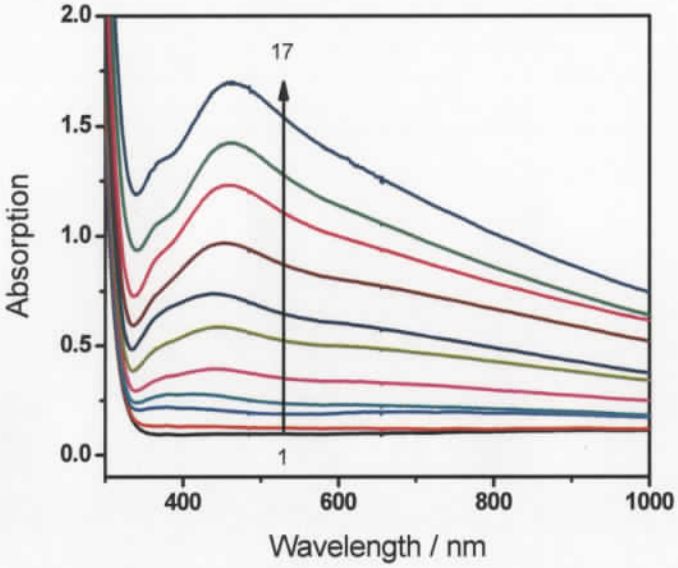

Figure 3- 3 UV-Vis absorption of Ag NPs modified slides. From bottom to top: 1, 2, 3, 4, 5, 7, 9, 11, 13, 15, 17 deposition(s) of Ag NPs on glass.

3.3.2 SERS performance

Substrate optimization for SERS

Nile blue A (NBA) and oxazine 720 were used as molecular probes to evaluate the SERS performance of the Ag NPs modified slides. Both dyes have very similar structure and have electronic absorption in the region of the 632.8 nm excitation. Therefore, experiments using that excitation wavelength contain contributions from the resonance Raman effect (surface-enhanced resonance Raman scattering (SERRS)). The dependence of the SER(R)S intensity of the ca 593 cm^{-1}-band of NBA with the number of Ag NPs depositions is presented in Fig. 3-4. Experiments were carried out for two laser excitations: 632.8 nm and 785 nm. The SER(R)S intensities in Fig. 3-4 are averages of 5 measurements from different spots of the slide surface and the error bars represents the standard error of these measurements. The SERS spectrum in the inset for 785 nm excitation present a weak broad shoulder around 680 cm^{-1} (indicated with an arrow), but this feature is absent in the case of 632.8 nm excitation. This shoulder is a background contribution from the substrate (Fig. 3-1). Notice that no resonance Raman contribution is expected at 785 nm, but additional Raman resonance effect is present at 632.8 nm excitation (SERRS effect) and the background signal from the substrate is negligible in that condition. The higher intensity (in cps) observed for the 785 nm excitation (Fig. 3-4b) is due to the larger power density and illuminated area for this excitation.

After 6 Ag NP depositions, the SER(R)S signal reached a maximum and stabilized after the peak, although some increase is still noted in Fig. 3-4a. It is difficult to rationalize the reason for this stabilization without any knowledge of the evolution of the near field distribution within the different morphologies, although an increase in scattering loss from large nanofeatures should contribute to this effect. The behavior, however, is in agreement with our previous results from Au NPs deposited on gold slides.[34] Interestingly, we didn't observe the strong dependence on the optimum SERS with the excitation wavelength as observed for Au NPs deposited in glass using a dithiol linker.[33] This may be rationalized by considering the differences in particle size and morphology between these substrates (Au deposited on glass using dithiol linkers[33] and Ag deposited on glass using MPTMS sol-gel (this work)). As shown in Figs. 3-2a to 3-2d, the coverage of Ag NPs aggregates changed with increasing deposition. This can be further confirmed from the line profiles in Fig. 3-2b' to 2d', which shows almost no change in the lateral dimensions of the nanostructures with increasing deposition numbers. This behavior differs from the results observed using Au NPs, where lateral sizes of the features increased with increasing deposition number.[33] This is a fundamental difference, certainly related to the nature of the linker, which might explain the different trends in SERS intensities observed from both Ag and Au deposited on glass.

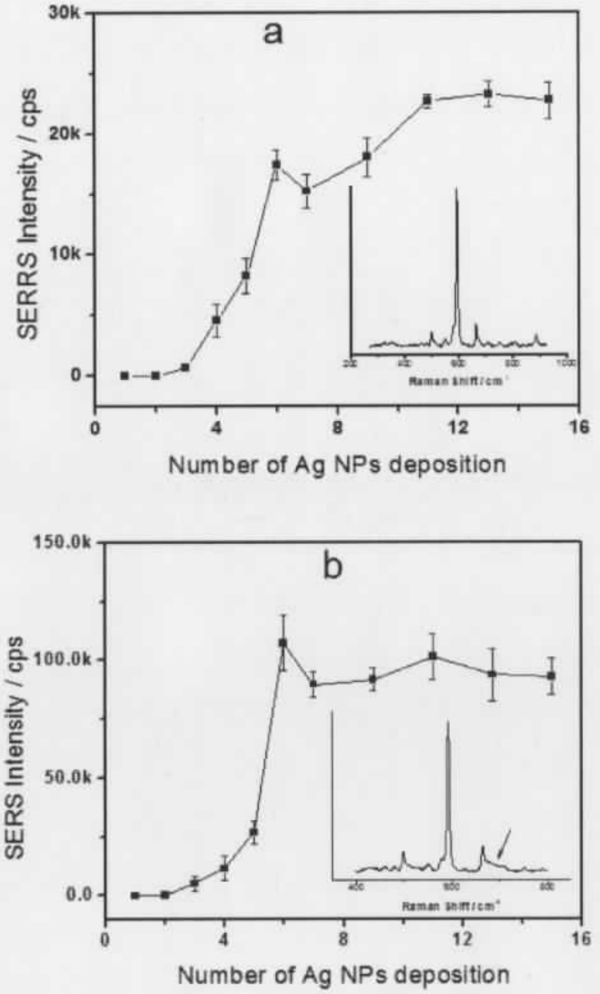

Figure 3- 4 SERS performance of the Ag NPs-modified glass slides. NBA was used as the molecular probe and its 593 cm^{-1}-band is plotted against the number of Ag NPs depositions. a) 632.8 nm excitation and power density equals to 10 $\mu W/ \mu m^2$; b) 785 nm excitation and power density equals to 21 $\mu W/\mu m^2$. The amount of NBA on each slide was constant (4μg/ml). 5 measurements were performed in different regions of each sample and the SER(R)S results were averaged. The bars show the standard error (SE) that represents this spatial variation. Insets show SER(R)S spectrum of NBA on a substrate after 7 Ag NPs deposition for each excitation.

The SER(R)S intensity obtained after 6 Ag NP depositions, normalized by the excitation conditions, from just one Ag NP deposition was about 2 orders of magnitude higher than what was observed for Au NPs.[33-34] Fig. 3-4 also shows that the SERS signal increased as a power function up to the peak at 6 depositions of Ag NPs, where our former result on Au showed roughly a linear increase until the maximum.[34] Zhu et al[56] considered that SERS intensities should depend on both size and population (i.e. inter-particle distance) of NPs, and they showed that there is a threshold particle density where the interaction between the particles become significant. When the population is lower than this threshold, the SERS intensity increased slowly with the particle density. However, the SERS intensity will increase fast due to the localized surface plasmons resonance (LSPR) coupling after the threshold value is reached. This effect is especially prominent for NPs with larger size, which is the case that we are reporting here.

The insets in Fig. 3-5 are the SERRS mappings from the Ag NPs substrate surfaces obtained using the 632.8 nm laser. The spatial distribution of SERRS intensity (in terms of peak area, see the caption in Fig. 3-5) can be also visualized in Fig. 3-5 by the analysis of the histograms obtained from these maps. The statistics of the mappings were done using a method proposed by Scott.[57] The histogram shows the distribution of SERRS intensities (normalized by the average). The inset in Fig. 3-5a shows that, for 1 Ag NPs deposition, there are several regions at the surface with weak SERS activity. This is confirmed by the large number of events with "zero" intensity in the histogram. In this case, more than one third of the surface area of the substrate presents very low SERRS intensity, although regions with SERRS signal as high as 32 times the average was also observed, indicating the presence of a SERS hot-spot.[3, 16] A skewed spatial distribution of SERRS intensities is also observed after 3 and 5 depositions, respectively (Figs. 3-5b, 3-5c). After 3 Ag NPs depositions (Fig. 3-5b), the distribution of SERRS signal narrows, and the distribution peak maximum appear closer to 1 (average) compared with that of Fig. 3-5a. The same observation was recorded after 5 Ag NPs depositions (Fig. 3-5c). A dramatic change in the shape of the distribution is observed after 7 Ag NPs depositions (Fig. 3-5d). The distribution in this case presents a normal (Gaussian) profile, with the distribution maximum centered at 1. Also note that the long distribution tails seen in Figs.

3-5a, 3-5b and 3-5c are not evident anymore after 7 Ag NPs depositions (Fig. 3-5d). The spatial variability of SERS intensity calculated from the FWHM of the Gaussian distribution from Fig. 3-5d is about ±20%. The mapping results from Fig. 3-5 indicate that the spatial variation of the SERRS intensities were greatly improved after 7 Ag NPs depositions.

Sample-to-sample reproducibility of SERS measurements

The sample-to-sample reproducibility of the slides prepared using our self-assembly procedure was tested and the results are presented in Fig. 3-6. Three different slides were used and the experiments were carried out at both excitations (632.8 nm and 785 nm). The SER(R)S intensity from each slide is the average from 10 randomly chosen spots and the error bars in Fig. 3-6 represent the calculated standard error (SE) for the spatial variation of the SER(R)S signal. The RSD% (among different slides) on the mean SERRS intensities is less than 10% for 632.8 nm excitation, but the RSD% under 785 nm is 18%. The difference in the spatial variation of SERS intensity for the same molecule at the same substrate but at different excitation wavelengths is an interesting effect. We attribute this difference to the nature of LSPR modes excited within the illuminated area at the laser frequency. It is anticipated that different LSPR-modes (surface features) are responsible for SERS at different wavelengths. The spatial distribution of surface structures that provide optimum SERS (hot spots) at 632.8 nm and 785 nm are not expected to be the same. This interesting result highlights the fact that a SERS substrate is "optimized" (not only in terms of enhancement efficiency but also in terms of reproducibility) for a particular excitation wavelength.

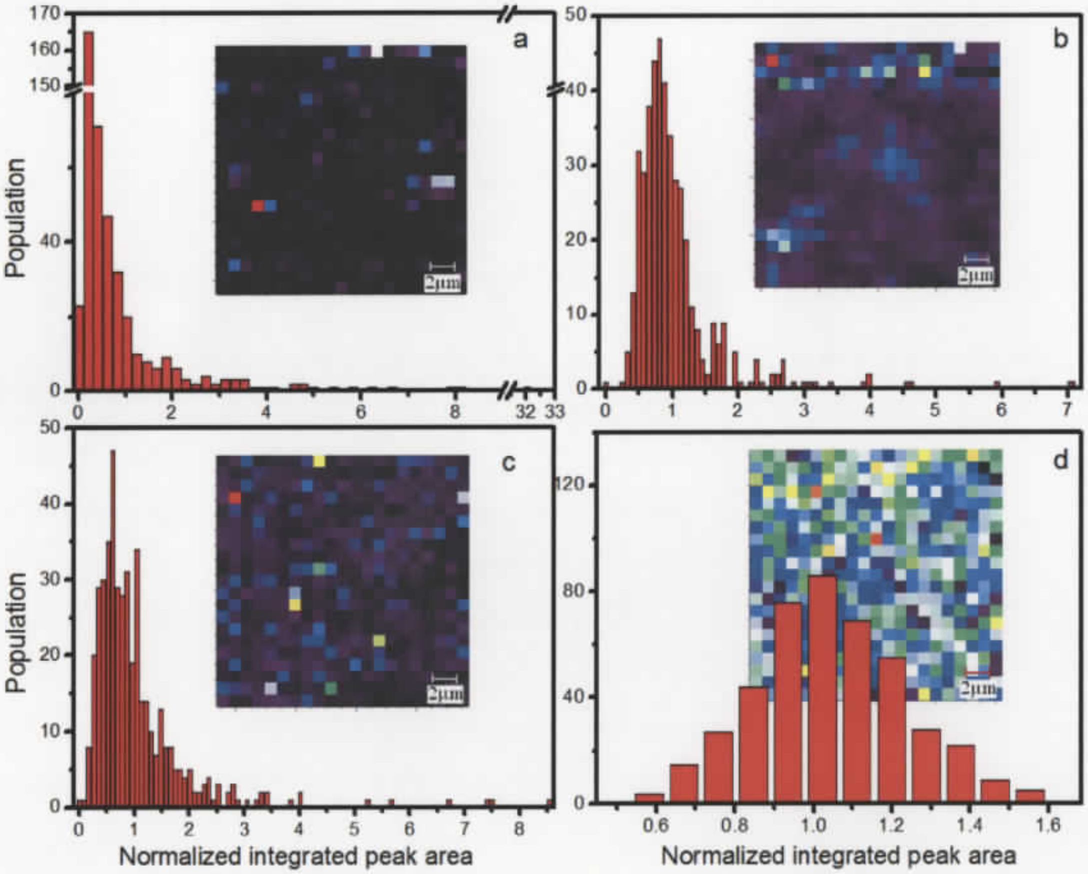

Figure 3- 5 SERRS mapping of the substrates coated with oxazine 720. Laser excitation at 632.8nm. The diagrams show the area of the dominant oxazine 720 SERRS peak at around 595 cm^{-1}. *a* to *d* represents the SERRS intensity (in peak area) distributions from the respective SERRS maps (inset). Note that the intensities for the histograms were normalized using the average SERRS intensity (in peak area).

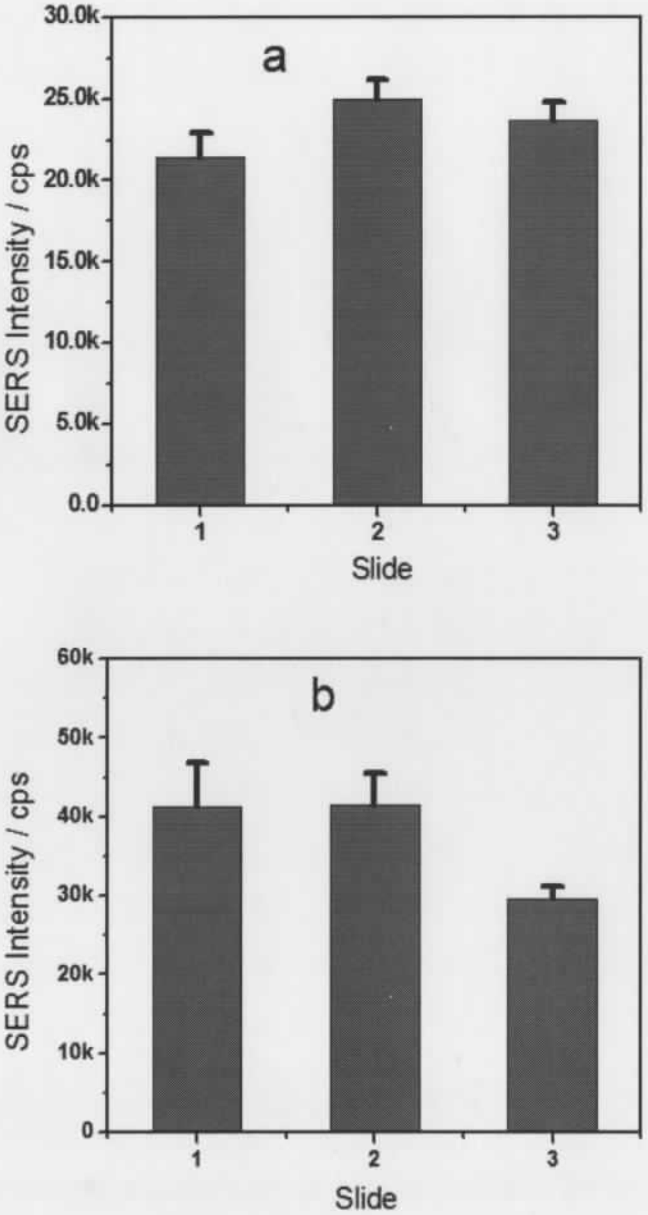

Figure 3- 6 Spatially-averaged SER(R)S intensities (at 593 cm^{-1}) for three 7-Ag NPs-deposition slides. a) 632.8 nm; b) 785 nm. The error bar shows the standard error of the spatial distribution of SER(R)S intensity. Concentration of NBA: 4μg/ml.

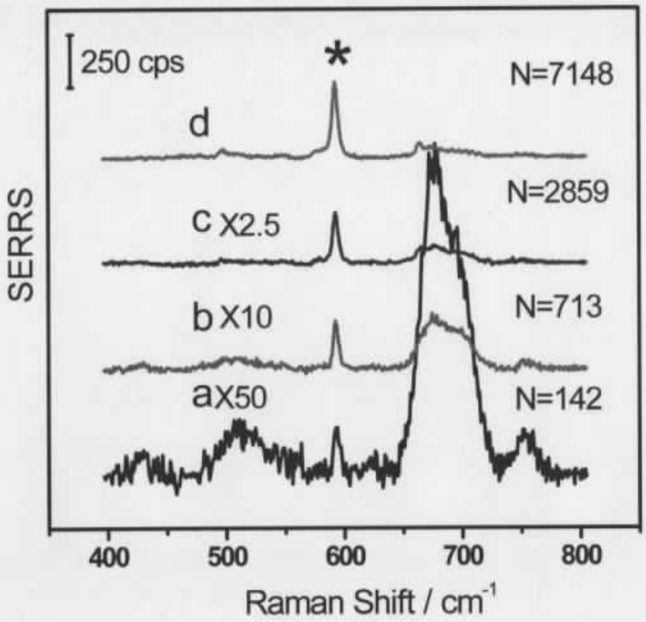

Figure 3- 7 Spatially-averaged (5 measurements) SERRS spectra at different concentration of NBA (background corrected). a) 2ng/mL; b) 10ng/mL; c) 40ng/mL; d) 100ng/mL. Spectra *a* to *c* were multiplied by a constant showed in the figure. Laser excitation was 632.8 nm and the substrate with 7 Ag NPs depositions were used. N is the estimated number of molecules within the laser spot. The asterisk (*) marks the position of the strongest NBA band.

Limit of detection (LOD) for the probe molecule NBA

The quality of the SERS substrate may also be evaluated by its limit of detection (LOD) for a particular molecular probe. Fig. 3-7 shows the spatially-averaged SERRS spectra of NBA obtained at different concentrations. A fluorescence-like background, present in some spectra, was corrected, and the spectra at lower concentrations were multiplied by a constant for better comparison. The strong bands at ~509cm^{-1}, ~677 cm^{-1},

~750 cm^{-1} are from the substrate (Fig. 3-1), but the NBA band (marked with an asterisk (*) in Fig. 3-7) can still be clearly indentified at very low analyte concentrations (Fig. 3-7a). Even the dominant band from the substrate at ~677 cm^{-1} doesn't constitute a strong interference at higher concentrations of the dye for 633 nm excitation (100 ng/mL, Fig. 3-7d), showing the strong efficiency of the SERRS effect in this case. The number of molecules in the laser spot, N, was calculated assuming a uniform coverage of the whole surface (see experimental section for details). SERRS was still observed even when only 142 molecules were estimated to populate the laser spot at 632.8 nm excitation and a 50× objective lens. Since it is unlikely that all 142 molecules populate hot-spots inside the laser illuminated region, it is possible that the amount of molecules that are actually contributing to the observed signal is even smaller

This is better illustrated in Fig. 3-8, where a SERRS mapping was performed for a sample with only ~142 molecules estimated in the laser spot. Since the coverage of NBA is small (assuming NBA molecule lies flat on the substrate (the maximum space it can occupy), the coverage would be roughly 0.06%), the chance of NBA molecules finding a hot spot is also small. Furthermore, the distribution of hot spots and the distribution of molecules are two independent factors, and the combination (to produce SERRS) is multiplicative. Thus, a lognormal (or tailed) rather than a normal distribution of intensities across the slide is expected.[58] This is exactly what is shown in Fig. 3-8b. Most of the surface presents signal levels smaller than the average (there are also spots with no SERRS signal), but the SERRS from a few spots can be much larger than the average value.

Similar results were obtained with a 100× objective and are presented in Fig. 3-9. The higher magnification and NA of the 100× lens allow the illumination of an even smaller spot size, probing a smaller number of molecules. A weak NBA signal is still present under these conditions. Since only 44 molecules are estimated in the laser-illuminated area, and not all of them will be at hot spots, it is likely that these results are approaching the single-molecule limit. No blinking was observed in our case, indicating that the molecules are immobilized in the hot spot in the dry conditions of our experiments.

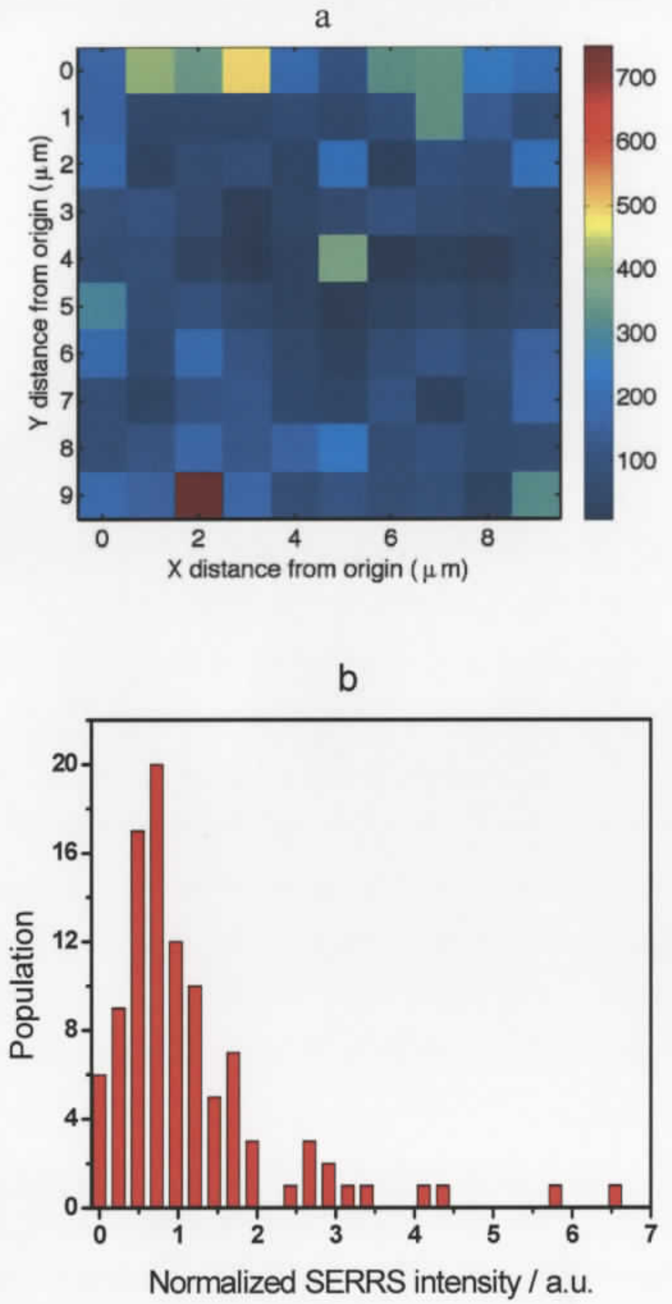

Figure 3- 8 a) SERRS mapping of the 593cm^{-1}-band of NBA; b) histrogram of the spatial distribution of SERRS intensity. 60s accumulation. Concentration of NBA 2ng/mL. 7 Ag NPs deposition. Laser excitation at 632.8 nm.

The performance of the substrate at near IR excitation was also probed. Fig. 3-10 shows the SERS from different concentration of NBA obtained using 785 nm laser excitation. Since NBA has no electronic absorption in this region, the Raman enhancement does not benefit from a resonance Raman mechanism, as it was the case for 632.8 nm excitation. Thus, the relative SERS signal is not as strong as for 632.8 nm excitation, and the interference of the background signal from the substrate is much more severe (Fig. 3-10 inset). In this case, the LOD determined using the same procedure as for 632.8 nm, was about 28 zeptomoles (2.8×10^{-20} moles) of molecules (10ng/mL, 50× objective, numerical aperture (NA)=0.75). Note that the laser spot at 785 nm is larger (see experimental section for details)).

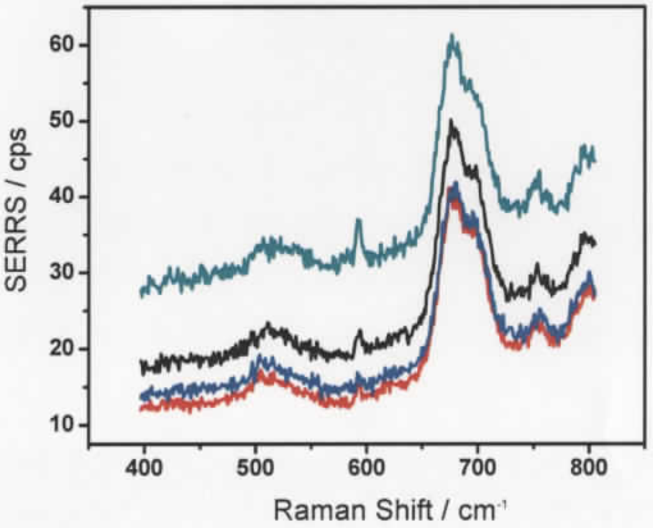

Figure 3- 9 SERRS spectra of NBA using a 100× objective from different spots at the same slide. Experimental conditions are the same as in Fig. 3-8. But only about 44 molecules are estimated in the laser spot. Laser excitation at 632.8 nm.

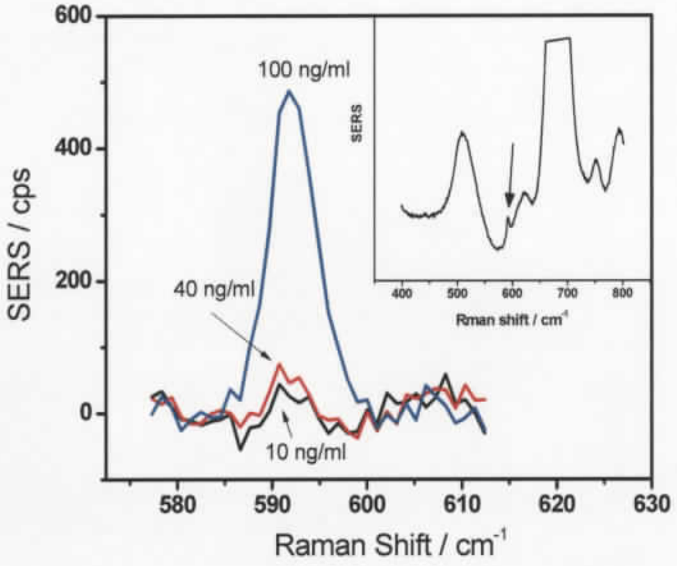

Figure 3- 10 SERS spectra of NBA at different concentrations (785 nm laser). Each spectrum is the averages of 5 measurements at different spots on the same slide. Inset shows an extended spectrum for 100 ng/mL of NBA. The arrow indicates the NBA band. The other strong features are the background from the substrate.

3.4 Conclusion

In this report, we used a multi-step deposition procedure to immobilize Ag NPs on glass using MPTMS sol-gel as linker. The procedure yielded highly sensitive SERS substrates. It is found that the Raman signal was dramatically enhanced (up to 3 orders of magnitude compared to just one deposition for both lasers (visible and near IR)) after 7 Ag NPs depositions. SERRS mapping showed that the number of hot spots increased with the deposition number, and the spatial distribution of intensities follows a normal statistics when the surface is covered by a homogeneous distribution of nanofeatures. The spatial and sample to sample variability of the SE(R)RS intensities were less than 20% in this case. Detectable SERRS signal was observed even when the number of molecules in the laser spot was around less than 100. Single molecule sensitivity is likely achieved, since not all molecules will populate the hottest spots. Even without the extra contribution from resonant Raman effects, the detection limit from these substrates is at sub-zeptomolar level for the dyes tested.

3.5 References :

1. Brolo, A. G.; Irish, D. E.; Smith, B. D., *Journal of Molecular Structure* **1997,** *405* (1), 29-44.

2. Campion, A.; Kambhampati, P., *Chemical Society Reviews* **1998,** *27* (4), 241-250.

3. Moskovits, M., *Journal of Raman Spectroscopy* **2005,** *36* (6-7), 485-496.

4. Vo-Dinh, T., *Trac-Trends in Analytical Chemistry* **1998,** *17* (8-9), 557-582.

5. Baker, G. A.; Moore, D. S., *Analytical and Bioanalytical Chemistry* **2005,** *382* (8), 1751-1770.

6. Moore, B. D.; Stevenson, L.; Watt, A.; Flitsch, S.; Turner, N. J.; Cassidy, C.; Graham, D., *Nature Biotechnology* **2004,** *22* (9), 1133-1138.

7. Ruan, C. M.; Wang, W.; Gu, B. H., *Analytical Chemistry* **2006,** *78* (10), 3379-3384.

8. Kneipp, J.; Kneipp, H.; Kneipp, K., *Chemical Society Reviews* **2008,** *37* (5), 1052-1060.

9. Doering, W. E.; Piotti, M. E.; Natan, M. J.; Freeman, R. G., *Advanced Materials* **2007,** *19* (20), 3100-3108.

10. Qian, X. M.; Nie, S. M., *Chemical Society Reviews* **2008,** *37* (5), 912-920.

11. Braun, G.; Lee, S. J.; Dante, M.; Nguyen, T. Q.; Moskovits, M.; Reich, N., *Journal of the American Chemical Society* **2007,** *129* (20), 6378-6379.

12. Olson, L. G.; Lo, Y. S.; Beebe, T. P.; Harris, J. M., *Analytical Chemistry* **2001,** *73* (17), 4268-4276.

13. Olson, L. G.; Uibel, R. H.; Harris, J. M., *Applied Spectroscopy* **2004,** *58* (12), 1394-1400.

14. Moskovits, M., Surface-enhanced Raman spectroscopy: a brief perspective. In *Surface-Enhanced Raman Scattering: Physics and Applications*, 2006; Vol. 103, pp 1-17.

15. Etchegoin, P.; Cohen, L. F.; Hartigan, H.; Brown, R. J. C.; Milton, M. J. T.; Gallop, J. C., *Journal of Chemical Physics* **2003,** *119* (10), 5281-5289.

16. Le Ru, E. C.; Etchegoin, P. G.; Meyer, M., *Journal of Chemical Physics* **2006,** *125* (20).

17. Albrecht, M. G.; Creighton, J. A., *Journal of the American Chemical Society* **1977,** *99* (15), 5215-5217.

18. Natan, M. J., *Faraday Discussions* **2006,** *132*, 321-328.

19. Henzie, J.; Lee, M. H.; Odom, T. W., *Nature Nanotechnology* **2007,** *2* (9), 549-554.

20. Kwak, E. S.; Henzie, J.; Chang, S. H.; Gray, S. K.; Schatz, G. C.; Odom, T. W., *Nano Letters* **2005,** *5* (10), 1963-1967.

21. Gordon, R.; Brolo, A. G.; McKinnon, A.; Rajora, A.; Leathem, B.; Kavanagh, K. L., *Physical Review Letters* **2004,** *92* (3).

22. Lesuffleur, A.; Kumar, L. K. S.; Brolo, A. G.; Kavanagh, K. L.; Gordon, R., *Journal of Physical Chemistry C* **2007,** *111* (6), 2347-2350.

23. Gordon, R.; Sinton, D.; Kavanagh, K. L.; Brolo, A. G., *Accounts of Chemical Research* **2008,** *41* (8), 1049-1057.

24. Anema, J. R.; Brolo, A. G.; Marthandam, P.; Gordon, R., *Journal of Physical Chemistry C* **2008,** *112* (44), 17051-17055.

25. Min, Q.; Santos, M. J. L.; Girotto, E. M.; Brolo, A. G.; Gordon, R., *Journal of Physical Chemistry C* **2008,** *112* (39), 15098-15101.

26. Laurent, G.; Felidj, N.; Grand, J.; Aubard, J.; Levi, G.; Hohenau, A.; Aussenegg, F. R.; Krenn, J. R., *Physical Review B* **2006,** *73* (24).

27. Laurent, G.; Felidj, N.; Truong, S. L.; Aubard, J.; Levi, G.; Krenn, J. R.; Hohenau, A.; Leitner, A.; Aussenegg, F. R., *Nano Letters* **2005,** *5*, 253-258.

28. Ward, D. R.; Grady, N. K.; Levin, C. S.; Halas, N. J.; Wu, Y. P.; Nordlander, P.; Natelson, D., *Nano Letters* **2007,** *7* (5), 1396-1400.

29. Qin, L. D.; Zou, S. L.; Xue, C.; Atkinson, A.; Schatz, G. C.; Mirkin, C. A., *Proceedings of the National Academy of Sciences of the United States of America* **2006,** *103* (36), 13300-13303.

30. Lu, Y.; Liu, G. L.; Kim, J.; Mejia, Y. X.; Lee, L. P., *Nano Letters* **2005,** *5* (1), 119-124.

31. Aroca, R. F.; Alvarez-Puebla, R. A.; Pieczonka, N.; Sanchez-Cortez, S.; Garcia-Ramos, J. V., *Advances in Colloid and Interface Science* **2005,** *116* (1-3), 45-61.

32. Freeman, R. G.; Grabar, K. C.; Allison, K. J.; Bright, R. M.; Davis, J. A.; Guthrie, A. P.; Hommer, M. B.; Jackson, M. A.; Smith, P. C.; Walter, D. G.; Natan, M. J., *Science* **1995,** *267* (5204), 1629-1632.

33. Addison, C. J.; Brolo, A. G., *Langmuir* **2006,** *22* (21), 8696 -8702.

34. Fan, M. K.; Brolo, A. G., *ChemPhysChem* **2008,** *9* (13), 1899-1907.

35. Musick, M. D.; Keating, C. D.; Lyon, L. A.; Botsko, S. L.; Pena, D. J.; Holliway, W. D.; McEvoy, T. M.; Richardson, J. N.; Natan, M. J., *Chemistry of Materials* **2000,** *12* (10), 2869-2881.

36. Jackson, J. B.; Halas, N. J., *Proceedings of the National Academy of Sciences of the United States of America* **2004,** *101* (52), 17930-17935.

37. Peng, C.; Song, Y.; Wei, G.; Zhang, W.; Li, Z.; Dong, W. F., *Journal of Colloid and Interface Science* **2008,** *317* (1), 183-190.

38. Aroca, R. F.; Goulet, P. J. G.; dos Santos, D. S.; Alvarez-Puebla, R. A.; Oliveira, O. N., *Analytical Chemistry* **2005,** *77* (2), 378-382.

39. Kho, K. W.; Shen, Z. X.; Zeng, H. C.; Soo, K. C.; Olivo, M., *Analytical Chemistry* **2005,** *77* (22), 7462-7471.

40. Zhao, S.; Zhang, K.; An, J.; Sun, Y. Y.; Sun, C. Q., *Materials Letters* **2006,** *60* (9-10), 1215-1218.

41. Tao, A.; Kim, F.; Hess, C.; Goldberger, J.; He, R. R.; Sun, Y. G.; Xia, Y. N.; Yang, P. D., *Nano Letters* **2003,** *3* (9), 1229-1233.

42. Wei, G.; Wang, L.; Sun, L. L.; Song, Y. H.; Sun, Y. J.; Guo, C. L.; Yang, T.; Li, Z. A., *Journal of Physical Chemistry C* **2007,** *111* (5), 1976-1982.

43. Pieczonka, N. P. W.; Goulet, P. J. G.; Aroca, R. F., *Journal of the American Chemical Society* **2006,** *128* (39), 12626-12627.

44. Li, X. L.; Xu, W. Q.; Zhang, J. H.; Jia, H. Y.; Yang, B.; Zhao, B.; Li, B. F.; Ozaki, Y., *Langmuir* **2004,** *20* (4), 1298-1304.

45. Goulet, P. J. G.; dos Santos, D. S.; Alvarez-Puebla, R. A.; Oliveira, O. N.; Aroca, R. F., *Langmuir* **2005,** *21* (12), 5576-5581.

46. Tan, S.; Erol, M.; Attygalle, A.; Du, H.; Sukhishvili, S., *Langmuir* **2007,** *23* (19), 9836-9843.

47. Han, Y.; Sukhishvili, S.; Du, H.; Cefaloni, J.; Smolinsko, B., *Journal of Nanoscience and Nanotechnology* **2008,** *8* (11), 5791-5800.

48. Tan, S.; Erol, M.; Sukhishvili, S.; Du, H., *Langmuir* **2008,** *24* (9), 4765-4771.

49. Ahonen, P.; Laaksonen, T.; Nykanen, A.; Ruokolainen, J.; Kontturi, K., *Journal of Physical Chemistry B* **2006,** *110* (26), 12954-12958.

50. Joo, S. W.; Han, S. W.; Kim, K., *Journal of Physical Chemistry B* **2000,** *104* (26), 6218-6224.

51. Jena, B. K.; Raj, C. R., *Analytical Chemistry* **2006,** *78* (18), 6332-6339.

52. Bauer, G.; Hassmann, J.; Walter, H.; Haglmuller, J.; Mayer, C.; Schalkhammer, T., *Nanotechnology* **2003,** *14* (12), 1289-1311.

53. Bertoluzza, A.; Fagnano, C.; Morelli, M. A.; Gottardi, V.; Guglielmi, M., *Journal of Non-Crystalline Solids* **1982,** *48* (1), 117-128.

54. Mondragon, M. A.; Castano, V. M.; Garcia, J.; Tellez, C. A., *Vibrational Spectroscopy* **1995,** *9* (3), 293-304.

55. Akbarian, F.; Dunn, B. S.; Zink, J. I., *Journal of Raman Spectroscopy* **1996,** *27* (10), 775-783.

56. Zhu, Z. H.; Zhu, T.; Liu, Z. F., *Nanotechnology* **2004,** *15* (3), 357-364.

57. Scott, D. W., *Biometrika* **1979,** *66* (3), 605-610.

58. Limpert, E.; Stahel, W. A.; Abbt, M., *Bioscience* **2001,** *51* (5), 341-352.

Chapter 4: Characterization of a Layer-by-layer biofuel cell anode by (*in-situ*) vibrational spectroscopy

This chapter is a manuscript submitted. It is a work based on a collaboration project with Harrington group in University of Victoria. Dr. Manuel Marechal and Amanda Finn contributed to the development of the anode, Dr. Marechal also performed the cyclic voltammetry analysis.

Polarization modulation infrared reflection absorption spectroscopy (PM-IRRAS) and (*in situ*) surface-enhanced (resonant) Raman scattering (SE(R)RS) were used as "quality control" tools during the construction of a model biofuel cell anode. The model anode was a layered structure formed by 4-hydroxythiophenol (HTP) attached to a coenzyme analog, Cibacron blue F3G-A (CB), which then supported the adsorption of the enzyme formaldehyde dehydrogenase (FalDH). *Ex situ* SERS and PM-IRRAS showed that HTP binds to a gold surface through its thiol group. The binding of CB to the HTP layer was shown by a combination of *ex situ* and *in situ* SERS data. *In situ* SERS spectra after immobilization of FalDH to the CB layer confirmed successful enzyme immobilization.

4.1 Introduction

Biofuel cells use microorganisms or enzymes, instead of inorganic catalysts, in at least one of their electrodes.[1-4] Their fuels can be as simple as hydrogen or methane or as complicated as sugars. Compared with conventional fuel cells, biofuel cells are more selective to a particular fuel, and have the advantages of working at ambient temperature and physiological pH. These advantages make them suitable for applications as implantable devices and portable power supplies.

Currently, however, enzyme-based biofuel cells still present two important disadvantages: low power density and short lifetime. Proper enzyme immobilization helps to minimize both of these issues.[2, 4-5] Enzymes immobilized at the right orientation are necessary to optimize the electron transfer efficiency to the electrode, producing higher power density.[4, 6] For example, it is found that catalytic activity of laccase was greatly affected by the immobilization method (physical adsorption versus chemical binding).[7]

To help understand and eventually solve some of these difficulties, many techniques have been developed and used to monitor the enzyme immobilization procedure. For example, AFM[8-11] can monitor the immobilization of enzymes and the morphological changes at the electrode. There are also reports about the application of scanning electrochemical microscopy (SECM)[12] and X-ray photoelectron spectroscopy (XPS)[13] for the same purpose.

Vibrational spectroscopic methods, which can give direct information about the presence and orientation of surface bound molecules, have also been applied in biofuel cell research.[1, 14] Surface-enhanced Raman scattering (SERS) is a very sensitive vibrational spectroscopic method.[15] The origins of SERS are generally linked to two groups of mechanisms: the charge transfer (CT) and the electromagnetic (EM) mechanisms.[16-18] The former originates from resonant transitions involving the metal's Fermi level and the molecule's frontier orbitals, and only affects molecules directly attached to the metal surface.[16, 19-20] The latter is related to LSPR and accounts for most of the observed features in SERS.[16, 19] For instance, the exponential decay of SERS signals with increasing distance from the substrate surface[21] is attributed to the decay of the LSPR field. Meanwhile, if the wavelength of the laser used to excite SERS is within the electronic absorption range of the adsorbed molecule, an extra enhancement of one to two orders of magnitude can be achieved in a process called surface-enhanced resonance Raman scattering (SERRS). However, despite the many merits of the SERS technique,[17, 19] examples of its application for the characterization of "multi-layers" of adsorbates on surfaces are still limited.[22-24] We are also not aware of any reports on the application of SERS in biofuel research. The objective of the present work is to demonstrate that SERS can be used to characterize a multilayer biofuel cell anode. A well established three "layers" sample anode (Scheme 4-1) was chosen as the model system.[1, 25-28] The results showed that the unique vibrational signature of each component of the "layer-by-layer" anode was present after each adsorption step.

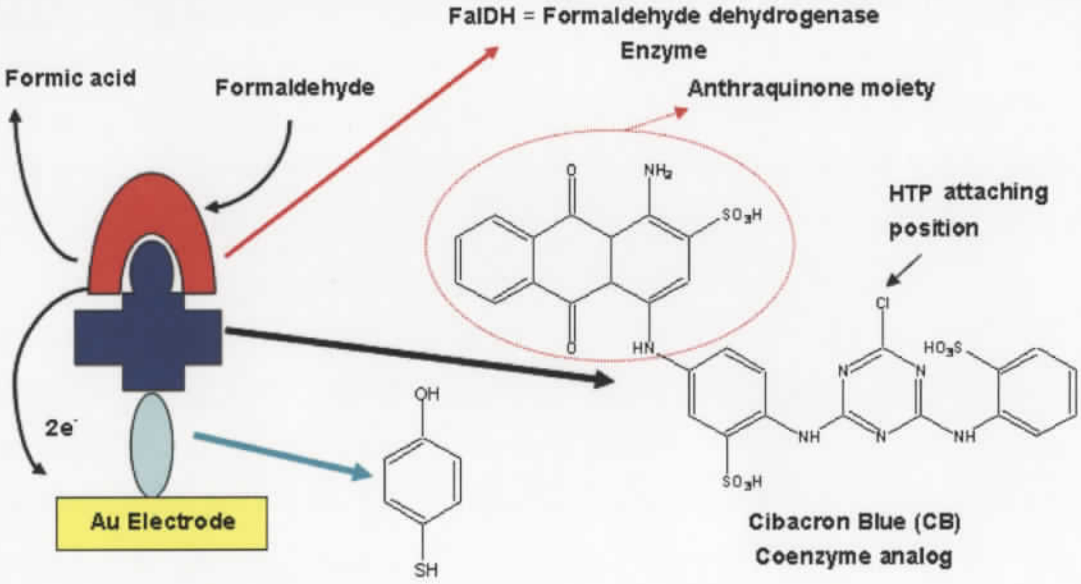

Scheme 4- 1 Schematic representation of the configuration of the model biofuel cell anode.

4.2 Materials and methods

4.2.1 Chemicals

Unless otherwise mentioned, ACS grade chemicals were used. $HAuCl_4$, sodium citrate dihydrate, 1,3-propanedithiol (PDT), 4-hydroxythiophenol (4-HTP), Cibacron Blue F3G-A (CB), and FalDH (5.06 units/mg) were obtained from Sigma-Aldrich. Methanol at HPLC grade was obtained from Caledon Laboratories Ltd. Gold slides (100 nm thick Au deposited on glass coated with a 5 nm Cr adhesion layer) were obtained from Evaporated Metal Films Inc.

Ultrapure water with a resistivity of 18.2 MΩ·cm (from Barnstead NANOpure Diamond water purification system) was used throughout the experiments.

4.2.2 Substrate preparation

SERS substrates are the nanostructured surfaces of noble metals (mainly Cu, Ag and Au) that support the surface-enhancement effect. All SERS measurements were realized using Au nanoparticles (NPs) deposited on Au slides, which were described elsewhere.[29-30] The 13 nm Au NPs were synthesized using established procedures and the NPs were deposited using PDT as linker. A total of nine Au NP "layers" were used in all experiments.

4.2.3 Sample preparation – biofuel cell anode (see Scheme 4-1)

HTP SAM preparation

2 mM of HTP was prepared in ethanol. The electrode (either the SERS substrate or a smooth gold film[30-31] used for PM-IRRAS) was immersed in the HTP ethanolic solution overnight. After that, the slides were rinsed with excess ethanol and dried with N_2. Samples containing a HTP monolayer on the gold (nanoparticle) surface are denoted throughout the text as Au/HTP.

Anchoring of CB

CB (1 mM) was dissolved in a H_3BO_3-KCl-NaOH buffer (pH 11). The reaction conditions were the same as described by Bertilsson et al[1] for their alcoholic type linker. Briefly, HTP modified slides were immersed in the 1 mM CB solution and left in a water bath (80°C) for 8 hours. After that, the slides were taken out and rinsed with excess water. This type of sample is denoted throughout the text as Au/HTP/CB.

FalDH enzyme binding

FalDH was dissolved in pH 8 phosphate buffer at 8 units/mL (~1.6 mg/mL). The FalDH solution was drop-coated onto the as-prepared Au/HTP/CB slides and refrigerated overnight. Then it was gently rinsed with phosphate buffer. This type of sample is denoted as Au/ HTP/CB/FalDH.

Control samples

Several control samples were prepared. Physisorbed CB on Au slides (Au/CB) was made by directly immersing the gold slides into CB solutions and using the same experimental procedure for the preparation of Au/HTP/CB (the lack of HTP being the only difference). Drop-coated Au/HTP/CB and Au/CB were prepared by applying a drop of CB dissolved in methanol to the gold surface, with and without the HTP SAM, respectively, and then rinsing with the same solvent.

4.2.4 PM-IRRAS measurement

PM-IRRAS measurement was performed using a Equinox 55 (Bruker) equipped with a photoelastic modulator (PEM-90 with II/ZS50 ZnSe 50 kHz optical head, HINDS instruments inc.) and a liquid N_2 cooled MCT IR detector (Kolmar Technologies). An external reflection configuration was used. The IR beam was directed to the sample surface at a grazing angle. The acquisition time was 10 min for the *difference* spectra and 2 min for the *sum* spectra. The resolution was set at 2 cm^{-1}. The final spectra were obtained by dividing the *difference* spectrum by the *sum* spectrum. The data presented were manually background corrected.

4.2.5 *In situ* and *ex situ* SERS measurement

All the Raman measurements were accomplished using a Raman microscope system equipped with a He-Ne laser source (632.8 nm, Melles Griot). *Ex situ* measurements were taken in air with the samples directly mounted on the stage of an Olympus BHSM microscope. The *in situ* measurements were taken with the substrate immersed in an electrolyte and under electrochemical control. The spectroelectrochemical cell used for *in situ* measurements was also mounted on the stage of the microscope. The Raman experiments were realized in a backscattering configuration, where the exciting laser and the scattered radiation passed through the same 50× Olympus microscope objective. An ultra-long working distance objective 50× (numerical aperture (NA) =0.55) was used for *in situ* measurements, and a regular 50× objective (NA=0.80) was used for the *ex situ* measurements. A Kaiser super notch filter was used to remove the unwanted radiation at the laser frequency. A Kaiser Holospec f/1.4 spectrograph equipped with an Andor CCD detector (model DV-401-BV) was coupled to the microscope. For *in situ* measurement, a three-compartment spectroelectrochemical cell with 1 mm glass window was used. The Au NP modified slides were used as working electrodes. Ag|AgCl|KCl(sat.) was used as reference electrode and a Pt wire was used as a counter electrode. An Autolab PGSTAT 30 potentiostat was used to control the applied potential. All the potential values quoted are versus Ag|AgCl|Cl^-(sat.).

4.3 Results and discussion

The sample biofuel cell anode investigated here (Scheme 4-1) is a slightly modified version of the system reported in the literature.[1, 25-28] The main difference is that a 4-hydroxythiophenol (HTP) was chosen to form the initial self-assembled monolayer (SAM) rather than a long chain alkanelthiol. HTP is a good SERS probe,[32] and, similarly to the long chain alkanethiol, it has a thiol group that attaches to the metal surface and a hydroxyl group that can be functionalized.[30, 33-36] There is an expectation that electron conductivity through the aromatic ring will be enhanced relative to an alkyl chain. In addition, the electrochemical activity of HTP SAM on Au colloids and on flat gold surfaces has been examined.[37-40] A different enzyme, FalDH, was used when compared to the anode previously reported in the literature. The characterization of each of these layers, i.e. the HTP SAM formation, the binding of CB, and the immobilization of the enzyme through the affinity reaction with CB, are presented below.

4.3.1 The "first layer": characterization of the HTP SAM

SERS and PM-IRRAS techniques were used to identify the adsorption of HTP on a gold surface. *In situ* SERS was performed to check the stability of the monolayer.

Adsorption of the HTP SAM on the Au electrode

The SERS and PM-IRAAS results for HTP adsorbed on gold are presented in Fig. 4-1. In Fig. 4-1a, both normal Raman of bulk HTP and the SERS spectrum of HTP SAM adsorbed on a gold electrode modified with Au NPs are presented. The relative intensities of the dominant bands in the bulk at 385, 814, and 918 cm^{-1}, are greatly reduced in the SERS spectrum. *Ab initio* calculations (DFT rb3lyp/6-311^{++}g (3df,3pd)) were performed and showed that all these bands have contributions from the S – H vibration. The PM-IRRAS spectrum of HTP SAM presented in Fig. 4-1b is consistent with this, since the band at 2559 cm^{-1}, which is due to S–H stretching, is completely missing after adsorption. Thus both techniques indicated that the SAM of HTP is formed via bonding of the S atom to the gold, and no evidence for a large amount of "unbound" HTP molecules, as reported before [41], was observed in our case.

Electrochemical stability of the HTP-SAM

The electrochemistry of HTP adsorbed on Au surfaces has been examined by two different groups.[38-40] Both groups reported an anodic current near 0 V at neutral pH. Two different reaction schemes for the HTP oxidation were proposed. Chen [38] suggested a two steps process with a carbonium ion intermediate. Stolarczyk et al,[39-40] on the other hand, pointed out that the oxidation of HTP could only happen after the applied potential was close to 0.5 V in phosphate buffer (pH 7.0), and no Faradaic current was observed when the applied potential was limited to the range between -0.3 and +0.3 V. Based on this observation, Stolarczyk et al[39-40] proposed another mechanism: at 0.5 V in neutral conditions, the HTP molecule loses an electron and a proton from the -OH group to form a radical. Once formed, the radical will quickly attack neighboring HTP and form a dimer. This dimer then is partially desorbed and hydrolyzed to form a species containing a quinone moiety. The last product corresponds to the observed Faradic current at around 0 V.

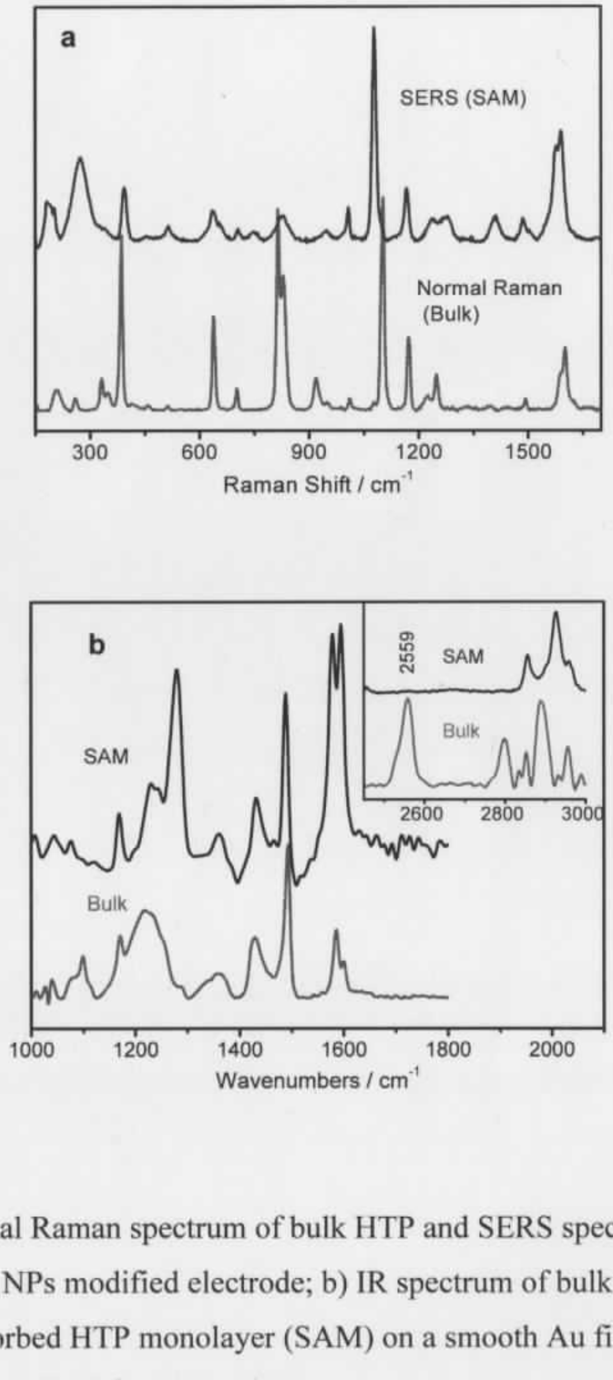

Figure 4- 1 a) Normal Raman spectrum of bulk HTP and SERS spectrum of adsorbed HTP (SAM) on Au NPs modified electrode; b) IR spectrum of bulk HTP and PM-IRAAS spectrum of an adsorbed HTP monolayer (SAM) on a smooth Au film. The intensities of all spectra were normalized for comparison.

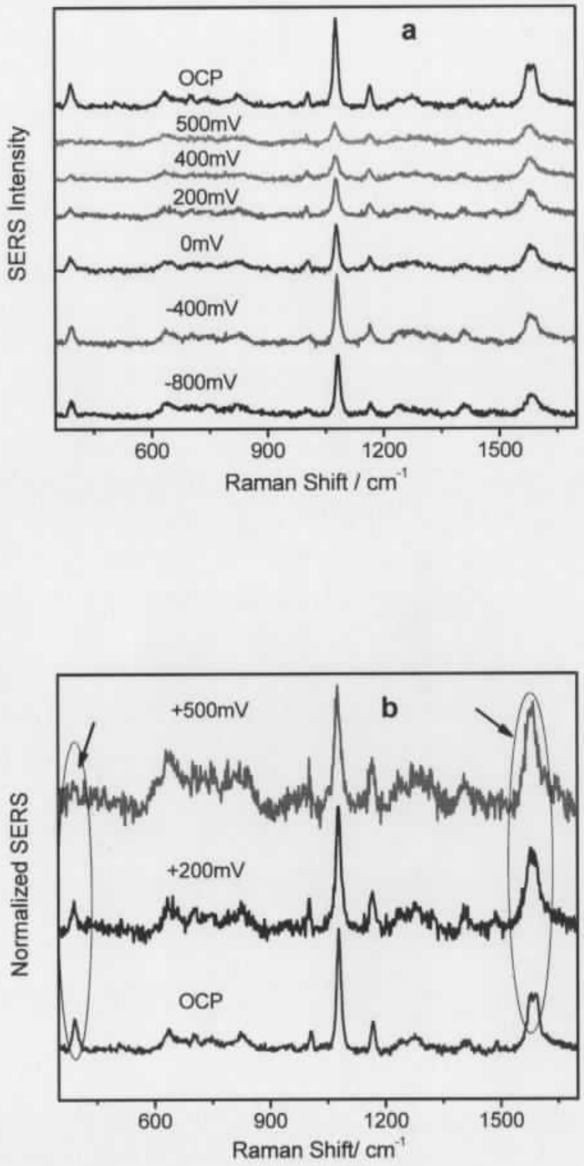

Figure 4- 2 (*a*) *in situ* SERS of HTP on Au NPs modified electrode from -800mV to +500 mV; (*b*) same as (a) but zoomed at selected potentials for comparison. Electrolyte: 0.1 M KCl. Potential was scanned from -800 mV towards positive values. OCP, measured independently, was close to -100 mV.

We are particularly interested in the electrochemical stability of the HTP SAM, because our biofuel cell sample anode operates up to 0.3 V. Fig. 4-2 shows the *in situ* SERS of HTP on an Au NP modified electrode at different applied potentials. The spectra were recorded within the potential range from -800 mV to +500 mV in steps of 100 mV. Fig. 4-2a shows that the overall SERS intensity decreases as the potential is made more positive. Three possible processes can contribute to the decrease in SERS intensity: 1) it might be an effect of losing the CT contributions to the SERS signal;[16, 20] 2) the substrate structure (adsorbed Au NPs) might not be stable at relative positive potentials; or 3) the electrochemical oxidation of the HTP molecule occurs. Analysis of normalized HTP spectra didn't show significant changes in the relative intensities from -800 mV to 200 mV, which indicates that no electrochemical reaction involving HTP took place in that potential range, contradicting the findings suggested by Chen.[38] The electrochemical stability of the Au NPs electrode was established in our previous work, and no major contributions from the substrate is expected for potentials more negative than +300 mV.[30] Hence, we concluded that the decreasing SERS signal up to 200 mV should be assigned to the losing of CT contribution. At potentials more positive than +200 mV, the electrochemical activity of HTP starts to play a major role. This is well illustrated in Fig. 4-2b, where the spectra of HTP from three potentials were normalized using the band at ~1080 cm^{-1}. Two regions with significant changes are identified in Fig. 4-2b. Note that only HTP bands and their relative intensities are compared, and no contribution from the substrate is observed (the background SERS from the substrate is much weaker than for HTP). The HTP SERS at +200 mV is very close to that at OCP (~ -100 mV). However, when the potential was further increased (more positive than +200 mV), the band at around 390 cm^{-1} disappeared, and the one at around 1580 cm^{-1} was enhanced (relative to the 1080 cm^{-1}). Our calculations showed that the C-O-H functional group contributed most to these two bands. Hence, these spectral changes indicate that an electrochemical reaction took place on the C-O-H functional group at +500 mV, which is consistent with the formation of a dimer suggested by Stolarczyk.[39-40]

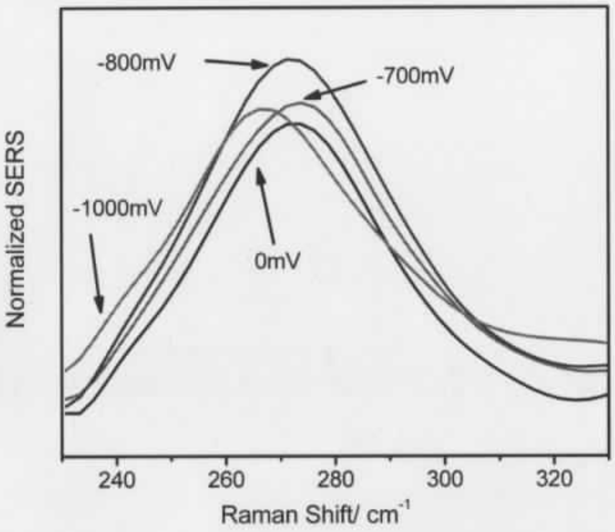

Figure 4-3 *In situ* SERS of HTP at different potentials. On the Au - S region is shown. The potential scan starts from 0 V towards negative values. Electrolyte: 0.1M KCl. The spectra were normalized using a band from the SERS substrate at around 1410 cm^{-1}.

The reductive desorption of the HTP monolayer was also investigated. Fig. 4-3 shows the *in situ* SERS measurement for HTP adsorbed on Au at negative potentials. The band shown in Fig. 4-3 is assigned to the Au – S stretch.[30] The Au – S band is recorded at 273 cm^{-1} at positive potentials and it does not shift between 0 to -700 mV. However, when the potential reached a region between -800 to -1000 mV, the Au-S band shifts to lower frequency (from 273cm^{-1} to 266cm^{-1}). This shift can be interpreted as weakening of the Au-S bond at the onset of the monolayer reduction. It is then possible to conclude that the HTP monolayer might start to desorb at around -800 mV. Note that this band will not totally disappear even if the HTP molecules are completely desorbed since the SERS substrate also has Au – S band in that region.[30]

The results from Figs. 4-2 and 4-3 suggest that the HTP monolayer is stable in the potential range between -700 mV and +200 mV. HTP will desorb from the surface at potentials more negative than -800 mV and the –OH group will be oxidized at +500 mV.

4.3.2 The second "layer": CB immobilization and characterization

As seen in Scheme 4-1, CB has a diaminoanthroquinone (DAAQ) chromophore, responsible for a broad electronic absorption band between 400 to 700 nm.[26, 42] Since the wavelength of the laser used in the SERS measurements was 632.8 nm (in resonance with a molecular electronic transition), the adsorbed CB yielded a very strong SERRS signal. Moreover, the SERRS spectrum of CB was very similar to that of 1,4-DAAQ. [43-44] However, as shown in Scheme 4-1, the suggested HTP attaching position is not on the DAAQ moiety. Also, due to the resonance effect, the CB signal is much stronger and practically obscures the bottom HTP layer. These difficulties were tackled by carefully designing experiments to help elucidate whether the CB was bound onto HTP from the SERS signal of the bilayer.

A series of *ex-situ* SERS experiment (in air and without potential control) was first carried out from samples consisting of CB simply drop-coated onto Au NPs modified slides with and without HTP SAMs (these samples will be referred to as drop coated Au/HTP/CB and drop coated Au/CB, respectively). After the SERS measurements, the same samples were then immersed in CB solution and incubated at 80 °C for 8 hours, which are the conditions to chemically react CB with HTP. The *ex situ* SERS spectra were recorded again after that treatment.

The SERS spectra of the drop coated CB samples were compared to the ones obtained after incubation in basic solution to determine any difference between CB just physisorbed and CB that actually reacted with the HTP monolayer. The spectra were normalized by the dominating CB band at 1268 cm^{-1} and the difference spectra (between Au/HTP/CB and Au/CB, before or after incubation, respectively) are shown in Fig. 4-4. Fig. 4-4a is the normalized and baseline corrected SERS spectra of Au/HTP/CB and Au/CB (both before and after incubation), where Fig. 4-4b is the difference between the Au/HTP/CB and Au/CB (black line: difference before incubation, i.e. drop coated; *red line*: difference after incubation, i.e. after reaction). The difference spectrum obtained from the drop-coated sample (drop coated Au/HTP/CB - Au/CB, Fig. 4-4b black line) closely resembles the SERS spectrum of HTP SAM (Fig. 4-1a). This is expected because CB is only physisorbed (drop-coated) in these cases. That is, the SERS spectrum of drop coated Au/HTP/CB is just the sum of both SER(R)S from CB and HTP. On the other hand, the difference spectrum obtained after incubation (Au/HTP/CB - Au/CB, Fig. 4-4b red curve) showed some interesting changes, although it still presented the main features of the HTP spectrum (Fig. 4-1a). As shown by arrows in Fig. 4-4b, the HTP bands shifted (4~12 cm^{-1}) after incubation in basic solution. These shifts suggest the successful immobilization of CB molecules through a chemical bond with the HTP molecules. Fig. 4-4b also clearly shows a valley at ~1350 cm^{-1}. This is caused by the changing of relative SERRS intensity of CB after incubation, which points towards some sort of surface re-organization for CB after binding (which might be connected to a preferential orientation of the chemically attached CB). Both the HTP band shifts and the changes in relative intensities of the CB features are consistent with a successful immobilization of CB mediated by HTP.

Further evidence of CB binding to the HTP linker was sought through *in situ* SERS measurements (under electrochemical control). The dependence of the strongest SERRS band of CB at 1268 cm^{-1} (Fig. 4-4a) at neutral pH (pH 6.7, i.e., in 0.1 M KCl as electrolyte) with the applied potential was obtained for both the Au/CB and the Au/HTP/CB sample (Fig. 4-5). As can be seen in Fig. 4-5, the overall SERRS signal of the CB band at 1268 cm^{-1} from Au/HTP/CB is lower than from the Au/CB in the whole potential range investigated. This suggests the presence of the HTP, since the SAM would keep the CB molecules further away from the surface, reducing their SERS activity (according to EM theory, the SERS signal should decrease with the distance from the surface[19]). Another interesting aspect of Fig. 4-5 is that both Au/CB and Au/HTP/CB show maximum SERRS signal when the potential reaches -800 mV, and the SERRS intensity decreases sharply as the potential is swept to more negative values. The decrease of SERRS signal at potentials more negative than -800 mV is assigned to the reduction of CB. The electrochemical reduction process is better illustrated in Figs. 4-6a and 4-6b. As the potential is swept to more negative values, the band around 1640 cm^{-1} diminishes for both systems, Au/CB and Au/HTP/CB, and a new band appears at around 1580 cm^{-1}(Figs. 4-6a and 4-6b). These changes are consistent with the reduction of the DAAQ moiety of CB from the quinone to the hydroquinone form at potentials more negative than -800 mV.[45-46] These results also show that CB binding to HTP does not affect the electrochemical properties of the DAAQ moiety.

In summary, for *ex situ* SE(R)RS experiments, the difference spectrum between drop-coated Au/HTP/CB and Au/CB resembles the HTP SERS spectrum. However, band-shifts were found for HTP after incubation in basic medium, indicating the successful reaction between CB and HTP. *In situ* SERRS consistently showed intensity differences between the Au/CB and the Au/HTP/CB. The overall SERRS signal from CB molecules is reduced by the presence of the HTP SAM, which is consistent with a spacer between CB molecules and the electrode surface. The drop of the SERRS signal at potentials more negative than -900 mV for both Au/CB and Au/HTP/CB is caused by the reduction of the DAAQ moiety. All these evidences suggest that CB molecules were successfully linked onto the electrode surface though HTP in the Au/HTP/CB system.

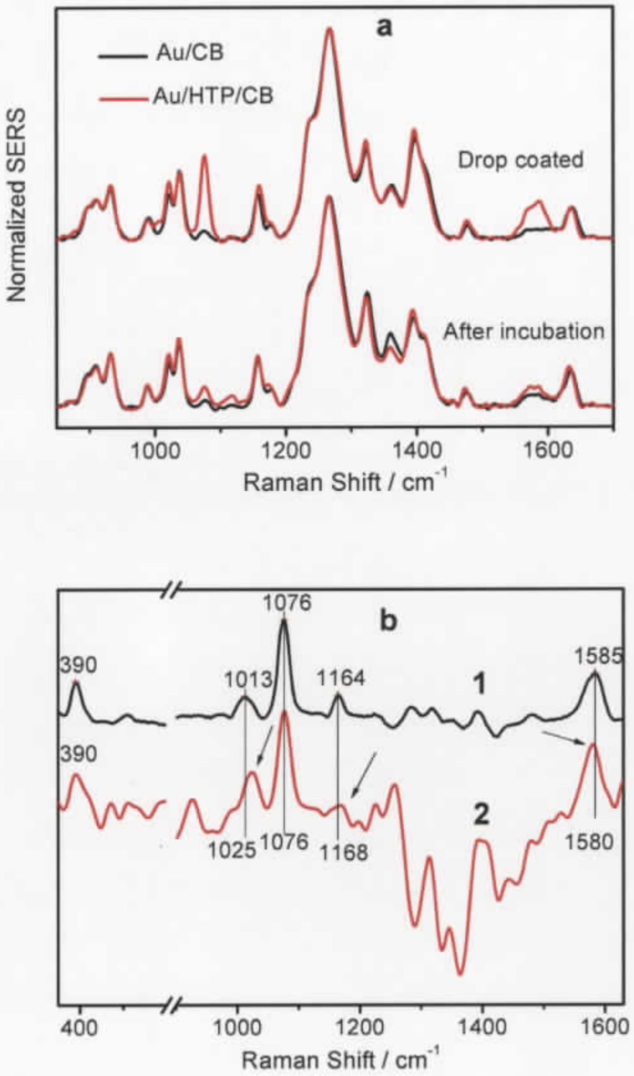

Figure 4- 4 a) *Ex situ* SERS spectra of drop coated Au/CB, drop coated Au/HTP/CB, Au/CB after incubated in conditions that promote the reaction between the OH group of the HTP and CB, and Au/HTP/CB after incubated in conditions that promote the reaction between the OH group of the HTP and CB. The spectra were normalized using the CB band at 1268 cm^{-1}; b) *Black line*. Difference spectrum between drop-coated Au/HTP/CB and drop coated Au/CB. *Red line*. Difference spectra between Au/HTP/CB and Au/CB

after incubation in basic solution (which promote chemical reaction between HTP and CB). The difference spectra were normalized using the HTP band at ~ 1080 cm^{-1}. The arrows indicate the bands that shifted after incubation. The difference spectra were obtained after all the spectra were normalized using the CB band at 1268 cm^{-1} and baseline corrected.

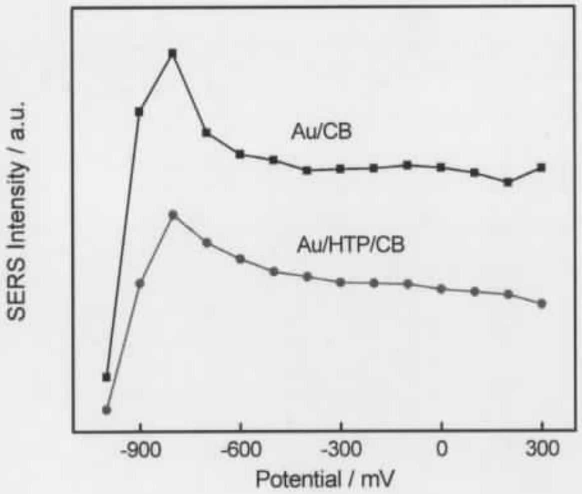

Figure 4- 5 SERS intensity vs. potential plots for the CB band at 1268 cm^{-1}. Electrolyte: 0.1 M KCl (pH≈6.7). The potential was scanned from positive towards negative values.

4.3.3 "The third layer": The enzyme immobilization and characterization.

Protein adsorption has been shown to change the SERS spectrum of linker molecules.[24] Since the SERRS signal from the CB will still be dominant after the adsorption of the enzymes, the direct observation of strong bands from the protein adsorption are not expected. Fig. 4-7 shows the *in situ* SERS spectra of the Au/HTP/CB anode with and without the enzyme FalDH (Fig. 4-7a) and their difference spectra (Fig. 4-7b) obtained at different applied potentials. The CB SERRS band at 1268 cm^{-1} was normalized to facilitate the comparison between the samples (with and without the presence of the protein). Changes in relative intensities were observed in Fig. 4-7a at ~1400 cm^{-1} and ~1580 cm^{-1} after incubation with FalDH (indicated by arrows). Some band shifts were also observed. For example, the band at ~1636 cm^{-1} at 0 mV, assigned to the C=O group in the DAAQ moiety, shifted to higher frequency (~1639 cm^{-1}) in the presence of FalDH. All these changes are better illustrated in the difference spectra (Fig. 4-7b), where two positive bands and a negative band were found at those positions shown in Fig. 4-7a.

These spectral differences indicate that the immobilization of the enzyme was successful. The CV data, shown in Fig. 4-8, confirmed the catalytic activity of the anode after the protein immobilization. The band shift at ~1636 cm^{-1} may be related to the disturbance of the intramolecular hydrogen bond of CB due to the protein binding.[45] The broad band at ~1580 cm^{-1} is a direct proof of the enzyme presence, since this band can be assigned to amide II and/or tyrosine residues of the enzyme.[47-48] The changes at ~1400 cm^{-1} –region are more complex. The increase of the shoulder at ~1412 cm^{-1} may be a contribution from the enzyme, since proteins have a band in this region.[47] It can also be the result of changes in the CB local environment since there is a report for 1,4-DAAQ[43], the chromophore in CB, indicating pH dependent SERS intensity changes in that region. The important point is that either of these possible explanations for the changes around 1400 cm^{-1} supports the presence of the enzyme adsorbed enzyme on the CB layer.

In summary, we showed that vibrational spectroscopy, particularly SERS, can be used to follow the formation of multilayers of different components in a biofuel cell model anode. Since every component and their interactions can be identified, we suggested that this type of characterization should be useful to prove successful immobilization and to further understand the proper adsorption modes that lead to successful biofuel cell electrodes.

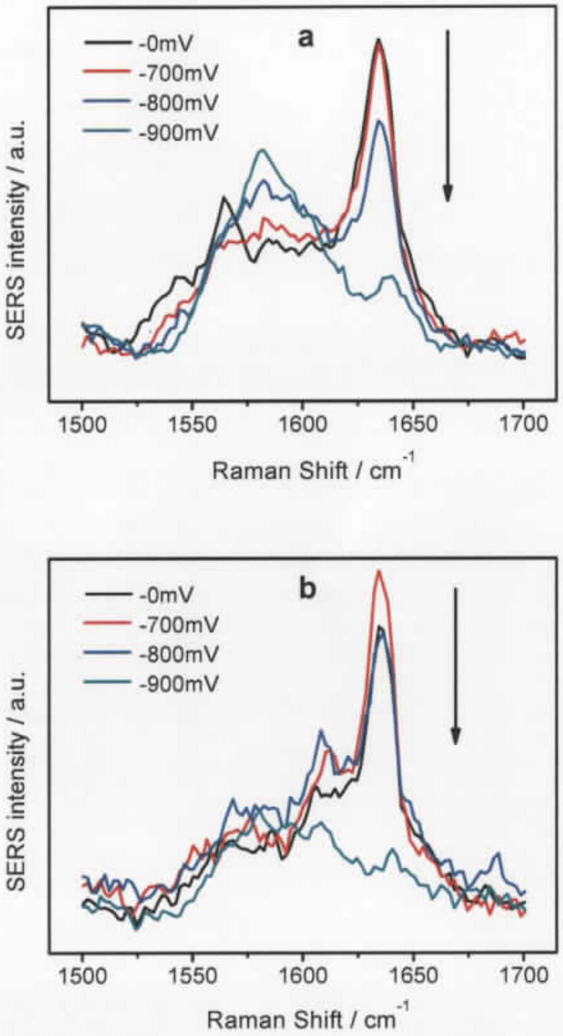

Figure 4-6 a) *In situ* SERS spectra of Au/CB at neutral conditions at different applied potentials; *b*) *In situ* SERS spectra of Au/HTP/CB at neutral conditions at different applied potentials. The potential scan was initiated at more positive values towards negative potentials. Electrolyte: 0.1 M KCl (pH≈6.7). Arrows show the directions of the changes in relative intensities.

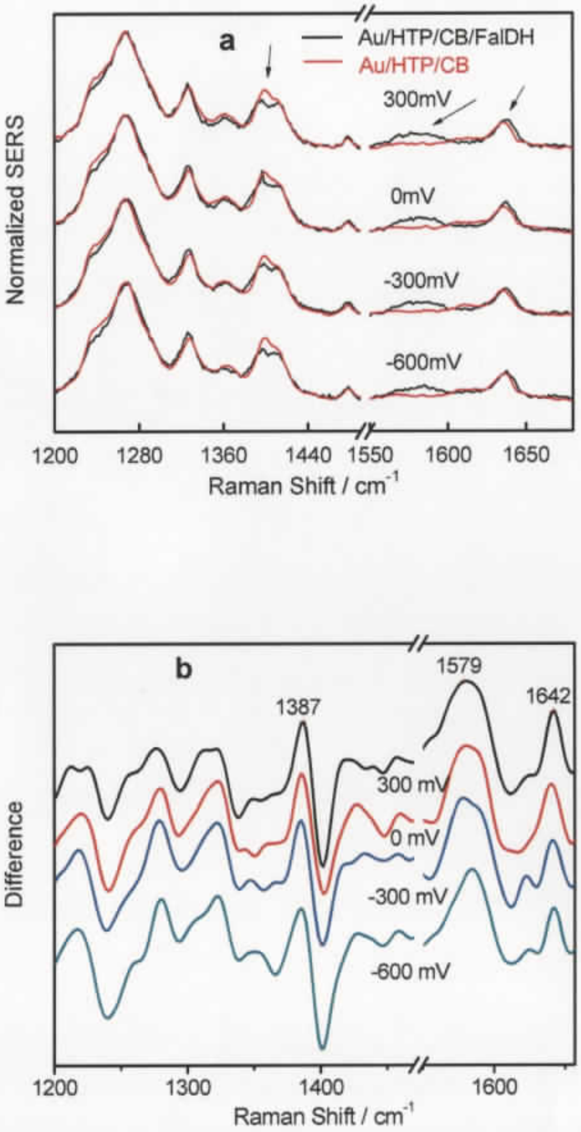

Figure 4- 7 a) *In-situ* SERS of the anode (with and without the enzyme FalDH) at different potentials; b) The difference between the SERS spectra with and without the enzyme. Electrolyte: 0.1 M KCl.

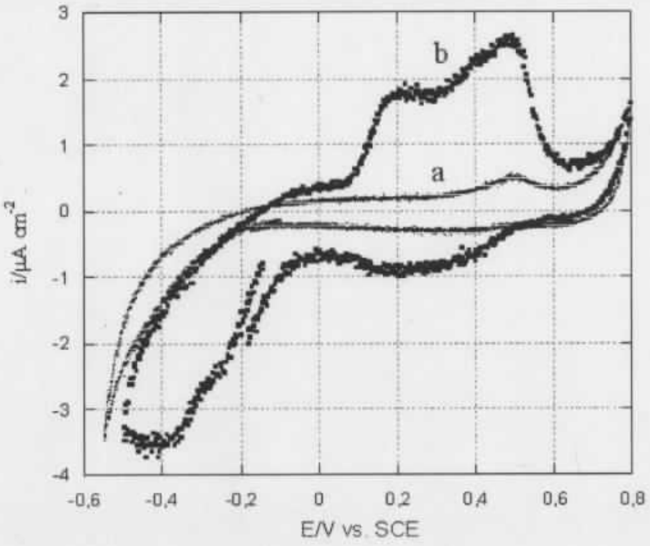

Figure 4-8 Cyclic voltammograms obtained with Au/HTP/CB/FalDH electrode before (a) and after (b) formaldehyde adding (50 μmol·L-1). Scan rate 50 mV·s-1 in 50 mM tris buffer (pH=7.4).

4.4 conclusion

A sample biofuel cell anode was investigated by vibrational spectroscopy. A SAM of HTP was first examined in terms of adsorption characteristics and the *in situ* electrochemical stability. Then, the enzyme linker, CB, was added to the HTP SAM. Although the SERS signal from the HTP was largely masked by the CB due to its large

SERRS effect, the chemical interaction between HTP-CB was obtained by examining combinations of *ex-situ* and *in situ* SERS. These suggest that the CB molecule was successfully linked onto the HTP SAM. *In situ* SERS of the anode in the presence of enzyme FalDH was recorded and compared with the situation where the enzyme was absent. The spectral changes provoked by the enzyme imply that its immobilization was successful, which is in agreement with electrochemical measurement (Fig. 4-8). In summary, we showed that the layer by layer modification of a biofuel cell electrode or a biosensor can be monitored *in situ* and in stepwise fashion by SERS.

4.5 References:

1. Bertilsson, L.; Butt, H. J.; Nelles, G.; Schlereth, D. D., *Biosensors & Bioelectronics* **1997,** *12* (8), 839-852.

2. Davis, F.; Higson, S. P. J., *Biosensors & Bioelectronics* **2007,** *22* (7), 1224-1235.

3. Sarma, A. K.; Vatsyayan, P.; Goswami, P.; Minteer, S. D., *Biosensors & Bioelectronics* **2009,** *24* (8), 2313-2322.

4. Kim, J.; Jia, H. F.; Wang, P., *Biotechnology Advances* **2006,** *24* (3), 296-308.

5. Siqueira Jr, J. R.; Caseli, L.; Crespilho, F. N.; Zucolotto, V.; Oliveira Jr, O. N., *Biosensors & Bioelectronics DOI: 10.1016/j.bios.2009.09.043.*

6. Barton, S. C.; Gallaway, J.; Atanassov, P., *Chemical Reviews* **2004,** *104* (10), 4867-4886.

7. Gupta, G.; Rajendran, V.; Atanassov, P., *Electroanalysis* **2004,** *16* (13-14), 1182-1185.

8. Cusma, A.; Curulli, A.; Zane, D.; Kauhs, S.; Padeletti, G., *Materials Science & Engineering C-Biomimetic and Supramolecular Systems* **2007,** *27* (5-8), 1158-1161.

9. Tan, Y. H.; Liu, M.; Nolting, B.; Go, J. G.; Gervay-Hague, J.; Liu, G. Y., *ACS Nano* **2008,** *2* (11), 2374-2384.

10. Willner, I.; Katz, E., *Angewandte Chemie-International Edition* **2000,** *39* (7), 1180-1218.

11. Zhang, P.; Tan, W. H., *Fresenius Journal of Analytical Chemistry* **2001,** *369* (3-4), 302-307.

12. Guadagnini, L.; Ballarin, B.; Mignani, A.; Scavetta, E.; Tonelli, D., *Sensors and Actuators B-Chemical* **2007,** *126* (2), 492-498.

13. Libertino, S.; Scandurra, A.; Aiello, V.; Giannazzo, F.; Sinatra, F.; Renis, M.; Fichera, M., *Applied Surface Science* **2007,** *253* (23), 9116-9123.

14. Han, E.; Shan, D.; Xue, H. G.; Cosnier, S., *Biomacromolecules* **2007,** *8* (3), 971-975.

15. Qian, X. M.; Nie, S. M., *Chemical Society Reviews* **2008,** *37* (5), 912-920.

16. Brolo, A. G.; Irish, D. E.; Smith, B. D., *Journal of Molecular Structure* **1997,** *405* (1), 29-44.

17. Baker, G. A.; Moore, D. S., *Analytical and Bioanalytical Chemistry* **2005,** *382* (8), 1751-1770.

18. Vo-Dinh, T., *Trac-Trends in Analytical Chemistry* **1998,** *17* (8-9), 557-582.

19. Campion, A.; Kambhampati, P., *Chemical Society Reviews* **1998,** *27* (4), 241-250.

20. Otto, A.; Futamata, M., Electronic mechanisms of SERS. In *Surface-Enhanced Raman Scattering: Physics and Applications*, 2006; Vol. 103, pp 147-182.

21. Barnes, W. L.; Dereux, A.; Ebbesen, T. W., *Nature* **2003,** *424* (6950), 824-830.

22. Jiao, L. S.; Wang, Z. J.; Niu, L.; Shen, J.; You, T. Y.; Dong, S. J.; Ivaska, A., *Journal of Solid State Electrochemistry* **2006,** *10* (11), 886-893.

23. Joo, S. W.; Han, S. W.; Kim, K., *Langmuir* **2000,** *16* (12), 5391-5396.

24. Kudelski, A., *Vibrational Spectroscopy* **2003,** *33* (1-2), 197-204.

25. Schlereth, D. C., *Sensors and Actuators B-Chemical* **1997,** *43* (1-3), 78-86.

26. Schlereth, D. D., *Journal of Electroanalytical Chemistry* **1997,** *425* (1-2), 77-85.

27. Schlereth, D. D.; Kooyman, R. P. H., *Journal of Electroanalytical Chemistry* **1997,** *431* (2), 285-295.

28. Schlereth, D. D.; Kooyman, R. P. H., *Journal of Electroanalytical Chemistry* **1998,** *444* (2), 231-240.

29. Addison, C. J.; Brolo, A. G., *Langmuir* **2006,** *22* (21), 8696 -8702.

30. Fan, M. K.; Brolo, A. G., *ChemPhysChem* **2008,** *9* (13), 1899-1907.

31. Grabar, K. C.; Freeman, R. G.; Hommer, M. B.; Natan, M. J., *Analytical Chemistry* **1995,** *67* (4), 735-743.

32. Lee, H. M.; Kim, M. S.; Kim, K., *Vibrational Spectroscopy* **1994,** *6* (2), 205-214.

33. Barriet, D.; Yam, C. M.; Shmakova, O. E.; Jamison, A. C.; Lee, T. R., *Langmuir* **2007,** *23* (17), 8866-8875.

34. Brust, M.; Fink, J.; Bethell, D.; Schiffrin, D. J.; Kiely, C., *Journal of the Chemical Society-Chemical Communications* **1995,** (16), 1655-1656.

35. Sabapathy, R. C.; Crooks, R. M., *Langmuir* **2000,** *16* (4), 1777-1782.

36. Sun, L.; Thomas, R. C.; Crooks, R. M.; Ricco, A. J., *Journal of the American Chemical Society* **1991,** *113* (22), 8550-8552.

37. Chailapakul, O.; Crooks, R. M., *Langmuir* **1995,** *11* (4), 1329-1340.

38. Chen, S. W., *Langmuir* **1999,** *15* (22), 7551-7557.

39. Stolarczyk, K.; Palys, B.; Bilewicz, R., *Journal of Electroanalytical Chemistry* **2004,** *564* (1-2), 93-98.

40. Stolarczyk, K.; Bilewicz, R., *Electroanalysis* **2004,** *16* (19), 1609-1615.

41. Lee, J. R. I.; Han, T. Y. J.; Willey, T. M.; Wang, D.; Meulenberg, R. W.; Nilsson, J.; Dove, P. M.; Terminello, L. J.; van Buuren, T.; De Yoreo, J. J., *Journal of the American Chemical Society* **2007,** *129* (34), 10370-10381.

42. Viana, E. R. C.; Pereira, F. C.; Zanoni, M. V. B., *Dyes and Pigments* **2006,** *71* (2), 145-152.

43. Lee, C. J.; Kang, J. S.; Park, Y. T.; Rezaul, K. M.; Lee, M. S., *Bulletin of the Korean Chemical Society* **2004,** *25* (12), 1779-1783.

44. Jayaraj, S. E.; Ramakrishnan, V., *Spectroscopy Letters* **1999,** *32* (1), 103-113.

45. Jamali, M.; Bernede, J. C.; Le Ny, R., *Thin Solid Films* **1999,** *346* (1-2), 181-185.

46. Carneiro, P. A.; Boralle, N.; Stradiotto, N. R.; Furlan, M.; Zanoni, M. V. B., *Journal of the Brazilian Chemical Society* **2004,** *15* (4), 587-594.

47. Kneipp, J.; Kneipp, H.; McLaughlin, M.; Brown, D.; Kneipp, K., *Nano Letters* **2006,** *6* (10), 2225-2231.

48. Kumar, G. V. P.; Shruthi, S.; Vibha, B.; Reddy, B. A. A.; Kundu, T. K.; Narayana, C., *Journal of Physical Chemistry C* **2007,** *111* (11), 4388-4392.

Chapter 5: Multilayer Silver Nanoparticles Modified Optical Fiber Tip for High Performance SERS Remote Sensing

This chapter is published in the ***Biosensors & Bioelectronics****. Dr. Gustavo F.S. Andrade contributed to the experiment design and performed all the SERS mappings.*
Doi:10.1016/j.bios.2010.03.00, reproduced with permission. Copyright 2010 Elsevier

This work presents the construction and optimization of nanoparticles-modified optical fiber tip (NPs-MOFT) devices for remote sensing by surface-enhanced Raman scattering (SERS). Silver nanoparticles (Ag-NPs) were self-assembled on optical fiber tips through a "layer-by-layer" procedure. It is shown that the SERS performance is at optimum when 5 "layers" of 50 nm Ag-NPs were deposited on the optical fiber tip. Using the optimized Ag NPs-MOFT device, it was possible to detect 200 nM of the R6G dye in remote sensing mode (backscattering through the fiber). It was also possible to detect dye molecules with different structures and charges at the micro-molar concentration level, including anions, cations and neutral species. It can be envisioned that the Ag-NPs-MOFT device reported in this work can be further developed for SERS-based remote biosensing.

5.1 Introduction

The discovery of the surface-enhanced Raman scattering (SERS) effect 35 year ago [1-3] paved the way for the extension of Raman spectroscopy to the realm of trace detection. The use of SERS as an analytical tool has grown over the past years [4-6], although there are still a few drawbacks that prevent its widespread application [4]. The SERS technique proved to be able to detect single molecules [7-8]. This property qualifies the technique as one of the few that reached this level of sensitivity, in addition to, for instance, fluorescence and scanning-tunnelling microscopy. This positions SERS as one of the few ultimate analytical tools available nowadays. Single-molecule SERS has been reported from different environments [9], including under electrochemical conditions [10], and in single living cells [5].

Fiber optics based sensors, on the other hand, have been developed for several spectroscopic techniques, including normal Raman and SERS [11-12]. Sensors based on optical fiber are suitable for remote detection and can easily be implemented to in-field measurements [13]. However, fiber optic sensors based on SERS received much less attention than normal Raman [13-14]. The several approaches that can be used for engineering optical fibers for SERS can be divided into two main groups: optrodes and cladding-coupled sensors.

The cladding-coupled sensor is based on the evanescent field between the core and the cladding of the optical fiber. The fiber is polished or etched carefully to decrease the cladding thickness allowing higher intensity for the evanescent field. The resulting fiber is then modified on the thin clad area with a silver or a gold layer. The evanescent field is used to excite the SERS [15]. This procedure usually leads to very fragile sensors, and the re-coupling of the Raman scattered light is very inefficient, resulting in limited Raman sensitivity.

For the optrode approach, the tip of one (or a bundle) of optical fibers are modified by the SERS-active layer, and the laser collection can be done either in backscattering through the same fiber or by forward scattering using a separated set of fibers. The first reports on optrodes relied on the concept of using a metal-modified optical fiber tip as the SERS substrate, and a collection fiber to couple the SERS signal to the spectrometer [16-17]. Stokes and Vo-Dinh reported the use of microparticles of alumina covered with Ag [18], and Polwart et al. reported the immobilization of Ag nanoparticles on the tip of an optical fiber [19] as single-fibers SERS optrodes. Several authors proposed other procedures to obtains optrodes, including photochemical modification [20], evaporation of metal films [21-22], nanoimprint lithography[23], and electron beam lithography [24]. However, some of these sensors showed a limited sensitivity and they were not suitable for carrying both excitation and Raman photons at the same time, which prevented their application in remote sensing.

In our previous works, it was found that the SERS performance of metallic nanoparticles (MNPs) modified substrate is greatly depended on the number of MNPs depositions [25-27], because larger deposition number tends to increase the density of NPs on the surface, which in turn yields to a higher population of SERS hot-spots. At optimized MNPs deposition numbers, the SERS signal can be orders of magnitude higher than for just one MNPs deposition, depending on the laser frequency, the solid support and the nature of the MNPs. Furthermore, the sample-to-sample reproducibility was also greatly improved with increasing deposition numbers [25-26]. In the present work, we extend the use of this methodology to modify OFTs with Ag NPs. We will show that the Ag nanoparticles-modified optical fiber tip (AgNPs-MOFT) devices fabricated in this way have very good sensitivity and reproducibility. Most importantly, this device is suitable for remote sensing. As a proof of concept, remote detection of several dyes with diverse chemical structures was performed using the AgNPs-MOFT device.

5.2 Materials and methods

5.2.1 Chemicals

Unless otherwise mentioned, ACS grade chemicals were used. $AgNO_3$, sodium citrate di-hydrate, 3-aminopropyltrimethoxysilane (APTMS) and Nile blue A (NBA) perchlorate were obtained from Sigma-Aldrich. Rhodamine-6G (R6G), 4-dicyanomethylene-2-methyl-6-(p(dimethylamino)styryl)-4H-pyran (DCM) and Congo Red (CR) were obtained from LambdaChrome. Ultrapure water with a resistivity of 18.2 MΩ cm (Barnstead NANOpure Diamond water purification system) was used throughout the experiments. Methanol (Calderon, HPLC grade) was used without further purification.

5. 2.2 Ag NPs synthesis and the immobilization on OFT

The preparation of Ag NPs follows the procedure reported in the literature [28]. Briefly, a 500 mL $AgNO_3$ solution (5.29×10^{-4} M) was brought to boiling under vigorous stirring. Then, 10 mL of 1% sodium citrate solution was quickly added. The heating and stirring were kept for an hour and then only with stirring until the solution cool to room temperature. The as prepared Ag NPs showed an absorption peak at ~399 nm.

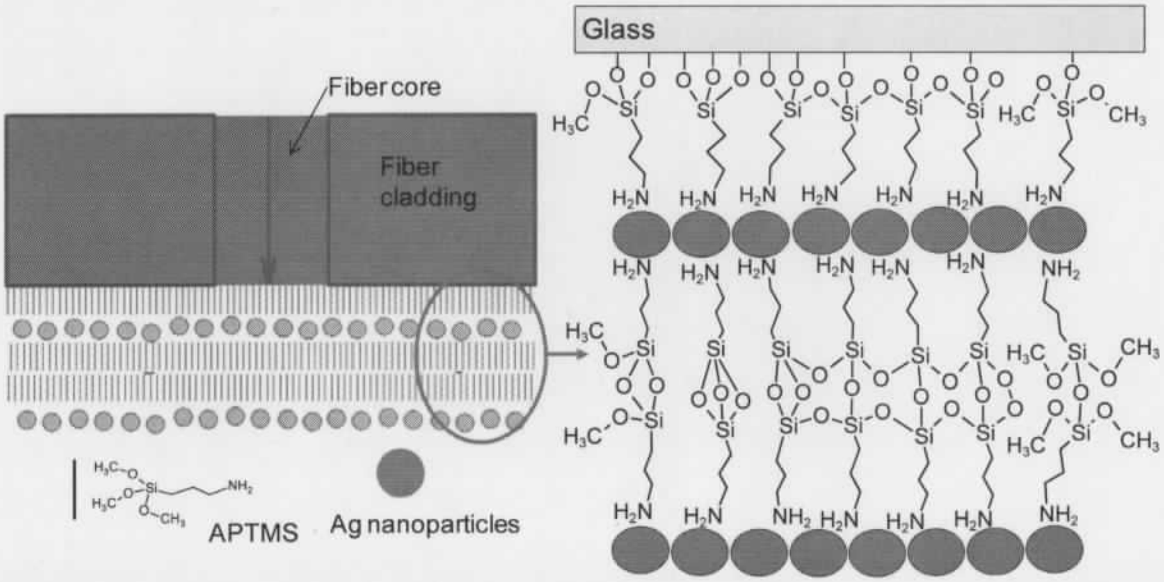

Figure 5- 1 Configuration of the optical fiber tip modified with "multi-layer" of Ag-NPs.

The APTMS sol-gel was prepared by following a method for 3-mercaptopropyltrimethoxysilane[25, 29]. Briefly, 400 µL of APTMS and 332 µL of 0.1M HCl were added into 33 mL of water. The solution was vigorously stirred for at least 1 hour. The sol-gel mixture shall be used the same day. The Ag-NPs self-assembly procedure was similar to our previous work of Ag-NPs on glass slide and it is illustrated in Fig. 5-1[25]. The single mode optical fiber (F-SA from Newport, with 2 µm core diameter) was cut into ~ 40 cm long segments.

Before the modification, the polymer protection layer close to the tip of the fiber (~3 cm) was peeled off, and then the tip was cleaved using a ceramic cuter to obtain a flat surface. The OFT was then cleaned in piranha solution for 20 min and washed thoroughly with deionized water. After drying under N_2 gas flow, it was soaked in a 10 mM APTMS ethanolic solution for 24 h. Following the modification with APTMS, the OFT was thoroughly washed with deionized water, dried and soaked for additional 24 h in the Ag-NPs suspension. Finally, it was washed with deionized water and dried under N_2 again. For the deposition of additional Ag-NPs layers, the OFT was soaked for 20 min in the APTMS sol gel solution and followed by 1 h in the Ag-NPs suspension, with vigorous rinsing with deionized water between steps. This procedure was repeated until the desired number of "layers" was obtained. After the last desired layer of Ag-NPs was deposited, the AgNPs-MOFT was heated up in N_2 atmosphere to ~110 °C for 15 min to induce cross linking among the APTMS sol gel and improve the stability of the modifier layers of Ag NPs [19].

5.2.3 SERS spectra

The SERS spectra were obtained in a Renishaw InVia Raman spectrometer, equipped with the 632.8 nm line from a He-Ne laser (4.5 mW of power on the objective). The objective used was a 50× magnification, with NA (numerical aperture) =0.75. The full-width at half-maximum (FWHM) of the He-Ne laser spot for this objective is 0.9 µm. The spectrometer is also equipped with a motorized stage that allows the computer-controlled XYZ positioning of the sample, which was used to obtain the Raman mappings.

The SERS spectra were obtained sending the laser light through the 50× objective to the unmodified proximal tip of the optical fiber, with the distal Ag-NPs-modified tip immersed in the analyte aqueous solution, as shown in Fig. 5-2. The SERS mapping was obtained by moving the motorized stage of the Renishaw InVia microscope in both X and Y directions at step size of 0.5 μm. A SERS spectrum was recorded in each spot from the proximal fiber tip (unmodified tip). To obtain the SERS map, the peak area of the strongest SERS band (1508 cm^{-1}) of R6G was plotted as a function of the X-Y position. The SERS intensity is color-coded; the brighter colors represent higher intensities. It should be noticed that methanolic solutions were also used, but the SERS performance of the AgNP-OFT was lower in this solvent. Both excitation and collection were in the proximal tip of the modified fiber, which is the configuration suitable for remote sensing [25].

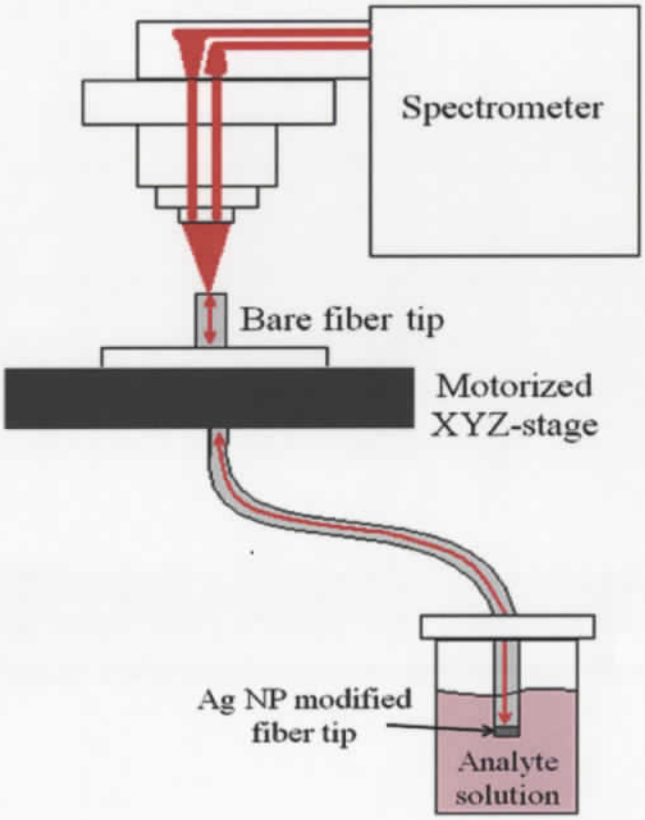

Figure 5- 2 Scheme for the the SERS experiments using the AgNP-OFT devices.

5.3 Results and Discussion

The optical fibers used in the work were single mode in the visible light range, and the diameter of their core was 2 μm. The diameter of the core used in this work is smaller than that in previous works [13], which is justified by the fact that it is a single-mode optical fiber in the 632.8 nm region. This will minimize light loss during the SERS measurements. The small core caused the coupling of light possible only in a small area of the fiber tip. In order to get the best possible coupling, the fiber holder was mounted on the motorized stage in the Raman microspectrometer as shown in Fig. 5-2.

SEM images were obtained for Ag NPs-MOFT device after 5-Ag NPs-depositions, and they are shown as supplementary material (Fig. 5-S1). The SEM images clearly showed that a homogeneous, high density assembly of Ag NPs on the fiber tip was achieved, as observed before for Ag NPs depositions on planar glass slides [25].

The Raman spectra were acquired sending the laser light from the proximal unmodified tip throughout the whole fiber length, and collecting the light back-scattered from the distal modified fiber tip, as depicted in Fig. 5-2. The setup shown in Fig. 5-2 is intended to allow the use of the device for remote sensing, because the modified tip can be directly introduced into the sampling environment. In the present work, the samples were in vials away from the spectrometer, the Ag-NPs modified optical fiber tip was simply immersed in the sample solution without any special mount.

A Raman mapping at the unmodified tip was performed to find an optimum spot that presents the maximum SERS signal, which is expected to be at the center of the fiber core. In this kind of measurement, the computer-controlled motorized XYZ-stage stop in one spot and one Raman spectrum is taken; following this, the XYZ-stage moves to the next spot and a new spectrum is obtained. This process is repeated in a pre-determined area of the sample. After the completion, the intensity of a certain band can be plotted as a function of the position on the sample, generating a 2D-plot. The Raman intensity is color-coded; the brighter colors representing higher intensities.

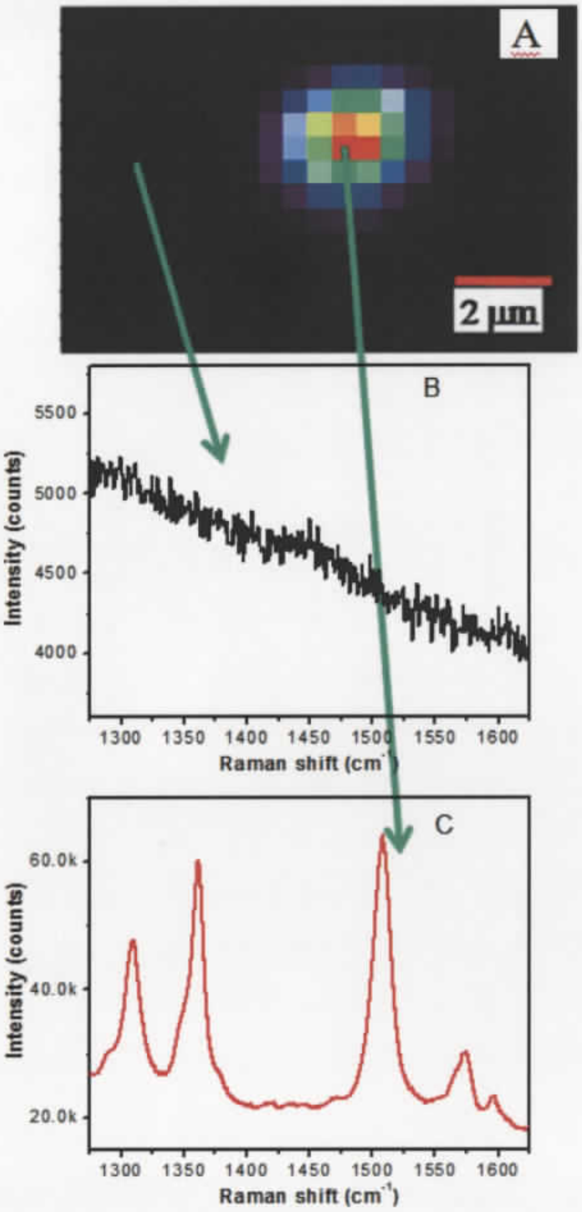

Figure 5- 3 A) Raman mapping for the 1508 cm^{-1} band of R6G on a 5 layers Ag NPs-MOFT. B) and C) Raman spectra corresponding to the points of the Raman mapping indicated by the green arrows from A.

Fig. 5-3 shows the Raman mapping for the 1508 cm^{-1}-region of the proximal unmodified tip for a Ag-NPs-MOFT immersed in a 10 μM R6G dye solution. The Raman mapping in Fig. 5-3A shows that no SERS from R6G can be detected in most of the area of the fiber tip (Fig. 5-3B), but only from a small spot, which corresponds to the fiber core, the R6G SERS spectra with a high signal-to-noise ratio can be observed (Fig. 5-3C). The SERS performance evaluation of the device was based on the most intense spectra from the Raman mappings, which corresponds to the middle of the fiber core, where most of the light is coupled.

The "layer-by-layer" procedure allows multiple depositions of Ag-NPs on glass using the APTMS sol gel as linker[25]. Fig. 5-4A presents the SERS intensity of the 1508 cm^{-1} band of 10 μM R6G on the NPs-MOFT devices as a function of the number of Ag-NPs layers deposited.

It can be noticed in Fig. 5-4A that the SERS intensity is maximized after 5 Ag NPs depositions. The maximum SERS intensity was roughly 10 times higher than for just one deposition. Further increase in the number of Ag NPs deposition decreased the SERS signal. Fan and Brolo studied the SERS intensity dependence with the number of Ag-NPs deposition on glass slides and found that the maximum intensity was from 6 layers of Ag-NPs[25]. Also, further increase in the number of Ag-NPs deposition on glass slides did not affect the SERS intensity after the maximum. The decrease in SERS signal after 5 Ag-NPs deposition, shown in Fig. 5-4A, can be rationalized by taking into account the SERS measurement configuration. The laser excitation must travel through the fiber, excite the Ag-NPs at the tip from the glass side and interact with molecules adsorbed at the Ag-NPs solution interface. The scattered light must couple back into the fiber to reach the spectrometer. Therefore, it must be a balance between the thickness of the metal layer and the arrangement of the nanostructures to generate the required hot-spots for SERS. The increase in SERS intensity from 1 to 5 depositions might be assigned to an increase in the number of hot spots accessible to the adsorbed species. After 5 Ag-NPs deposition, the thickness of the metal layer become significantly large, decreasing the efficiency of both excitation and collection through the metal film.

One of the major concerns on the development of SERS substrates is the sample-to-sample reproducibility of the SERS signal. Fig. 5-4B presents the SERS intensity from

R6G 10 μM solution for seven samples of the optimized 5 layers Ag-NPs-MOFT device. The relative standard deviation (RSD%) for this device was around 25%, which is consistent with previous reports[25-26].

The minimum amount of analyte that can be detected by the Ag-NPs-MOFT was also explored. Fig. 5-5A presents SERS spectra from 200 and 500 nM R6G solutions obtained using an optimized Ag-NPs-MOFT device. It is worth mentioning that the two measurements were made with the same Ag-NPs-MOFT, starting from the lowest concentration and with a washing step between measurements. One can notice in Fig. 5-5A that it is possible to observe the characteristic SERS bands of R6G for concentration as low as 200 nM. In previous reports on metal-modified single optical fibre tips for back-scattering detection using SERS, Polwart [19] detected crystal violet down to 100 nM and Lan [30] reported optrodes that could detect R6G down to 10 nM with the addition of NaCl to the solution containing the dye. Shi [31] reported the detection of R6G in concentrations as low as 1 nM with the addition of Ag NPs to the analyte solution, and Kostovski [23] reported the detection of one monolayer of thiophenol and 100 μM of R6G. In Fig. 5-5B, a calibration curve for one of our Ag-NPs-MOFT is shown. The SERS intensity (in peak area) versus the concentration of R6G was well fitted using a Langmuir-Freundlich isotherm (R^2 = 0.998), and the limit-of-detection (LOD) was determined to be 3 nM for the AgNP-MOFT device in remote sensing mode. To our knowledge, this report is probably one of the lowest concentrations achieved using the real time remote sensing configuration, and without the help of any extra reagents other than the analyte. The equilibrium constant for R6G adsorption on AgNPs and the saturation coverage were also obtained from the isotherm, and they are in good agreement with a previous work [32], as discussed in more details in the Supporting Information (supporting information, 5- S2).

Hence, this high sensitivity property, in addition to the ease fabrication and high reproducibility, shows a considerable promise for this SERS device in remote sensing.

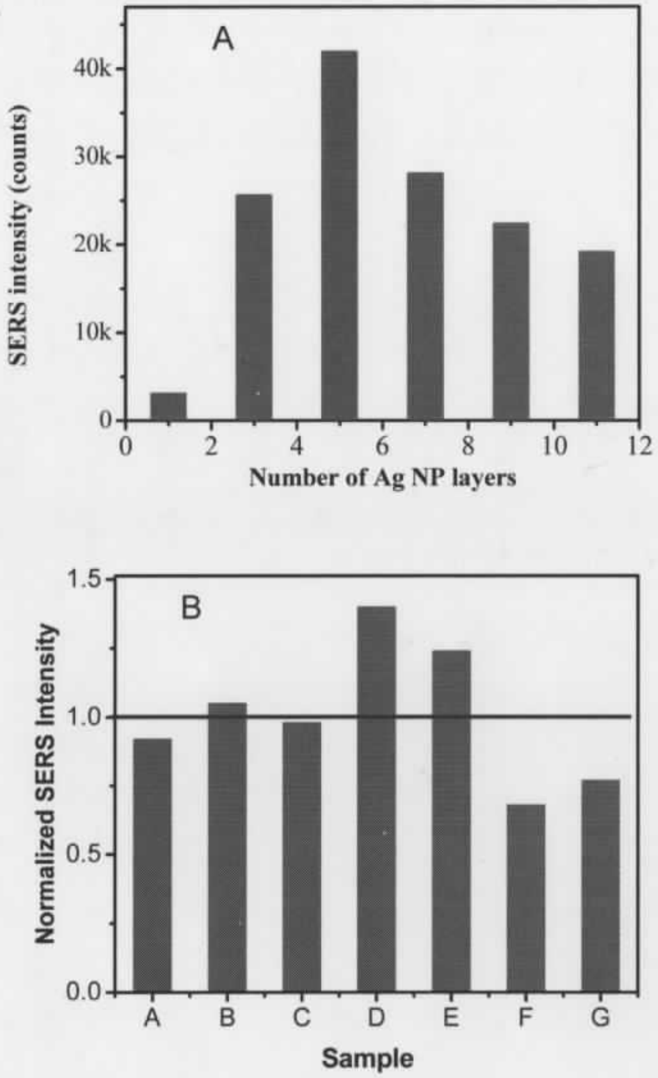

Figure 5- 4 A – SERS performance of the NPs-MOFT as a function of the number of Ag-NPs deposited (only the odd deposition numbers are shown). B – Average normalized SERS Intensity distribution of the 1508 cm^{-1} band intensity for 7 different 5 Ag-NPs monolayers samples.

It is also worth mentioning that the sensor area that actually contributes to the SERS signal contains hot-spots within the ca. 3 μm^2 fiber core. The surface coverage of R6G is expected to be low at these concentrations [10, 32], the combination of low surface coverage and small number of hot spots limits the probability of R6G molecules to populate the sites that contribute mostly to the signal (hot spots) [10]. The detection of R6G for concentrations lower than 200 nM, as observed in our previous report for Ag-NPs adsorbed on glass slides[25], could be achievable, but it would probably require a long immersion time to collect the sample due to the even lower probability of R6G molecules to find a hot spot.

The stability of the Ag NPs-MOFT device was also examined. It was found that there is no loss of SERS activity for the device when stored in air for 72 hours. However, the SERS performance of the device decreased dramatically after storage in water for 24 h, and it was completely lost after storage in methanolic solution for the same period of time. The decrease in SERS intensity might be related to the solvolysis of the silane linker layer [33]. This limitation affects prolonged measurements using a single Ag-NPs-MOFT device, especially in methanolic environment. These limitations are offset by some of the advantages of the device; including easy fabrication involving standard chemicals and well-established wet chemistry methods that can be easily extended to mass production, and, most importantly, the reasonable sample to sample reproducibility (RSD% of ~25%).

Metallic NPs made from different methods usually are known to have different surface charges, and hence favour the adsorption of certain types of analytes, which strongly correlates with the average SERS intensity[34]. Hence, the ability to detect molecules with very different structures and charges without pre-treatment of sample is an extremely desirable property for SERS remote sensors. This kind of property could make the sensor useful for cellular studies in the future, where labeling with multiple organic dyes are common practice[35]. The AgNPs-MOFT device was then tested using a large range of analytes. Fig. 5-6 presents the SERS spectra of NBA, DCM and CR in concentration of 1 μM on NPs-MOFT devices. These dyes were chosen because they have different charges, as can be noticed by the chemical structure in the right-hand side of Fig. 5-6. NBA is a cation, DCM is neutral and CR is an anion and they would have very different affinities for the Ag-NPs surface.

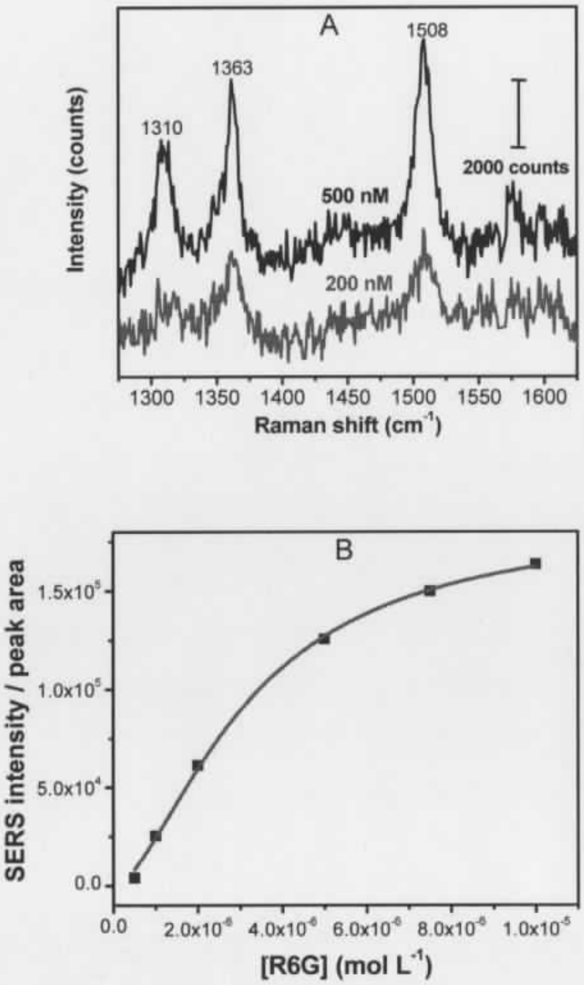

Figure 5- 5 A) SERS of R6G at different concentrations obtained from a 5 deposition made Ag NPs-MOFT. The baseline was subtracted and the spectra were offset for clarity; B) (black squares) a signal-dose curve for R6G in water using the band (peak area) at 1508 cm^{-1}; (red line) fitting of a Langmuir-Freundlich isotherm curve to the experimental points, used to obtain the LOD for the Ag NPs-MOFT device.

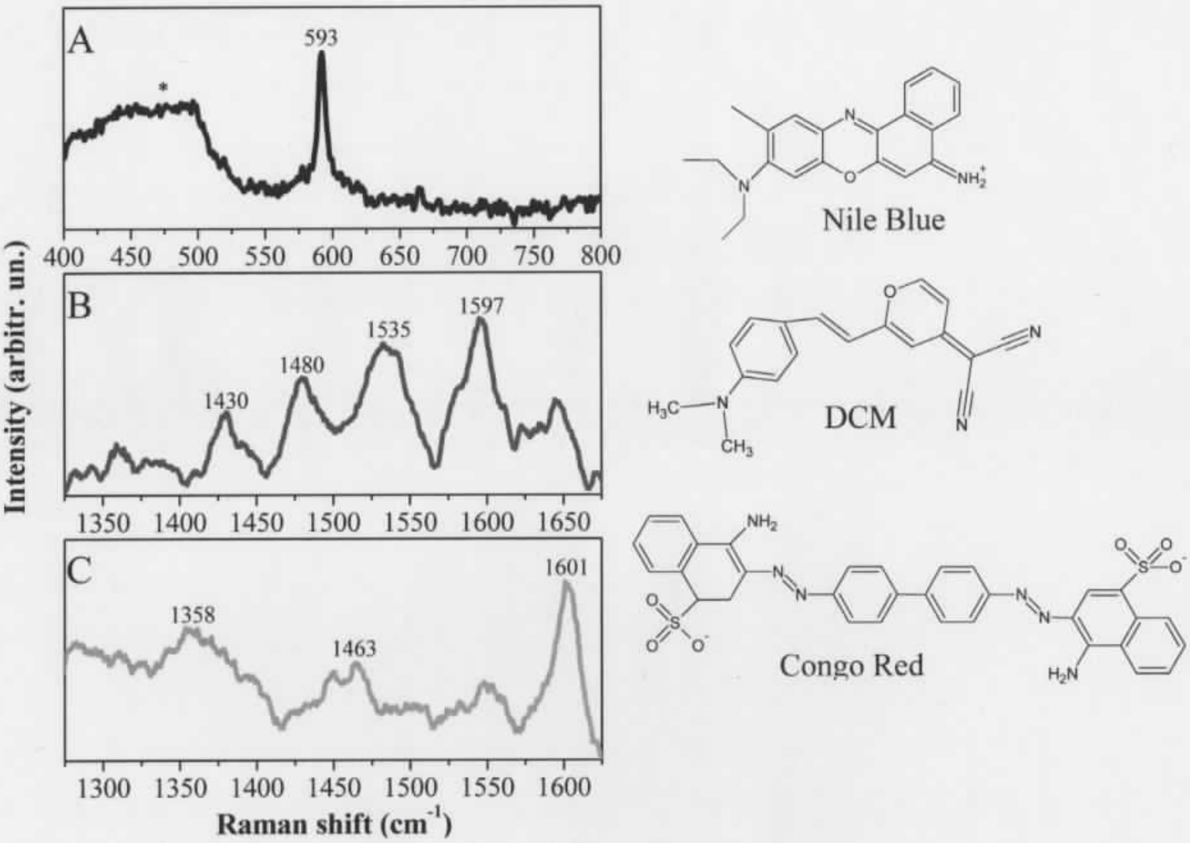

Figure 5- 6 SERS spectra of 1.0 μM aqueous solutions of the dyes: A – Nile Blue A; B – DCM; C – Congo Red. The chemical structure of the dyes is shown on the right of the SERS spectra. 632.8 nm laser excitation.

The SERS spectra shown in Fig. 5-6 confirm that the NPs-MOFT device is able to detect molecules with very different chemical structures at a concentration as low as 1 μM, also without the needs of additional reagents, but with comparable sensitivities to literature reports [19]. In the NBA case, the HeNe laser line is inside the absorption band of the analyte, and presents an additional enhancement due to resonance Raman, characteristics of the surface-enhanced resonance Raman scattering (SERRS) effect. Due to this additional enhancement, the SERS intensity for the 1 μM NBA solution is higher than for the other dyes. It is also worth noticing that the well known silica interference, with a maximum at 460 cm^{-1} (marked with an asterisk in Fig. 5-6A) is much weaker than the NBA band at 593 cm^{-1}.

5.4 Conclusions

This work presented the construction and optimization of the NPs-MOFT device for SERS detection of several analytes. The optimization procedure showed that the highest SERS intensity can be obtained after 5 depositions of 50 nm Ag-NPs by a sol-gel procedure on the tip of the optical fiber. Using the optimized 5-layer Ag-NPs modified device it was possible to detect 200 nM of the R6G dye, and it is also possible to detect molecules with different net charge at the micro-molar concentration limit, including anions, cations and neutral molecules.

The results showed a flexible remote SERS sensor with a very high sensitivity. Although there is some issue with the long time stability when expose to solvents, this problem does not hinder the usage of the device when stored in air. The AgNPs-MOFT device can be used as a single-use remote sensing element, since it is easy to fabricate and provide good sample to sample reproducibility. It can be envisioned that this kind of device could also be used as a SERS-based biosensor.

5.5 References:

1. Albrecht, M. G.; Creighton, J. A., *Journal of the American Chemical Society* **1977,** *99* (15), 5215-5217.

2. Fleischm.M; Hendra, P. J.; McQuilla.Aj, *Chemical Physics Letters* **1974,** *26* (2), 163-166.

3. Jeanmaire, D. L.; Vanduyne, R. P., *Journal of Electroanalytical Chemistry* **1977,** *84* (1), 1-20.

4. Bell, S. E. J.; Sirimuthu, N. M. S., *Chemical Society Reviews* **2008,** *37* (5), 1012-1024.

5. Scaffidi, J. P.; Gregas, M. K.; Seewaldt, V.; Vo-Dinh, T., *Analytical and Bioanalytical Chemistry* **2009,** *393* (4), 1135-1141.

6. Spuch-Calvar, M.; Rodriguez-Lorenzo, L.; Morales, M. P.; Alvarez-Puebla, R. A.; Liz-Marzan, L. M., *Journal of Physical Chemistry C* **2009,** *113* (9), 3373-3377.

7. Kneipp, K.; Wang, Y.; Kneipp, H.; Perelman, L. T.; Itzkan, I.; Dasari, R.; Feld, M. S., *Phys. Rev. Lett.* **1997,** *78* (9), 1667-1670.

8. Nie, S. M.; Emery, S. R., *Science* **1997,** *275* (5303), 1102-1106.

9. Pieczonka, N. P. W.; Aroca, R. F., *Chemical Society Reviews* **2008,** *37* (5), 946-954.

10. dos Santos, D. P.; Andrade, G. F. S.; Temperini, M. L. A.; Brolo, A. G., *Journal of Physical Chemistry C* **2009,** *113* (41), 17737-17744.

11. Lieberman, R. A., *Sensors and Actuators B: Chemical* **1993,** *11*, 43-55.

12. McDonagh, C.; Burke, C. S.; MacCraith, B. D., *Chemical Reviews* **2008,** *108* (2), 400-422.

13. Stoddart, P. R.; White, D. J., *Analytical and Bioanalytical Chemistry* **2009,** *394* (7), 1761-1774.

14. Vo-Dinh, T.; Stokes, D. L., Optical Conduits for Vibrational Specroscopy. In *Handbook of vibrational spectroscopy*, Chalmers, J. M.; Griffiths, P. R., Eds. John Wiley & Sons: Chichester, 2002; pp 1302–1317.

15. Zhang, Y.; Gu, C.; Schwartzberg, A. M.; Zhang, J. Z., *Applied Physics Letters* **2005,** *87* (12), -.

16. Mullen, K. I.; Carron, K. T., *Analytical Chemistry* **1991,** *63* (19), 2196-2199.

17. Bello, J. M.; Narayanan, V. A.; Stokes, D. L.; Vodinh, T., *Analytical Chemistry* **1990,** *62* (22), 2437-2441.

18. Stokes, D. L.; Vo-Dinh, T., *Sensors and Actuators B-Chemical* **2000,** *69* (1-2), 28-36.

19. Polwart, E.; Keir, R. L.; Davidson, C. M.; Smith, W. E.; Sadler, D. A., *Applied Spectroscopy* **2000,** *54* (4), 522-527.

20. Zheng, X. L.; Guo, D. W.; Shao, Y. L.; Jia, S. J.; Xu, S. P.; Zhao, B.; Xu, W. Q.; Corredor, C.; Lombardi, J. R., *Langmuir* **2008,** *24* (8), 4394-4398.

21. Viets, C.; Hill, W., *Sensors and Actuators B: Chemical* **1998,** *51*, 92-99.

22. Hankus, M. E.; Li, H. G.; Gibson, G. J.; Cullum, B. M., *Analytical Chemistry* **2006,** *78* (21), 7535-7546.

23. Kostovski, G.; White, D. J.; Mitchell, A.; Austin, M. W.; Stoddart, P. R., *Biosensors & Bioelectronics* **2009,** *24* (5), 1531-1535.

24. Smythe, E. J.; Dickey, M. D.; Bao, J. M.; Whitesides, G. M.; Capasso, F., *Nano Letters* **2009,** *9* (3), 1132-1138.

25. Fan, M.; Brolo, A. G., *Physical Chemistry Chemical Physics* **2009,** *11* (34), 7381-7389.

26. Fan, M. K.; Brolo, A. G., *ChemPhysChem* **2008,** *9* (13), 1899-1907.

27. Addison, C. J.; Brolo, A. G., *Langmuir* **2006,** *22* (21), 8696 -8702.

28. Cui, Y.; Ren, B.; Yao, J. L.; Gu, R. A.; Tian, Z. Q., *Journal of Physical Chemistry B* **2006,** *110* (9), 4002-4006.

29. Jena, B. K.; Raj, C. R., *Analytical Chemistry* **2006,** *78* (18), 6332-6339.

30. Lan, X. W.; Han, Y. K.; Wei, T.; Zhang, Y. N.; Jiang, L.; Tsai, H. L.; Xiao, H., *Optics Letters* **2009,** *34* (15), 2285-2287.

31. Shi, C.; Yan, H.; Gu, C.; Ghosh, D.; Seballos, L.; Chen, S. W.; Zhang, J. Z.; Chen, B., *Applied Physics Letters* **2008,** *92* (10).

32. Hildebrandt, P.; Stockburger, M., *Journal of Physical Chemistry* **1984,** *88* (24), 5935-5944.

33. Plueddemann, E. P., *Silane coupling agents*. 2nd. ed.; Plenum Press: New York, 1991; p 253.

34. Alvarez-Puebla, R. A.; Aroca, R. F., *Analytical Chemistry* **2009,** *81* (6), 2280-2285.

35. Hanson, G. T.; Hanson, B. J., *Combinatorial Chemistry & High Throughput Screening* **2008,** *11* (7), 505-513.

5.6 Supporting information

Multilayer Silver Nanoparticles Modified Optical Fiber Tip for High Performance SERS Remote Sensing

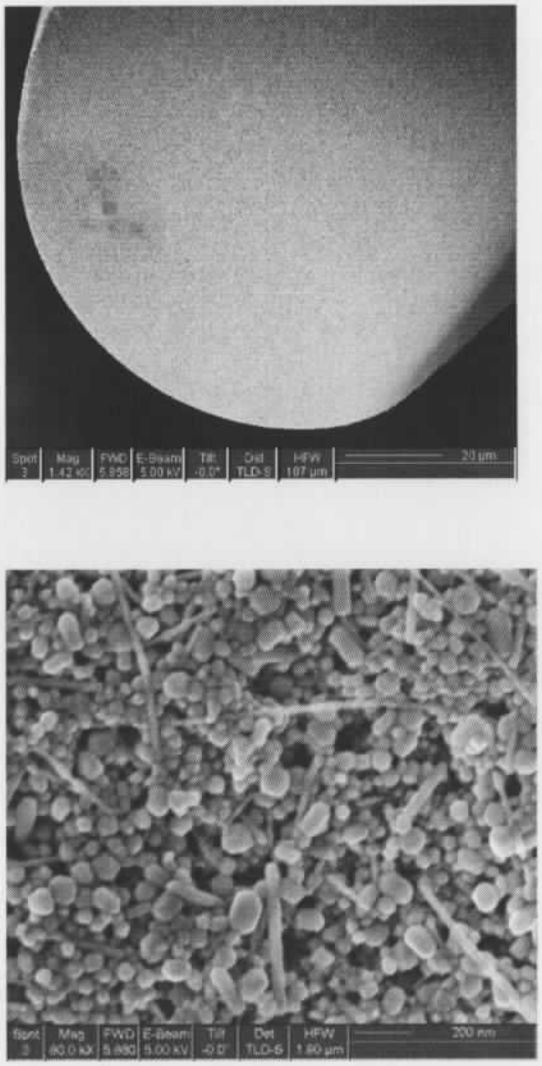

Figure 5-S 1 SEM images at different magnifications of the 5 Ag NPs deposition modified fiber tip.

5-S2. Langmuir-Freundlich fitting to the SERS intensity versus [R6G] curve and LOD determination.

The calibration curve presented in Figure 5B was fitted by a Langmuir-Freundlich isotherm:

$$\frac{c^{(1-a)}}{\Gamma} = \frac{c^{(1-a)}}{\Gamma_{\max}} + \frac{1}{K\Gamma_{\max}}$$

Where c is the [R6G], Γ is the SERS intensity, K is the equilibrium constant for the adsorption of R6G and Γ_{max} is the maximum SERS intensity expected for this system, *a* is a value dependent on the nature of the R6G-Ag interactions.

From the Langmuir-Freundlich isotherm, by plotting $c^{(1-a)}/\Gamma$ versus $c^{(1-a)}$ we get a straight line equation relating the SERS intensity with the R6G concentration. The best fitting we gor for the data in Figure 5 is: $c^{(1-a)}[1/\Gamma-4{,}949x10^{-6})] = 6.396x10^{-15}$.

From these values, the following values for K and Γ_{max} were obtained:

$K = 7.7x10^{8}\ M^{-1}$

$\Gamma_{max} = 2.0x10^{5}\ M$

The value for Γ_{max} obtained by Hildebrandt and Stockburger fitting SERRS data for R6G on AgNPs by a Langmuir isotherm was $1x10^{5}\ M^{1}$, which is in good agreement with our results.

The values for K obtained in the present work, on the other hand, is between the two values obtained by the authors of the previous work [1]: for a non-aggregated colloid, $K = 4x10^{4}\ M^{-1}$, but for a Cl^{-} aggregated colloid the author obtained $K = 5.5x10^{9}\ M^{-1}$. The much higher value for the equilibrium constant can be easily assigned to the creation of a greater number of SERS active sites with the aggregation using Cl^{-}. The K obtained in the present work is an intermediate value, indicating the substrate obtained has a high number of hot spots, but not as high as for AgNP aggregated by Cl^{-} in suspension.

The LOD was determined by the intensity measurement of eight blank samples, and determined as [2]:

$$x_L = x_{blank}^{average} + k*SD_{blank}$$

where: x_L is the minimum intensity that can be measured with this device, $x_{blank}^{average}$ is the average of (in our case) 8 measurements of the maximum range of intensity measured in the region of the R6G band, and SD_{blank} is the standard deviation for the blank measurements, and k is the numerical factor at given confidence level (assumed as 0.95).

After measuring the minimum intensity that can be measured, we determined the LOD for R6G as 3 nM.

References:

1. Hildebrandt, P.; Stockburger, M., *Journal of Physical Chemistry* **1984,** *88* (24), 5935-5944.

2. IUPAC, *Compendium of Chemical Terminology (the "Gold Book")*. 2nd. ed.; Blackwell Scientific Publications: Oxford, 1997.

Chapter 6: Silver nanoparticles on a plastic platform for bio-sensing

This chapter is a manuscript submitted. Matthew Thompson and Maria Luiza Andrade performed some of the absorption tests.

A cost-effective fabrication method for the preparation of localized SPR biosensors supported on plastics is described. The silver-nanoparticles-on-plastic sensor was fabricated by chemically modifying the surface of one of the most common plastics, polyethylene terephthalate, which then allows the efficient immobilization of Ag NPs. The localized SPR of the silver-nanoparticles-on-plastic sensor strip showed good sample to sample reproducibility and a moderate response to bulk refractive indices changes (~150 nm/RIU (refractive index unit)). The analytical performance of the sensor strip for monitoring both thiol and protein adsorption, including bio-affinity, was examined. The limit of quantification to the adsorption of the sample thiol molecule 11-mercaptoundecanoic acid was 500 nM and for the detection of streptavidin was ~9.5 nM. The capability of using the as developed sensor strip to monitor protein-protein interactions was shown by immobilizing anti-human IgG at the sensor surface and detecting the binding of human IgG. The silver-nanoparticles-on-plastic sensor can then be used as a cheap, versatile, and yet sensitive localized SPR biosensor.

6.1 Introduction

Localized surface Plasmon resonance (LSPR) spectroscopy has attracted lots of attention from the bioanalytical community.[1-6] It is believed that LSPR offers similar merits as the conventional propagating SPR in smooth metal films for chemical sensing, but with some important advantages. For instance, LSPR sensors are more suitable to integrate into microchips; they can operate in either transmission or reflection geometries; they provide faster response time; and they have much better spatial resolution.[7-8] Moreover, the LSPR wavelength can be tuned throughout the visible and near infrared region by a judicious choice of size, shape and material, providing extra flexibility for sensor designing and sometimes higher sensitivity as well.[4, 9-10]

Suspensions of metallic nanoparticles (MNPs), especially Au NPs, have been used to detect DNA hybridization[11-14] and in immunoassays.[12, 15] The former takes advantages of the significant color change induced by LSPR coupling (through small range inter-particle interaction), and the latter is related to the LSPR wavelength shift caused by the change in local RI at the surface due to the adsorption of biomolecules. This is the same principle that forms the basis of the conventional propagating SPR sensor.

However, chemical analysis using MNPs suspended in a liquid phase suffers from the inherent stability issues related to the colloidal system. The experimental conditions have to be carefully controlled. Furthermore, the approach is not suitable for high throughput analysis,[16] as is the case for MNPs immobilized on a solid support. [1, 8, 10, 17-18]

Many groups have vastly contributed to the development of LSPR sensors in planar substrates. For instance, Van Duyne group [1, 7, 19-22] used nanosphere lithography technique to fabricate periodic Ag NPs arrays to detect biomarkers of Alzheimer's disease. Core-shell structured NPs layer, [8, 23-24] fabricated by thermal evaporation, has the capability of monitoring both antibody-antigen reaction and DNA hybridization, and it is suitable for high throughput multi-analytes assays.[8] LSPR sensor chips on glass fabricated through wet chemistry method have also been reported[10, 16, 18, 25-29] and used for monitoring biotin-streptavidin (SA) binding,[4, 10, 16] antigen-antibody interactions,[18] and even detecting small molecules with high sensitivity.[10, 28-29]

Glass has been the most popular supporting material for LSPR sensors platforms. Although glass is inexpensive, it is fragile, non flexible and relatively heavy. Efforts to develop alternative supporting substrate, such as paper,[17, 30] for LSPR based sensor have been reported.

Polymeric materials, such as polyethylene terephthalate (PET), are transparent, flexible, low weight, cheap and have very good mechanical strength. Biosensors supported on polymer films have been widely reported in order to explore these attractive properties.[31-34] In the specific case of PET, it is a material that has been used as a substrate for transparent flexible displays, organic electronic devices and biomedical devices.[35-37] Recently, PET has been used as a substrate for nanofabrication,[35] protein microarrays,[38] and glucose biosensors.[39] Surprisingly, there is very limited efforts on using PET as substrate to support LSPR-based sensors. Bauer et al[40] reported a DNA hybridization analysis using Au NPs supported on PET films. The PET film was vacuum-coated with aluminum followed by nitrocellulose-lacquer. After that, single stranded DNA was immobilized on the nitrocellulose film and used to capture Au NPs modified with complementary DNA strands. In that case, however, Au NPs were not immobilized on the substrate as in typical LSPR -sensor platforms, and the procedure to modify the PET surface was complex.

Previously, we have reported on methods[41-43] to self-assemble MNPs on different solid support for SERS detection with very high sensitivity. Here, we expand on those efforts by using PET as solid support for Ag NPs self-assembly. As shown in Scheme 6-1, the PET surface was activated in a plasma oven and further modified with a diamine to impart the required functionality for NPs immobilization. The resulting silver-nanoparticles-on-plastic sensor (SNOPS) strips were simple to fabricate, presented good sample-to-sample reproducibility and sensitive to biomolecule adsorption, and were low cost.

6.2 Results and discussion

LSPR (bio-)sensors supported on planar platforms have inspired tremendous interests.[3, 5, 8, 17, 21, 44] The SNOPS sensor reported here resembles a "pH-paper strip" that can be used to detect the adsorption of biomolecules. The SNOPS strips are fabricated through a wet chemistry self-assembly process using a common plastic, PET, as a solid support. The plastic platform makes the sensor flexible, resistant to mechanical stress and it is inexpensive. The versatility of the SNOPS strips in chemical and biochemical detection was shown. Procedures for surface chemistry modification of the SNOPS with either amine or carboxylic acid functionality were developed. These chemical moieties provided the starting point for further surface modification and protein immobilization. As a proof of concept, the SNOPS sensing performance was examined by monitoring the chemical adsorption of thiols and proteins, including the ability of the sensor to probe protein-protein interactions, and biotin-streptavidin binding. In the following sections, the optimization of the SNOPS strip fabrication, the procedures for surface modification and biomolecule immobilization, and the proof-of-concept (bio)analytical applications are discussed.

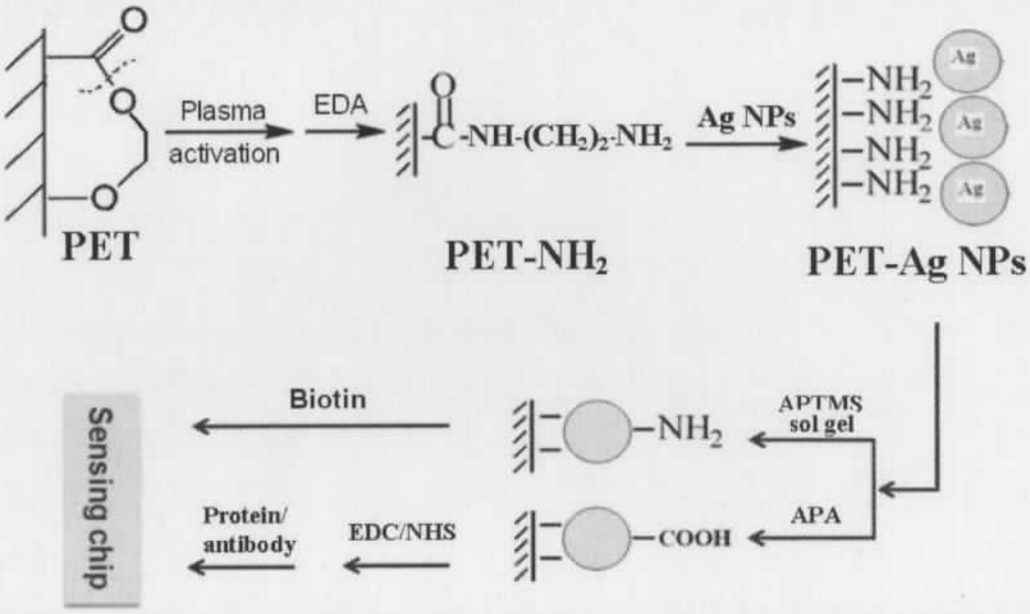

Scheme 6- 1 Preparation of SNOPS strip for biosensing. Illustration of the surface activation and modification (see text for details).

6.2.1 Optimization of the Ag NPs immobilization on PET

The plasma activated PET film was incubated overnight in different concentrations of methanolic solution of EDA before being immersed overnight in a Ag NPs dispersion (see Scheme 6-1). The effect of 1,2-ethylenediamine (EDA) concentration on the load of Ag NPs on PET surfaces is shown in Fig. 6-1a. The absorbance significantly changed up to 30% (V:V) of EDA, and it stabilized after that. The error bars in Fig. 6-1a represent the sample-to-sample (N=5) reproducibility and this relative standard deviation (RSD) in absorbance is shown to be less than 10% after the concentration of EDA reaches 30% (V:V). Considering these results, 40% (V:V) methanolic EDA solution were used in all subsequent experiments. The effect of the immersion time of Ag NPs deposition was also explored and it is illustrated in Fig. 6-1b. The absorbance of the film after just 2 hours of incubation in Ag NPs solution was about 0.4, indicating that a significant amount of Ag NPs were deposited. The amount of Ag NPs immobilized increased slightly up to 6 hours of incubation, where an absorption plateau was reached. Interestingly, the relative sample-to-sample standard deviation decreases with the incubation time. The position of the LSPR peak is also plotted in Fig. 6-1b. The blue shift of the LSPR maximum wavelength (λ_{max}) with the Ag NPs deposition time is not unusual. Previous reports[7, 19, 21] have assigned this behavior to adsorbed electron donating species which increase the electron density of the MNPs.[7] The Ag NPs strongly interacts with the amine modified PET film leading to the blue shift in the LSPR peak observed in Fig. 6-1b. The LSPR maximum wavelength stabilized after 6 hours, similarly to the observed for the absorption.

The effect of the Ag NPs incubation time on the sensitivity of the SNOPS strip to bulk refractive index (RI) changes was also examined. The results of the sensitivity to LSPR wavelength shifts are listed in Table 6-1. A sensitivity of ~150 nm/RIU (refractive index unit), independent of the deposition time, was obtained. This level of sensitivity is comparable to earlier literature reports.[45-47] The results from Fig. 6-1 and Table 6-1 suggest that a minimum of 4 hours of incubation in Ag NPs dispersion is required to achieve a reasonable sample-to-sample RSD% of the LSPR wavelength shifts. All the chemical and biochemical sensing experiments reported here were performed using

SNOPS strips prepared with 40% (V:V) EDA methanolic solutions and 6-hours of incubation in Ag NPs.

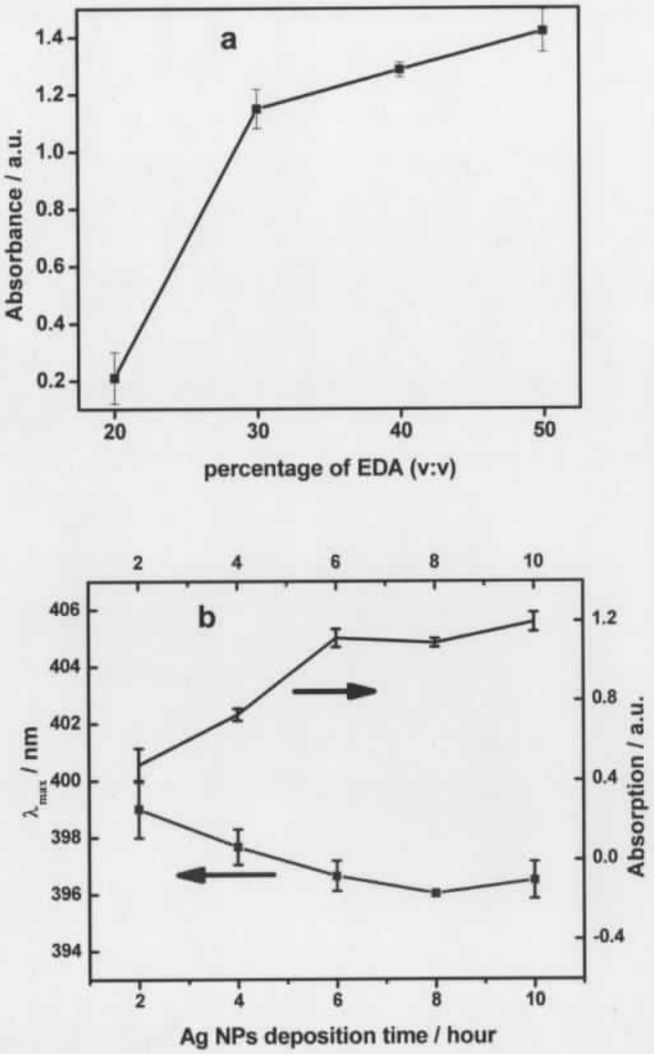

Figure 6- 1 Optimization of the Ag NPs immobilization on PET strips. a) Effect of the EDA concentration; b) effect of the incubation time in Ag NPs solution (with 40% of EDA in methanol (V:V)). The error bars are the sample-to-sample standard deviation (N=5). The lines in the graphs are only connecting the experimental points.

Table 6- 1 Sensitivities of SNOPS strips fabricated with different incubation times in Ag NPs dispersion.*

Ag NPs incubation time	Sensitivity	R^2
2-hour	146.6	0.9956
4-hour	146.1	0.9852
6-hour	135.3	0.9939
8-hour	154.3	0.9964
10-hour	152.5	0.9933

*The LSPR wavelength was measured for strips immersed in glucose solutions of different concentrations. Fitting equation: $y = Bx + A$, where x is the RI, y is the LSPR peak position, and B is the sensitivity. The sensitivities are in nm/RIU (bulk).

6.2.3 Monitoring the adsorption of thiol containing molecules

The SNOPS strip was first tested for the detection of a long chain thiol. Fig. 6-2 shows the response of the LSPR shift of an optimized strip with the concentration of 11-mercaptoundecanoic acid (MUA). The SNOPS strip presented good response to the presence of MUA, in terms of changes in both the LSPR full-width at half maximum – FWHM (Fig. 6-2a) and peak position (Fig. 6-2b), until a plateau is reached after 500 μM of MUA. The dependence of the LSPR FWHM with the MUA concentration for diluted ethanoic solutions is shown as an inset in Fig. 6-2a. A linear response was observed in the limit of low MUA concentrations (between 500nM to 6 μM), which is one order of magnitude lower than reported for Ag nanosensors fabricated by electron beam lithography.[48] It is known that the shape of the LSPR envelope depends on the degree of aggregation,[49] especially the bandwidth (in terms of FWHM). Thus, our results point towards strong morphological changes at the sensor strip surface upon the binding of MUA. These changes are related to the aggregation of the NPs driven by the MUA adsorption. The large changes in the optical properties of the strips due to aggregation contribute to the higher sensitivity for MUA detection, relative to the literature, observed in this report. Similar results were observed in Fig. 6-2b for the LSPR wavelength shift. The colour changes due to the MUA adsorption could be verified by visual inspection for concentrations in the micromolar range, as illustrated in the inset of Fig. 6-2b. This type of "detection" is akin to the colour changes observed using "pH-papers", and might provide a new opportunity for inexpensive LSPR-based strips (like SNOPS) to be used as disposable biosensors.

6.2.4 Monitoring protein adsorption.

The selectivity of a LSPR sensor is enabled by the immobilization of molecules on the metallic surface that target specific biological relevant species from solutions. The SNOPS strip must then be modified by different functional groups and proteins for biosensing. As discussed above; however, the presence of strong binding functional group, such as thiols, induces the Ag NPs to aggregate. The modification of the surface of the SNOPS strips was realized by carefully choosing amine-containing surface modification reagents to achieve a good degree of stability and reproducibility without strong aggregation.

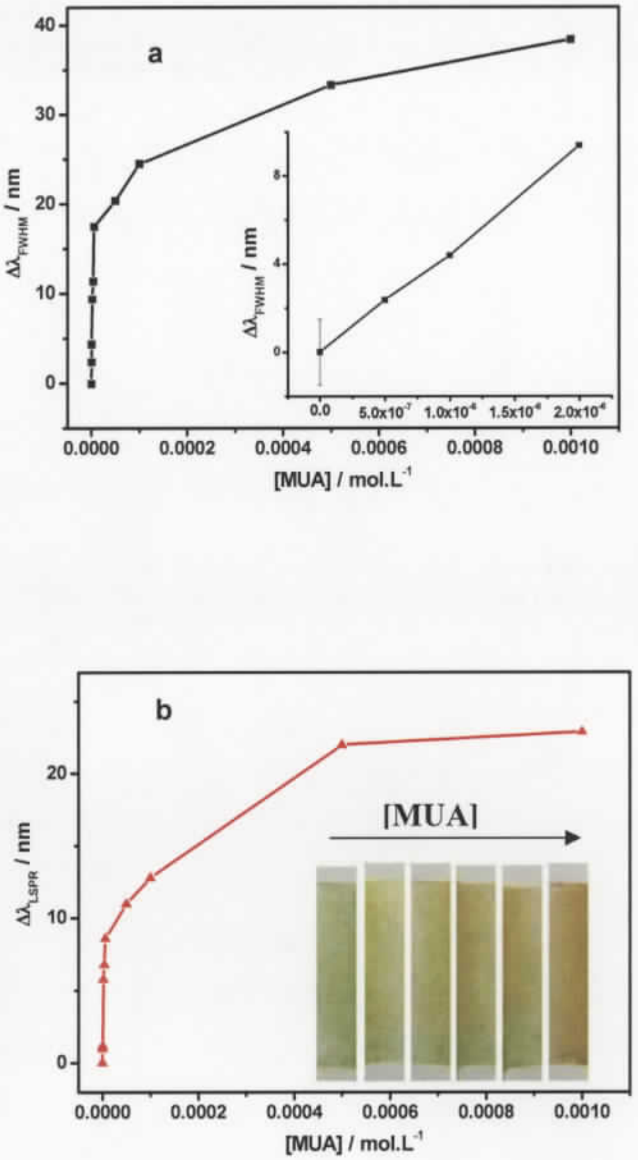

Figure 6- 2 SNOPS strip response to the presence of MUA. The strips were incubated in MUA solutions of various concentrations for 2 hours before measurements: a) changes in FWHM of the LSPR peak; b) LSPR peak shift with increasing MUA concentration in ethanol. Inset in *a* shows the zoom-in of the FWHM change at low MUA concentration. The zero MUA concentration in the inset was obtained by incubate 3 SNOPS strips in pure ethanol for the 2 hours. The inset in *b* shows the image of the SNOPS strip after exposed to MUA at different concentrations (left to right: 0, 1μM, 5μM, 10μM, 100μM, and 10 mM). Images were taken in air.

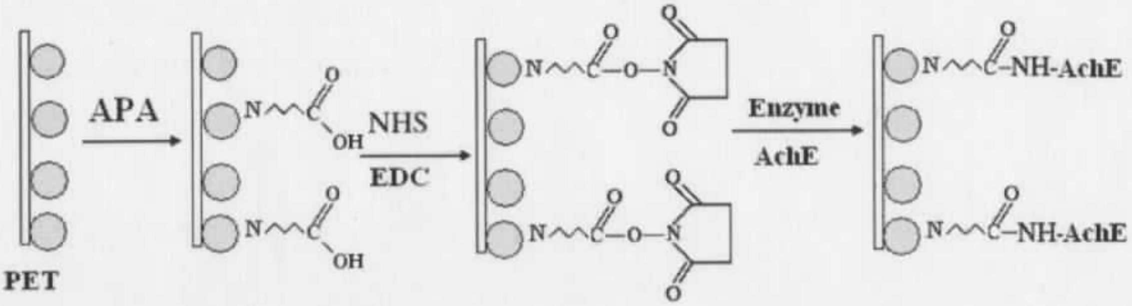

Scheme 6- 2 Surface modification steps for protein immobilization on a SNOPS strip.

The surface modification procedure, described in Scheme 6-2, was tested using a model protein, Acetylcholinesterase (AchE), on multiple SNOPS strips. The sequential steps leading to the protein immobilization was followed by measuring the LSPR peak shifts of the strips and the results are shown in Fig. 6-3. The LSPR peak shift following the adsorption of 3-aminopropionic acid (APA) was rather small (~0.5 nm), despite the fact that this species binds directly to the surface of the Ag NPs, in a region where the local electromagnetic field is expected to be strongest.[1, 45] This small shift can be rationalized by taking into account the size of the molecule and the binding group. APA is a relatively small molecule (MW = 89 a.m.u.) and the perturbation of local RI due to its adsorption is expected to also be small. Another contribution to the small shift is that APA binds to the silver surface through its amino group. It is known that amine is an electron donating specie and the adsorption of amino-containing species to MNPs can cause the LSPR to blue shift.[7, 19, 21] This effect was corroborated in the next step of surface modification, the coupling of N-hydroxysuccinimide (NHS), which led to a further ~ 2.5 nm redshift, despite the fact that this molecule would be away from the surface of the Ag NPs (hence experiencing weaker SP field than APA) and has comparable size (MW = 115 a.m.u.) to APA. The largest LSPR peak shift observed in Fig. 6-3 is caused by the adsorption of protein AchE. A shift of ~6.5 nm (after APA modification) was observed (notice that the binding of the protein replaces the NHS group, see Scheme 6-2) in this case. More importantly, a percent relative standard deviation of only 4% was observed by considering the LSPR peak shifts from all the different SNOPS strips measured (5 samples), indicating a good degree of sample-to-sample reproducibility for the SNOPS strips.

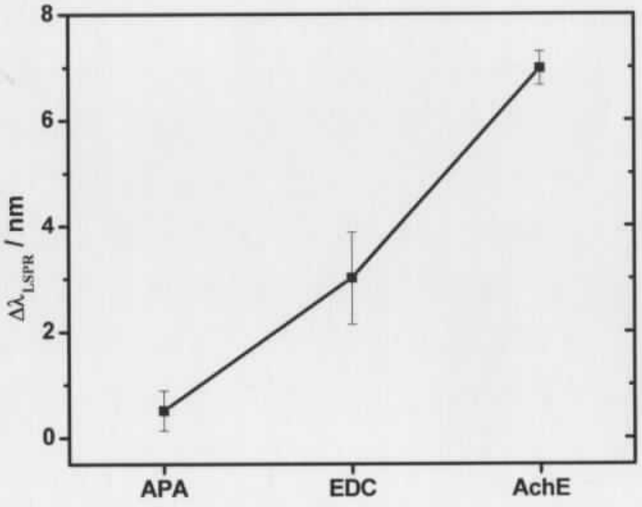

Figure 6- 3 LSPR peak shift due to surface modifications (relative to unmodified Ag NPs). Error bar shows the sample-to-sample standard deviation from 5 SNOPS strips.

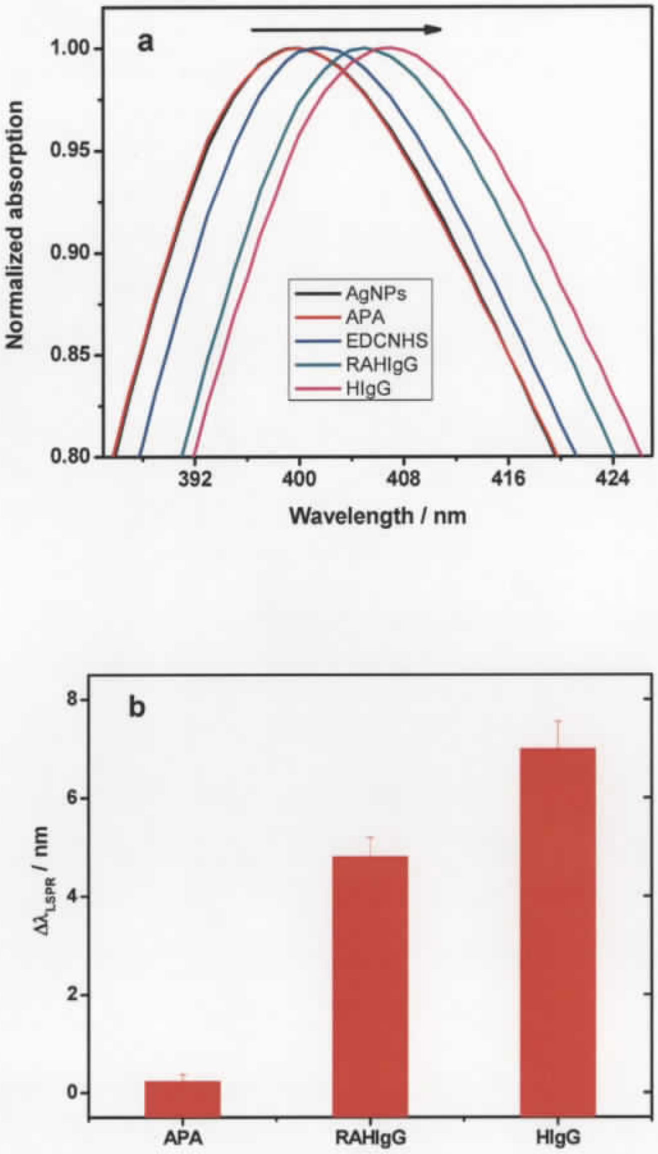

Figure 6- 4 a) LSPR spectra of SNOPS strips after different stages of surface modification; b) shift of LSPR peak relative to unmodified Ag NPs.

6.2.5 Monitoring protein-protein adsorption

In the above section, the SNOPS strips were used to monitor the immobilization of a model protein with good sample-to-sample reproducibility. In this section, we further explored the capabilities of the SNOPS strip by monitoring protein – protein interactions.

The surface modification steps were the same as in above section, described in Scheme 6-2, where APA was immobilized first and then followed by activation with EDC/NHS. The normalized LSPR spectra after each adsorption step are shown in Fig. 6-4a. The binding of APA shows small shift, as discussed for Fig. 6-3. After incubation of the NHS terminated SNOPS strip with Anti-human lambda light chain antibody from rabbit (RAHIgG), a ~4.5 nm further shift was observed. Finally, the binding of human IgG antibody (HIgG) onto RAHIgG provoked a further shift of ~2 nm (relative to RAH IgG) (Fig. 6-4b). The relative smaller shift of the second protein, HIgG, is expected, since the LSPR field penetration depth is about 20 nm and decays exponentially away from the surface.[7, 45, 50] The LSPR decay length is then comparable to the size of a typical IgG protein molecule (about 10 nm).[50] The binding of the second protein, HIgG, cannot cause a LSPR shift as large as the first one because it will experience a weaker LSPR field away from the surface (Fig. 6-4b). Nevertheless, the LSPR shift due to HIgG was still clearly detectable, indicating the potential application for the sensor strip in monitoring protein-protein interactions.

6.2.6 Protein immobilization through amino groups and the limit of quantification for streptavidin (SA) detection

The first step of the procedure for modification of the Ag surface with proteins presented in the above two sections was to introduce carboxyl functionality to the silver surface (Scheme 6-2). However, other strategies for protein detection are based on supported amino functional group on the sensor surface.[26] As a proof of concept, here biotin was immobilized on the SNOPS strips using APTMS sol gel to produce an amino-functionalized surface. The LSPR peak shifts following each step of the surface modification is presented in Fig. 6-5a. The treatment of the SNOPS strip with APTMS sol gel yielded a shift of ~2 nm. APTMS sol gel, similarly to MPTMS sol gel,[41, 51] is a cross-linked silane "polymer" with large molecular weight, which explains the larger shift compared to APA. The binding of biotin further shifts the LSPR position by ~1 nm. Finally, after binding of SA (50 μg.mL^{-1}), an additional shift of ~4 nm was observed (Fig. 6-5a). Fig. 6-5b presents a calibration curve for the detection of SA in solution using the SNOPS strips. The sensor presented a linear response in the SA concentration range between 9.5 nM to 189.4 nM, and the limit of determination (LOD) for SA was estimated as 3.5 nM (0.19 μg.mL^{-1}).

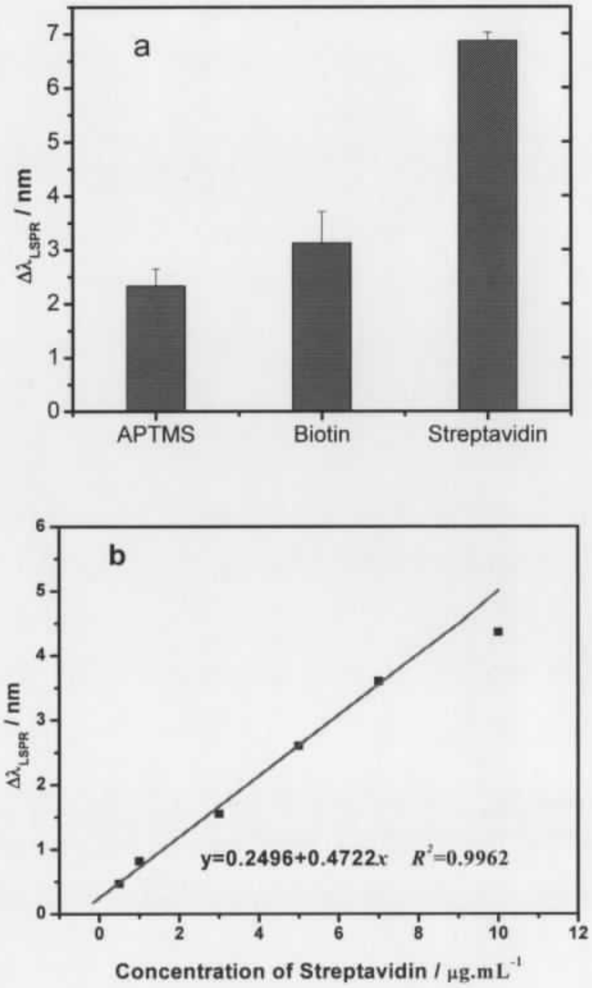

Figure 6- 5 Monitoring the biotin-streptavidin binding. a) LSPR peak shift after each surface modification step (relative to unmodified Ag NPs); b) calibration curve for detection of streptavidin in solution at different concentrations. LOD (2σ)=0.19 μg.mL^{-1}.

6.3 Conclusion

In this work, we developed a cheap, flexible, reproducible and sensitive LSPR sensor platform. The sensor platform is fabricated by using chemically modified PET film as supporting material. Ag NPs were self-assembled on the PET strip to provide LSPR sensing capabilities. At optimized condition, the SNOPS strips showed a sensitivity of ~150 nm/RIU for bulk refractive index changes. The SNOPS strip is very sensitive to the adsorption of thiol containing molecules. We found that as low as 500 nM of MUA can cause a detectable signal. Meanwhile, the SNOPS strips can also be used as very versatile platform for monitoring protein-protein interactions and biotin-(strept)avidin binding by simply changing the surface functionality. In the experiments carried out for the detection of streptavidin, a LOD of 0.19 $\mu g.mL^{-1}$ (~3.5 nM) was observed.

6.4 Materials and methods

6.4.1 Materials.

Unless otherwise mentioned, ACS grade chemicals were used. $AgNO_3$, sodium citrate dihydrate, glucose, 3-aminospropyltrimethoxysilane (APTMS), 11-Mercaptoundecanoic acid (MUA), 1,2-ethylenediamine (EDA), 3-aminopropionic acid (APA), N-hydroxysuccinimide (NHS), N-(3-Dimethylaminopropyl)-N'-ethylcarbodiimide hydrochloride (EDC), (+)-biotin N-hydroxysuccinimide ester (Biotin), Streptavidin (SA) from *Streptomyces avidinii*, human IgG (HIgG, lambda light chain from human mycloma plasma), Anti-human lambda light chain antibody from rabbit (RAH-IgG), and Acetylcholinesterase (AchE) from Electrophorus electricus are all from Sigma-Aldrich. PET films were the regular overhead transparency from BASICS office products LTD, Cambridge, Ontario. Before use, the PET sheets were cut into 9×40 mm strips. Ultrapure water with a resistivity of 18.2 MΩ.cm (from Barnstead NANOpure Diamond water purification system) was used in all experiments.

6.4.2 Synthesis of Ag NPs and MPTMS sol-gel.

The preparation of Ag NPs followed the procedure reported in the literature.[52] Briefly, a 500 mL $AgNO_3$ solution (5.29×10^{-4} M) was brought to boiling under vigorous stirring. Then, 10 mL of 1% sodium citrate solution was quickly added. The heating and stirring were kept for an hour and then only with stirring until the solution cool to room temperature. The as prepared Ag NPs showed an absorption peak at ~399 nm. The APTMS sol-gel preparation was following a sol-gel preparation method for 3-mercaptopropyltrimethoxysilane.[41, 51] Briefly, 400 μL of APTMS and 332 μL of 0.1M HCl were added into 33 mL of water. The solution was vigorously stirred for at least 1 hour. The sol-gel solution shall be used the same day.

6.4.3 SNOPS strip fabrication (Scheme 6-1).

The PET film was cut into 9×40 mm strips, sonicated in MeOH for 5min, and then mounted onto a custom made Teflon holder after dried with flowing N_2. Then, the strips were left in a plasma oven (Harrick Scientific Corp, Ossinng, New York) at high radio frequency for 20 min to activate the surface. Later, the strips were immersed overnight into EDA methanolic solution. After that, the strips were removed from the solution and sonicated in methanol and water for 3 min, respectively. Finally, the strips were rinsed with copious amount of water, and then soaked in Ag NPs solution for a desired amount of time. The Ag NPs modified PET strips then were rinsed with water to eliminate loosely bound Ag NPs and stored in water for future use. The SNOPS strips stored in this way were good for at least 3 weeks.

6.4.4 Surface chemical modification and binding test (Scheme 6-1).

In order to obtain carboxyl functionality on the surface, the SNOPS strips were immersed in 2 mM APA aqueous solution for 5 hours. After rinsing with water, the carboxyl group was activated through EDC/NHS procedure (2 hours) before test its capability of binding proteins. Two experiments were carried out after this step. We firstly tested the reproducibility of the SNOPS strips for monitoring the protein adsorption. As shown in Scheme 6-2, the EDC/NHS activated sensor strips were incubated in AchE (50 $\mu g.mL^{-1}$) overnight. Then they were rinsed thoroughly with PBS buffer before absorption measurements. The second experiment is to examine the protein-protein interaction. Firstly, the EDC/NHS activated strips were incubated in RAH-IgG (60 $\mu g.mL^{-1}$) PBS buffer solution for 40 min. After rinsing with PBS buffer, the SNOPS strips were left in IgG (50 μg.mL^{-1}) PBS buffer solution for another 40 min. PBS buffer was used to rinse off the non-binding HIgG.

In order to modify the Ag NPs surface with amine functionality, the SNOPS strips were left in APTMS sol gel for 20 min (Scheme 6-1). After rinsing with water then PBS buffer (pH 7.4), the amine activated sensor strips were incubated in Biotin DMSO solution (4 mg.mL^{-1}) for 1 hour followed by rinsing with water.[53] To bind SA, the strips were left in SA PBS buffer solution for 30 min. After rinse with PBS buffer, the SA bound SNOPS strips were stored in PBS buffer again before absorption measurement.

6.4.5 Absorbance measurements.

A Cary 50 UV-vis spectrometer was used to record the absorption spectrum. The SNOPS strips were immersed in a quartz cuvette filled with glucose solutions of different concentrations to measure the sensor response to bulk RI changes (the RIs were measured using Pocket Refractiometer (ATAGO CO., Ltd). Water was used for all the remaining measurements.

6.5 References:

1. Willets, K. A.; Van Duyne, R. P., *Annual Review of Physical Chemistry* **2007,** *58*, 267-297.

2. Anker, J. N.; Hall, W. P.; Lyandres, O.; Shah, N. C.; Zhao, J.; Van Duyne, R. P., *Nature Materials* **2008,** *7* (6), 442-453.

3. Mayer, K. M.; Lee, S.; Liao, H.; Rostro, B. C.; Fuentes, A.; Scully, P. T.; Nehl, C. L.; Hafner, J. H., *ACS Nano* **2008,** *2* (4), 687-692.

4. Nusz, G. J.; Curry, A. C.; Marinakos, S. M.; Wax, A.; Chilkoti, A., *ACS Nano* **2009,** *3* (4), 795-806.

5. Neely, A.; Perry, C.; Varisli, B.; Singh, A. K.; Arbneshi, T.; Senapati, D.; Kalluri, J. R.; Ray, P. C., *ACS Nano* **2009,** *3* (9), 2834-2840.

6. Hiep, H. M.; Yoshikawa, H.; Saito, M.; Tamiya, E., *ACS Nano* **2009,** *3* (2), 446-452.

7. Malinsky, M. D.; Kelly, K. L.; Schatz, G. C.; Van Duyne, R. P., *Journal of the American Chemical Society* **2001,** *123* (7), 1471-1482.

8. Endo, T.; Kerman, K.; Nagatani, N.; Hiepa, H. M.; Kim, D. K.; Yonezawa, Y.; Nakano, K.; Tamiya, E., *Analytical Chemistry* **2006,** *78* (18), 6465-6475.

9. Chen, H. J.; Kou, X. S.; Yang, Z.; Ni, W. H.; Wang, J. F., *Langmuir* **2008,** *24* (10), 5233-5237.

10. Kabashin, A. V.; Evans, P.; Pastkovsky, S.; Hendren, W.; Wurtz, G. A.; Atkinson, R.; Pollard, R.; Podolskiy, V. A.; Zayats, A. V., *Nature Materials* **2009,** *8* (11), 867-871.

11. Elghanian, R.; Storhoff, J. J.; Mucic, R. C.; Letsinger, R. L.; Mirkin, C. A., *Science* **1997,** *277* (5329), 1078-1081.

12. Sepulveda, B.; Angelome, P. C.; Lechuga, L. M.; Liz-Marzan, L. M., *Nano Today* **2009,** *4* (3), 244-251.

13. Storhoff, J. J.; Lucas, A. D.; Garimella, V.; Bao, Y. P.; Muller, U. R., *Nature Biotechnology* **2004,** *22* (7), 883-887.

14. Li, H. X.; Rothberg, L., *Proceedings of the National Academy of Sciences of the United States of America* **2004,** *101* (39), 14036-14039.

15. Englebienne, P., *Analyst* **1998,** *123* (7), 1599-1603.

16. Nath, N.; Chilkoti, A., *Analytical Chemistry* **2002,** *74* (3), 504-509.

17. Zhao, W. A.; Ali, M. M.; Aguirre, S. D.; Brook, M. A.; Li, Y. F., *Analytical Chemistry* **2008,** *80* (22), 8431-8437.

18. Ling, J.; Li, Y. F.; Huang, C. Z., *Analytical Chemistry* **2009,** *81* (4), 1707-1714.

19. Zhao, J.; Jensen, L.; Sung, J. H.; Zou, S. L.; Schatz, G. C.; Van Duyne, R. P., *Journal of the American Chemical Society* **2007,** *129* (24), 7647-7656.

20. Haes, A. J.; Zou, S. L.; Zhao, J.; Schatz, G. C.; Van Duyne, R. P., *Journal of the American Chemical Society* **2006,** *128* (33), 10905-10914.

21. Haes, A. J.; Chang, L.; Klein, W. L.; Van Duyne, R. P., *Journal of the American Chemical Society* **2005,** *127* (7), 2264-2271.

22. Haes, A. J.; Zou, S. L.; Schatz, G. C.; Van Duyne, R. P., *Journal of Physical Chemistry B* **2004,** *108* (1), 109-116.

23. Endo, T.; Kerman, K.; Nagatani, N.; Takamura, Y.; Tamiya, E., *Analytical Chemistry* **2005,** *77* (21), 6976-6984.

24. Endo, T.; Yamamura, S.; Nagatani, N.; Morita, Y.; Takamura, Y.; Tamiya, E., *Science and Technology of Advanced Materials* **2005,** *6* (5), 491-500.

25. Frederix, F.; Friedt, J. M.; Choi, K. H.; Laureyn, W.; Campitelli, A.; Mondelaers, D.; Maes, G.; Borghs, G., *Analytical Chemistry* **2003,** *75* (24), 6894-6900.

26. Wang, Y.; Qian, W. P.; Tan, Y.; Ding, S. H., *Biosensors & Bioelectronics* **2008,** *23* (7), 1166-1170.

27. Ling, J.; Li, Y. F.; Huang, C. Z., *Analytical Biochemistry* **2008,** *383* (2), 168-173.

28. Kreuzer, M. P.; Quidant, R.; Badenes, G.; Marco, M. P., *Biosensors & Bioelectronics* **2006,** *21* (7), 1345-1349.

29. Kreuzer, M. P.; Quidant, R.; Salvador, J. P.; Marco, M. P.; Badenes, G., *Analytical and Bioanalytical Chemistry* **2008,** *391* (5), 1813-1820.

30. Zhao, W.; Brook, M. A.; Li, Y. F., *ChemBioChem* **2008,** *9* (15), 2363-2371.

31. Li, Y.; Wang, Z.; Ou, L. M. L.; Yu, H.-Z., *Analytical Chemistry* **2006,** *79* (2), 426-433.

32. Wolter, A.; Niessner, R.; Seidel, M., *Analytical Chemistry* **2007,** *79* (12), 4529-4537.

33. Banuls, M.-J.; Garcia-Pinon, F.; Puchades, R.; Maquieira, A., *Bioconjugate Chemistry* **2008,** *19* (3), 665-672.

34. Banuls, M.-J.; Gonzalez-Pedro, V.; Puchades, R.; Maquieira, A., *Bioconjugate Chemistry* **2007,** *18* (5), 1408-1414.

35. Hwang, S. Y.; Jung, H. Y.; Jeong, J. H.; Lee, H., *Thin Solid Films* **2009,** *517* (14), 4104-4107.

36. Liu, Y.; Chen, J. R.; Yang, Y.; Wu, F., *Journal of Biomaterials Science-Polymer Edition* **2008,** *19* (4), 497-507.

37. Singh, N.; Bridges, A. W.; Garcia, A. J.; Lyon, L. A., *Biomacromolecules* **2007,** *8* (10), 3271-3275.

38. Liu, Y. S.; Li, C. M.; Hu, W. H.; Lu, Z. S., *Talanta* **2009,** *77* (3), 1165-1171.

39. Yan, X. B.; Chen, X. J.; Tay, B. K.; Khor, K. A., *Electrochemistry Communications* **2007,** *9* (6), 1269-1275.

40. Bauer, M.; Haglmuller, J.; Pittner, F.; Schalkhammer, T., *Journal of Nanoscience and Nanotechnology* **2006,** *6* (12), 3671-3676.

41. Fan, M. K.; Brolo, A. G., *Physical Chemistry Chemical Physics* **2009,** *11* (34), 7381-7389.

42. Fan, M. K.; Brolo, A. G., *ChemPhysChem* **2008,** *9* (13), 1899-1907.

43. Addison, C. J.; Brolo, A. G., *Langmuir* **2006,** *22* (21), 8696 -8702.

44. Peng, G.; Tisch, U.; Adams, O.; Hakim, M.; Shehada, N.; Broza, Y. Y.; Billan, S.; Abdah-Bortnyak, R.; Kuten, A.; Haick, H., *Nat Nano* **2009,** *advance online publication*.

45. Stewart, M. E.; Anderton, C. R.; Thompson, L. B.; Maria, J.; Gray, S. K.; Rogers, J. A.; Nuzzo, R. G., *Chemical Reviews* **2008,** *108* (2), 494-521.

46. Malynych, S.; Chumanov, G., *Journal of Optics a-Pure and Applied Optics* **2006,** *8* (4), S144-S147.

47. Li, H. Y.; Luo, X. G.; Du, C. L.; Chen, X. A.; Fu, Y. Q., *Sensors and Actuators B-Chemical* **2008,** *134* (2), 940-944.

48. Barbillon, G.; Bijeon, J. L.; Plain, J.; de la Chapelle, M. L.; Adam, P. M.; Royer, P., *Surface Science* **2007,** *601* (21), 5057-5061.

49. Li, X. L.; Xu, W. Q.; Zhang, J. H.; Jia, H. Y.; Yang, B.; Zhao, B.; Li, B. F.; Ozaki, Y., *Langmuir* **2004,** *20* (4), 1298-1304.

50. Zhou, Y.; Xu, H.; Dahlin, A. B.; Vallkil, J.; Borrebaeck, C. A. K.; Wingren, C.; Liedberg, B.; Hook, F., *Biointerphases* **2007,** *2* (1), 6-15.

51. Jena, B. K.; Raj, C. R., *Analytical Chemistry* **2006,** *78* (18), 6332-6339.

52. Cui, Y.; Ren, B.; Yao, J. L.; Gu, R. A.; Tian, Z. Q., *Journal of Physical Chemistry B* **2006,** *110* (9), 4002-4006.

53. Ferreira, J.; Santos, M. J. L.; Rahman, M. M.; Brolo, A. G.; Gordon, R.; Sinton, D.; Girotto, E. M., *Journal of the American Chemical Society* **2009,** *131* (2), 436-437.

Chapter 7: Summary and conclusions

This chapter contains the summary and conclusion of this thesis. An outlook and future directions for this work is briefly discussed.

7.1 Thesis summary

In this work, the application of MNPs assembly in surface enhanced vibrational spectroscopy and LSPR sensing has been examined.

We first started with the self-assembly of Au NPs on gold electrode as (*in situ*) surface enhanced vibrational spectroscopy substrates. It was found that after 9 Au NPs depositions the SERS signal reached a maximum. The maximum SERS was ~2 orders of magnitude higher than the intensity observed after one Au NPs deposition. A very important observation was that the sample-to-sample reproducibility also increased with the number of Au NPs deposition. However, this was not the case for surface enhanced PM-IRRAS measurements. This is because higher number of depositions leads to rougher surfaces, which scrambles the polarization of the incident light beam. This polarization scrambling effect makes the absorption difference for surface species between the two orthogonal polarized beams disappear (equation 1.18). The optimum deposition number of Au NPs for PM-IRRAS measurement was found to be just one. We further tested the stability of the substrate in electrochemical environment and found a potential window from -800 mV to +200 mV versus Ag|AgCl.

Then, a procedure for the self-assembly of Ag NPs on glass substrate was developed using APTMS sol gel. SERS imaging reveals that, similar to Au NPs on gold electrode, both the SERS signal and reproducibility improved with the number of depositions. In this case, the SERS signal was 3 to 4 orders of magnitude larger than observed from a single Ag NPs self-assembly, at optimum conditions. The spatial variation of the SERS signal also decreased with increasing deposition number, and reached less than 20% at optimum conditions. Using this glass substrate, a near single molecule level sensitivity was achieved for NBA as a sample analyte.

After developing new SERS substrates by self assembly of MNPs on metals (Au) and on dielectrics (glass), we moved towards the application of those procedures in solving analytical and electrochemical problems.

The multi-"layers" Au NPs structure was used to construct a model biofuel cell anode on a Au electrode. The biofuel cell anode consisted three molecular layers, and each of them was characterized by SERS. This was the first example of application of the SERS technique in the biofuel cell field. Also, that work showed that, although SERS is normally considered a powerful characterization method for molecules that directly adsorbed on a roughened metal surface, it is possible to apply the technique to exam a layer-by-layer adsorbates structure.

The methodology developed for the deposition of Ag NPs on glass was applied for their immobilization on fiber optic tips. The Ag NPs-MOFT device, reported in this thesis, is an unique example in the literature, since it combines high sensitivity and reproducibility for remote sensing. For example, the device can detect Rh6G in aqueous solution at 200 nM level without the addition of any extra reagents or NPs. It is also capable of detecting analytes with different structures and charges at high sensitivity in remote sensing mode.

Finally, the procedure for assembling Ag NPs was used to develop a LSPR sensor. The solid support was a common plastic, PET. The PET surface was activated with amine functionalities, and Ag NPs were successively immobilized. Optimization of the self-assembly of Ag NPs was done to achieve better reproducibility. The sensor strips, SNOPSs, were tested for their analytical performance. The response to bulk RI change was found to be ~ 150 nm/ RIU. The application for biosensing was proved by using streptavidin as sample analytes, and a LOD of 3.5 nM was achieved. We also showed that the SNOPS can be used to monitor protein-protein interaction, which shows that the SNOPS sensor is highly versatile in terms of applications.

The main contributions of this work can then be summarized as following:

New methods based on the "layer-by-layer" self-assembly of MNPs were developed for the fabrication of SERS substrates. We found that both the enhancement efficiency and reproducibility/sample-sample variation could be greatly improved using this method. Near single molecule SERS detection was achieved using substrates built by this procedure. In another application, a biofuel cell anode, consisting multi-layers of adsorbates, was successfully characterized. This may expand the SERS technique in the biofuel cell and biosensor research area. The Ag NPs-MOFT sensor constructed using this method, showed both high sensitivity and small RSD% in remote sensing.

The concept of using plastics, such as PET, as solid support for fabricating LSPR sensors, was introduced. MNPs on PET is cheap, easy to fabricate, and can be used in several bioanalytical applications.

7.2 Outlook

7.2.1. SERS substrate development

It is expected that "layer-by-layer" SERS substrates will gain wide applications in the future. This can be interpreted in the following directions:

1. The Au NPs on Au structures can be expanded into biofuel cell/biosensor development, where it can serve as one powerful quality control tool, other than AFM[1] and scanning electrochemical microscopy.[2]
2. The Ag NPs on glass may be used in real sample analysis. The procedure can be easily scaled up and; hence, the production of "standard" SERS substrates in industrial scale is possible. Since the substrate is very sensitive and reproducible, quantitative analysis using such kind of structure for real environmental samples is plausible.
3. The Ag NPs-MOFT device is among one of the most sensitive SERS remote sensors reported, and showed response to analytes with different structures and charges. These properties make it ideal candidate to be used both in environmental analysis and biomedical diagnostics. In fact, a project to develop a SERS endoscopic probe based on this work is underway.

7.2.2 LSPR sensor

For the LSPR sensor developed, it can be envisioned that a pH stick type medical diagnostic device can be developed based on the method proposed in this work. Same as the SERS sensor, the SNOPS sensor is cheap and easy to fabricate, and the surface functionalization is very adaptable. The readout for this type of sensor is absorbance,, which is very mature technique and can be miniaturized. It would be possible to use such kind of sensors in, for example, the sugar monitoring for patients with diabetes, or diagnosing pregnancy.

It is also possible to integrate this LSPR sensor into microfluidics, enabling lab-on-chip devices for biomedical applications. This is being carried out in our lab.

7.2.3 Problems to be solved

There are still a few points to be solved before a SERS substrate based on the work developed in this thesis could be used commercially. For example, in case of Au NPs on electrode, the potential window is limited. Meanwhile, in all the sensors developed, the long term stability (shelf life in months) still needs to be addressed. For the Ag NPs-MOFT device, it was verified that the stability in organic solvent is poor. This is related with the linker molecule used. To make it adaptable to samples contains organic solvent, new fabrication method has to be considered.

7.3 References:

1. Willner, I.; Katz, E., *Angewandte Chemie-International Edition* **2000,** *39* (7), 1180-1218.

2. Guadagnini, L.; Ballarin, B.; Mignani, A.; Scavetta, E.; Tonelli, D., *Sensors and Actuators B-Chemical* **2007,** *126* (2), 492-498.